THE DNA DAMAGE RESPONSE IN TP53 DEFICIENCY

Rashmi Janaki Kumar

A dissertation submitted to the faculty at the University of North Carolina at Chapel Hill in partial fulfillment of the requirements for the degree of Doctor of Philosophy in the Curriculum in Genetics and Molecular Biology.

Chapel Hill
2020

Approved by:

Adrienne Cox

Ian J. Davis

Gaorav P. Gupta

Charles M. Perou

Jeremy Purvis

Dale A. Ramsden

ABSTRACT

Rashmi Janaki Kumar: The DNA Damage Response in TP53 Deficiency
(Under the direction of Dr. Gaorav P. Gupta)

The DNA Damage Response (DDR) is an evolutionarily conserved network of proteins that maintain genome stability in cells and serve as an anti-cancer barrier. The DDR is activated in early pre-neoplastic lesions and is often dysregulated or functionally deficient in late-stage neoplasia. The signaling and repair arms of the DDR pathways can serve as both cancer drivers and as important therapeutic targets. The following work is divided into two parts: (1) how altered double strand break repair pathways may serve as therapeutic targets for restoring sensitivity to DNA damaging agents in cancers and (2) the role of Mre11-Rad50-Nbs1 (MRN) complex, the first-responder to DNA double strand breaks, in pre-neoplastic lesions as a key cell-cycle regulator.

TP53 deficiency has long been associated with poor patient outcomes and decreased response to DNA damaging agents, specifically radiotherapy. Chapter 2 of this dissertation identifies hyperactive end-joining pathways as a significant mediator of radio-resistance. We show that p53-deficiency in an isogenic model system is sufficient to induce resistance to radiation. The resistance to therapy can be partially reversed with inhibition of DNA Protein Kinase (DNA-PK), a serine-threonine regulatory kinase involved in Non-Homologous End Joining. Further, we identify a potential resistance pathway that a subset of p53-deficient cells with inhibition of DNA-PK may employ to avoid cell-death. Finally, we suggest that dual-suppression of DNA-PK and Polymerase Theta may be a

clinically relevant mechanism to restore treatment sensitivity in p53-deficient cancers. Our data show that repair of S phase DNA damage by hyperactive end-joining repair pathways mediates therapeutic resistance in p53-deficient cells.

The MRN complex binds to DNA DSBs, activates master signaling kinases, and initiates end resection at the break to begin repair. Data in this dissertation demonstrate that the MRN complex regulates a p53-independent, G2/M checkpoint in response to burgeoning replication stress during oncogenesis. This checkpoint response regulates mitotic entry of under-replicated DNA, enabling cells with genome instability to exit the cell-cycle via permanent G2 arrest or by mitotic catastrophe. This checkpoint response provides insight into how the DDR restrains genome instability during oncogenesis.

To my parents, Sreemathi and Kumar.

Thank you for your faith and infinite love.

To my pediatric oncologists, Edy, Greffe, and Stork, and my nurses, Margaret and Sally.

Thank you for helping me get here.

ACKNOWLEDGEMENTS

Special thanks to the Gaorav P. Gupta Laboratory and my entire thesis committee for their support and insightful feedback throughout my PhD. Thank you to Dennis Simpson for his development of the Volunder analysis pipeline and aid in analysis of break-site sequencing results. Thank you to Sherry Chao in the Purvis Lab for her guidance with live-cell imaging and wonderful peer mentorship. Thanks to Wanjuan Feng for her help in creating the TP53 mutant cell lines and her expertise in colony forming assays. Thank you to Katerina Fagan-Solis for her mentorship and teaching on mammary gland harvest, lentiviral transduction in animal models, and for the creation of the mammary epithelial cell harvest protocol. Thank you to Sunil Kumar for his help in digital droplet PCR and quantitative analysis of ddPCR results. Thank you to my undergraduate research mentees Victoria Roberts, Sonam Shah, and Aurora Sullivan for their contributions in image analysis and help with colony forming assay analysis. I cannot thank them enough for their encouragement and enthusiasm for our projects.

To the members of my committee; thank you to Dr. Adrienne Cox, the chair of my committee, for her helpful feedback in many aspects of this work and for her mentorship throughout my graduate career. Dr. Cox has also served as my mentor through the Cancer Cell Biology Training Program (CCBTP). Participation in this program will forever be one of the highlights of my PhD experience. Thank you to Dr. Charles Perou for sharing key resources such as the Rb-/- p53-/- mouse model for triple negative breast cancer and

his feedback on the genetic analyses performed. His questions always pushed me to evaluate my science further. Thank you to Dr. Jeremy Purvis for his mentorship on live-cell imaging and computational analyses of images. In addition to being insightful in his questioning and always encouraging, Dr. Purvis' generosity in sharing many of his lab's resources, including the tri-reporter cell line and the use of the Nikon Ti microscopes, made this dissertation possible. I have the utmost gratitude to him and Purvis lab members Kasia Kedziora and Sam Wolff for their time and help in key aspects of my project. Special thanks to Dr. Dale Ramsden who served as an expert in DNA repair on my committee and without whom I would not have been introduced to the world of DNA repair through his lecture series in medical and graduate school. I cannot thank Dr. Ian Davis enough for being a member of my committee and also serving as a clinical preceptor during my PhD years as part of the longitudinal clinical curriculum. In addition to being incredibly kind, Dr. Davis taught me many tenets of pediatric oncology and his patients constantly inspired me throughout my PhD and motivated me to think of clinical applications for my project. Thank you to Dr. Gaorav Gupta and the Gupta lab members for their valuable feedback, help and guidance in the experiments that compose this dissertation, this dissertation and work would not have been possible without them.

The MD-PhD experience is a lengthy journey and one that would not be possible without the endless support of my loving parents, Sreemathi and Kumar. I am eternally fortunate and blessed to have them as my parents and to have a wonderful family. They have always inspired me to do my very best in whatever I do and they have joined me in all of my adventures with laughter and joy. Thank you to my paternal grandfather, Ramiah, for being the first in the family to obtain a PhD at a time when India was a brand-

new country. His zoological manuscripts and love for drawing have encouraged me to be creative and thoughtful about scientific illustration. I am surrounded by a group of amazing friends and I am so thankful for the new friends I've made in medical and graduate school and the old friends who have always been by my side. I would like to acknowledge my oldest friend Richa Bhatia for always answering my calls and for making me laufgh. I would like to thank Alison Mercer-Smith, Hunter Bomba and Willis for their constant encouragement and positive presence in my life, their friendship has been a key component in my well-being and happiness throughout my PhD.

This work was directly funded by the UNC Chapel Hill MD/PhD Program through the Medical Scientist Training Program Grant, the University Cancer Research Fund, the Department of Genetics NIGMS T32 Training Grant, and the Lineberger T32 Cancer Cell Biology Training Program. I'd also like to thank Drs. Deshmukh and Darville, the co-directors of the MST Program for their wonderful mentorship and scientific advice. Finally, many thanks to Alison Regan for her invaluable support and assistance with grants during this training period. © BioRender Software was utilized to make the schematics found in this dissertation.

TABLE OF CONTENTS

LIST OF TABLES

LIST OF FIGURES

CHAPTER 1 - INTRODUCTION

1.1. Chromosomal Instability

Cancer begins when a single cell acquires driver mutations to proliferate in an uncontrolled manner, eventually giving rise to tumors. In the process of expansion, there are two broad stages which are recognized as part of the genetic transformation. First, the initial mutational acquisition which allows for cancer development (i.e. the drivers of cancer) and second, an additional phase of diversification due to selection pressures during the evolutionary process[1,2]. Both processes give rise to inter- and intra-tumoral heterogeneity[1,3]. Tumor heterogeneity is a clinically relevant topic as it poses substantial challenges for therapeutic consideration and efficacy[4,5]. Chromosomal Instability (CIN) is a hallmark of cancer and considered to be a major instigator of tumor heterogeneity[4,6]. CIN is defined as ongoing genomic alterations that result in loss and/or gain of whole chromosomes, partial chromosomes, structural aberrations, and gross chromosomal rearrangements. These changes lead to somatic copy number alterations (SCNAs) which are prevalent across various types of cancers. Amongst the most common cancer types (lung, breast, and colorectal), up to 80% of these tumors are characterized by SCNAs and a lack of diploid karyotype[7–9].

The central questions addressed in this dissertation are how cells give rise to chromosomally unstable genomes that create complex genomic alterations and how these genomic insults are continuously tolerated in the duration of a cancer cell's life. The

vast majority of cancer therapies rely on DNA damaging agents which cause cell death through the induction of cytotoxic double strand breaks (DSBs) in the genome[10]. Thus, the study of the origin, tolerance, and maintenance of genome instability will give us greater insight into novel therapeutic vulnerabilities of chromosomally unstable genomes to DNA damaging agents as well as resistance mechanisms utilized by cancer cells to avoid cell death.

DNA damage is an umbrella-term that can describe a wide variety of genetic lesions that alter the chemical structure of DNA. Most DNA lesions alter one of the DNA strands and the other undamaged strand can serve as a template for repair to restore fidelity to the original DNA sequence. DNA DSBs are considered the most cytotoxic form of DNA damage because both strands of the double helix are cleaved and the DNA is fragmented[10]. The DSB lesion is highly mutagenic and can even serve as a nidus for chromosomal translocations. In mammalian cells, there are at least 10-50 DNA DSBs per day per cell that arise due to endogenous stressors[11]. It is imperative that the cell recognize and repair DNA DSBs quickly and efficiently by activating the DNA Damage Response (DDR).

1.2. The Mammalian DNA Damage Response

The DDR is an evolutionarily conserved pathway whose purpose is to maintain the genome and to protect it against both exogenous and endogenous forms of DNA damage[12,13]. DNA damage is considered to be exogenous when it is environmentally or extracellularly induced. Examples of exogenous DNA damaging agents include UV exposure, ionizing radiation, and clastogenic chemotherapies[12]. Endogenous DNA damage is more complex and often due to dysregulation of cellular processes[13].

Currently, the most commonly recognized sources of endogenous DNA damage include reactive oxygen species, toxic metabolic accumulates, spontaneous deamination, errors in DNA replication or editing, inactivation of DDR pathway components, and oncogene activation[14]. In the context of cancer biology, the last two sources are considered key contributors to endogenous DNA damage.

The DDR is composed of four categories of proteins: sensors, signal transducers, mediators and effectors[12,15]. Sensors bind to and recognize DSBs; the mammalian DSB sensor is composed of the Mre11-Rad50-Nbs1 trimer, known as the MRN complex[16]. Signal transducers are primarily master kinases that amplify the signal that a DSB has occurred and coordinate repair with cell-cycle control. Two important signal transducers in the eukaryotic DDR are the proteins Ataxia-Telangiectasia Mutated (ATM) and Ataxia-Telangiectasia Related (ATR)[17]. While ATM is the primary master kinase for DSBs and ATR plays a similar role for single-stranded DNA (ssDNA) lesions, they have the ability to cross-talk and activate each other respectively[17]. Mediators are the DNA binding proteins that eventually mediate repair of the DSB. Examples of well-known mediators in cancer include the Breast Cancer Gene 1 and 2 (BRCA1 and BRCA2). Finally, effectors are proteins involved in regulating the cell-cycle such that the cell has ample time to conduct repair prior to transitioning to the next phase of the cell-cycle. Therefore, effectors are often strong tumor-suppressors such as TP53, which enact DNA damage checkpoints or trigger apoptotic cascades if repair is unsuccessful[18].

There are three recognized DSB repair pathways: Non-Homologous End-Joining (NHEJ), Homologous Recombination (HR), and Theta-Mediated End Joining (TMEJ)[19]. NHEJ-based repair is the most rapid and dominant form of DSB repair in cells as it can

occur throughout the cell-cycle[20]. During NHEJ, as the name suggests, the broken fragments are directly ligated without utilizing a homologous template. The DSB is first recognized by two Ku proteins (Ku 70/80) which act as a platform for other NHEJ proteins to dock[21]. The next critical protein that is loaded is the DNA-dependent protein kinase (DNA-PK) whose catalytic subunit phosphorylates itself and other key proteins to trigger the NHEJ repair cascade[21,22]. Often, at the site of the DSB the DNA ends are fragmented in a manner that is incompatible with direct ligation and so, nucleases must first process the DSB to allow for the two ends to be joined. NHEJ is characterized by minimal removal of nucleotides to enable clean-up from either end of the break (5' or 3'). The endonuclease Artemis performs resection after being recruited by DNA-PK. After resection, human DNA Pol X family polymerases (Pol μ and Pol λ) incorporate either dNTPs or even rNTPs (which are then removed by base excision repair) into the ends[23,24]. The unique feature of these polymerases is their ability to incorporate nucleotides in both a template-dependent or independent manner. Thus, NHEJ is more error-prone than HR due to the incorporation of small INDELS (insertions/ deletions) at the site of the DSB lesion[25]. Finally, the last step is the NHEJ pathway is DNA ligation which is mediated by DNA ligase IV with XRCC4 activating the ligase complex[26]. Summarily, we can categorize the NHEJ pathway into sensors (Ku 70/80), transducers (DNA-PK), and mediators (Artemis, DNA X Family Polymerases, and Lig IV)[20,22,23,26,27].

In contrast to NHEJ, HR requires the presence of a sister template for recombination and is confined to phases of the cell-cycle where the chromosomes have been duplicated[28]. In addition to DSB repair, HR is also involved in rescue of replication fork collapse, and physiological processes such as telomere maintenance and

meiosis[29,30]. Accordingly, HR is both a mechanism for repair and a manner by which we enhance genetic diversity. Uninhibited HR can lead to accumulation of chromosomal rearrangements, toxic HR intermediates, and most importantly, a loss of heterozygosity[30].

HR begins with the MRN complex binding to DSBs as a dimer of trimers[16]. Mre11 primarily exists bound to Rad50 in $Mre11_2Rad50_2$ complexes *in vivo*, and mutations in Mre11 are sufficient to de-stabilize the entire MRN complex and decrease levels of Rad50 as well as Nbs1[31]. These findings highlight that the complex is important for both function and protein stability. The globular domains of the Mre11 dimers are thought to enable "short-range" spatial organization of the broken DNA ends, and Rad50 dimers mediate "long-range tethering" via their zinc hooks[31]. Once MRN has bound to the DSB, it activates ATM master kinase and promotes autophosphorylation at S1981, which is key for retaining ATM at the DSB[17]. When ATM is activated, mediators and effectors are further recruited to the MRN complex. MRN is unusual in that it can participate in initial strand resection via its nuclease function[32].

Unlike NHEJ, HR is characterized by deep resection that leaves long ssDNA overhangs capable of strand invasion. Thus, processive resection enzymes such as hExo1 and DNA2 nucleases are required[33,34]. Following resection, the newly exposed ssDNA overhang is immediately protected by the binding of Replication Protein A (RPA)[31]. BRCA2 binds to the dsDNA-ssDNA junction and the formation of the BRCA1-PALB2 (Partner and localizer of BRCA2)-BRCA2 complex is required for the recruitment of an essential HR protein: Rad51 Recombinase[29,35]. For HR to occur, the RPA must be displaced by the nucleation protein Rad51 in an ATP dependent manner[36]. Rad51 coated

filament must now find sequence complementarity through homology search and form a synaptic complex with the homologous genomic sequence.

Homologous recombination is further complicated by the fact that there are two slightly different processes to synthesize and resolve the two different ends, which are known as the first-end and second-end synthesis steps[34,37]. Furthermore, because HR can result in crossover events where recombination occurs to induce genetic diversity, in the context of DNA DSB repair an altered version of HR is utilized, known as synthesis-dependent strand annealing (SDSA), where crossover does not occur. SDSA is the preferred HR method in mitotic cells[38]. To simplify these key steps, it is hypothesized that Polymerase δ is the primary polymerase involved in HR first-strand synthesis and other minor polymerases have been implicated for second-end synthesis respectively[33]. Once synthesis occurs, the HR complex is dissolved to complete repair. In summary, the key steps for HR are resection, strand invasion, homology search, strand pairing, and resolution.

The final pathway, TMEJ has been an area of active investigation in recent years. The TMEJ pathway is not the first choice for DSB repair; however, in cases where either NHEJ or HR-based repair fails, it becomes essential[39]. Polymerase theta-mediated end joining is also important in disease states where the HR or NHEJ pathways are deficient or mis-regulated[40]. In particular, DNA Polymerase Theta (Pol θ), the key polymerase-helicase protein involved in TMEJ, is upregulated in many HR deficient cancers[41]. TMEJ is thought to be independent of classical-NHEJ and does not require Ku, DNA-PK, or other NHEJ factors to perform repair. However, TMEJ does require end resection which is thought to be initiated by HR initiating factors and this resection enables the search for

microhomologies flanking the break site. As a result, deficiency in proteins that prevent end resection (such as Ku or p53 Binding Protein – 53BP1) also leads to increased TMEJ usage[39,41]. The current accepted TMEJ repair pathway has the following five steps: resection, annealing of microhomology sites, flap removal, gap synthesis, and ligation. As previously mentioned, resection processes may be shared with HR, but excessive resection is not required to expose microhomologies. The flap removal is performed by ERCC1, and Pol θ performs gap synthesis, with DNA Ligase III performing the final ligation step[42]. TMEJ is by nature an error-prone pathway as microhomology mediated repair often results in loss of the nucleotides in between the two sites of homology (i.e. due to flap removal).

1.3. DDR AND THE CELL-CYCLE: THE DNA DAMAGE CHECKPOINTS

The eukaryotic cell-cycle is characterized by four distinct phases: Gap phase 1 (G1), Synthesis (S), Gap Phase 2 (G2), and Mitosis (M). The sequential nature of the cell-cycle is coordinated by Cyclin Dependent Kinases (CDKs) and this elegant system is closely attuned to the DDR (Figure 1.2)[18,43]. The cell-cycle has several checkpoints that halt progress to ensure that DNA damage does not disrupt genomic integrity from one cellular generation to another[44]. DNA damage checkpoints can trigger cell-cycle arrests, providing time for DSB resolution. If repair is unsuccessful, downstream DDR effectors also have the capacity to trigger senescence or apoptosis. There are four main checkpoints: the G1-S transition checkpoint, intra-S checkpoint, G2 phase checkpoint, and Mitotic checkpoint (Figure 1.1)[12,18,44].

The G1-S checkpoint is dependent on activation of the p53 tumor suppressor protein by ATM phosphorylation[45]. Activated p53 induces transcriptional upregulation of

CDKN1A, which results in production of p21[46]. Levels of p21 signaling determine the stringency of the G1/S checkpoint through inhibition of CDKs[45,46]. The second checkpoint in the sequence is the intra-S checkpoint. The most critical function of the intra-S checkpoint is to ensure replication fidelity[47]. ATR kinase is thought to be the more crucial mediator of the intra-S checkpoint as it can be activated by a wide variety of genotoxic insults unlike ATM, which is primarily activated by DSBs[47,48]. Activation of the intra-S checkpoint results in inhibition of further origin firing and allows time for replication forks that encounter DNA damage to undergo fork reversal or fork restart. However, several elegant studies show that the intra-S checkpoint does not behave similarly to the G1 or G2 checkpoints as the gap phase checkpoints often trigger an extended “arrest” of cell-cycle[49–51] Triggering the intra-S checkpoint is more often associated with a slowdown of S phase progression, prolonging the time spent in S phase[49]. In many cases, cells that complete S phase with substantial damage will then arrest or be halted by the G2 checkpoint. The G2 checkpoint is termed the “threshold” checkpoint due to the observation that at a certain level of total DNA damage, this checkpoint is permanently activated, resulting in exit from cell-cycle[49,52,53]. The sensitivity of the G2 checkpoint is crucial as it is the final barrier before mitosis where entry of unrepaired DSBs can result in mitotic failure[54,55]. The final checkpoint is the mitotic checkpoint. The primary purpose of the mitotic checkpoint is to ensure proper attachment of spindle poles to chromosomes [56,57]. Figure 1.1 visually describes all checkpoints in greater detail.

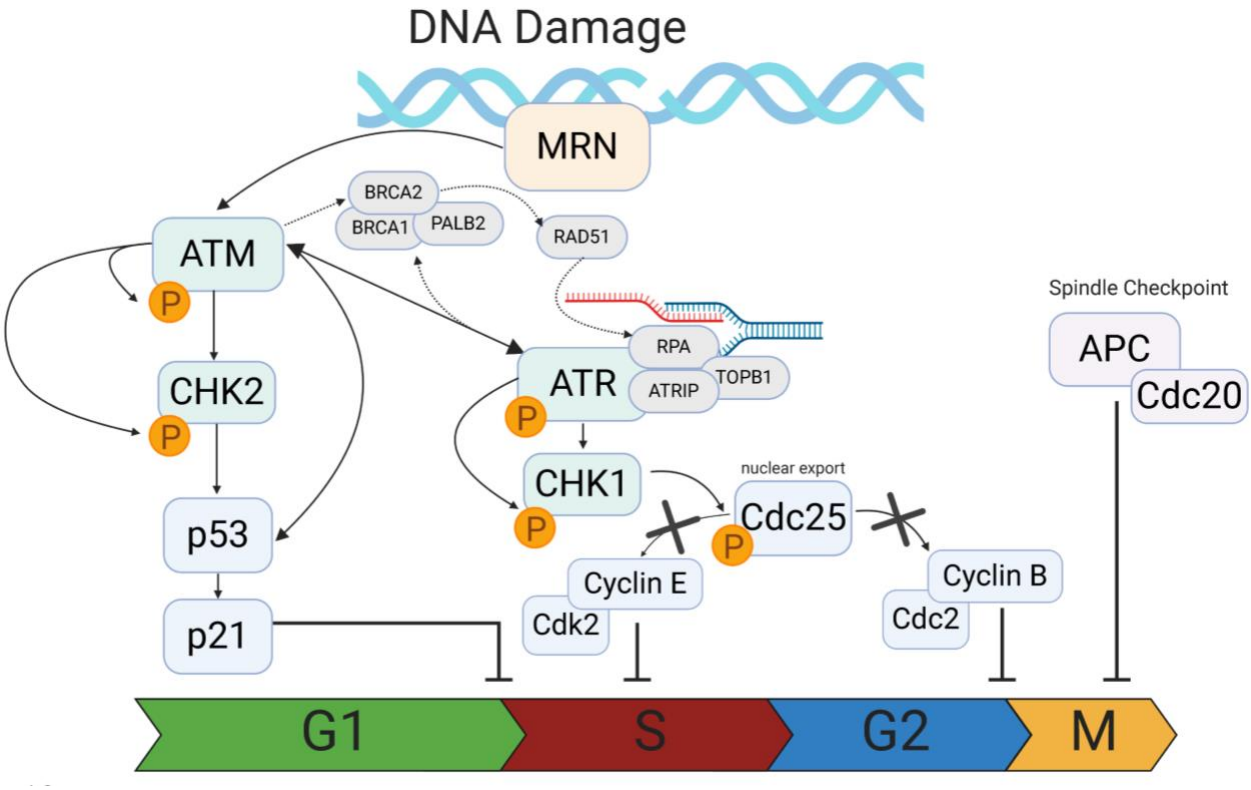

Figure 1.1 : DNA Damage Checkpoints. DNA damage is first detected by the MRN complex with downstream activation and cross-talk between ATM and ATR kinases[58]. These master kinases activate the checkpoint kinases, CHK2 and CHK1, which regulate p53 and Cdc25 respectively[59]. The CHK2-p53-p21 axis induces the G1/S DNA damage checkpoint[59]. ATR activation is critical for intra-S and G2/M checkpoints as it binds to RPA which coats single-stranded DNA at DNA damage sites in S phase replication forks[58]. CHK1 activity sequesters Cdc25C in the cytoplasm, causing G2 arrest. CHK1 activity also regulates Cyclin E through Cdc25A, which prolongs S phase via the intra-S checkpoint[47]. Finally, the spindle-assembly checkpoint serves as a major regulator for mitotic separation of chromosomes. Of note, these pathways have predominantly been evaluated with the use of ionizing radiation and DNA damaging agents.

While these four checkpoints have been broadly characterized, single-cell studies and analyses are revealing that activation of checkpoints can vary greatly within a population of cells treated with DNA damaging agents[49,60–62]. Insights from live-cell imaging have highlighted how cell-fate is dependent on the temporal kinetics of damage detection as well as repair[71,80–82]. Fluctuations in signaling and dysregulation of repair can greatly alter cell-fate outcomes in populations. Thus, critical portions of both chapter 2 and 3 of this dissertation will utilize single-cell analyses to gain greater insight into the mechanisms of checkpoint activation and altered repair kinetics in states of DDR deficiency.

1.4. The DNA Damage Response in Cancer

Although the purpose of the DDR is to maintain the genome, components of these three pathways may suppress or promote genome instability[12]. Alterations in DNA damage responses and repair can give rise to cancer. Many of the members of the DDR have been implicated in tumorigenesis[63]. The link between the DDR and cancer was first observed through the prevalence of cancers in human patients with genome instability syndromes[64]. Genome instability syndromes are characterized by a predisposition to early incidence of cancers, familial history of cancer, and recurrent incidence of multiple types of cancers[64]. These disorders are genetically characterized by germline loss of function mutations in key DDR proteins[64,65]

Moreover, the oncogene-induced DNA damage response model in cancer proposes that the DDR is activated in early pre-neoplasia by the presence of oncogenic replication stress (Figure 1.2). Oncogene activation results in increased de-regulation of origin licensing, nucleotide synthesis, an imbalance in metabolic stress, and increased

replication fork collapse directly leading to the formation of DSBs. These DSBs activate the DDR via the MRN-ATM-p53 axis which in turn regulates anti-proliferative measures to inhibit tumor growth. However, continued activation of oncogenes and accumulating stress create selection pressures for DDR deficiency and dysregulation which then contribute to the development of neoplasia (Figure 1.2). Thus, the DDR is intrinsically linked to tumor development and progression.

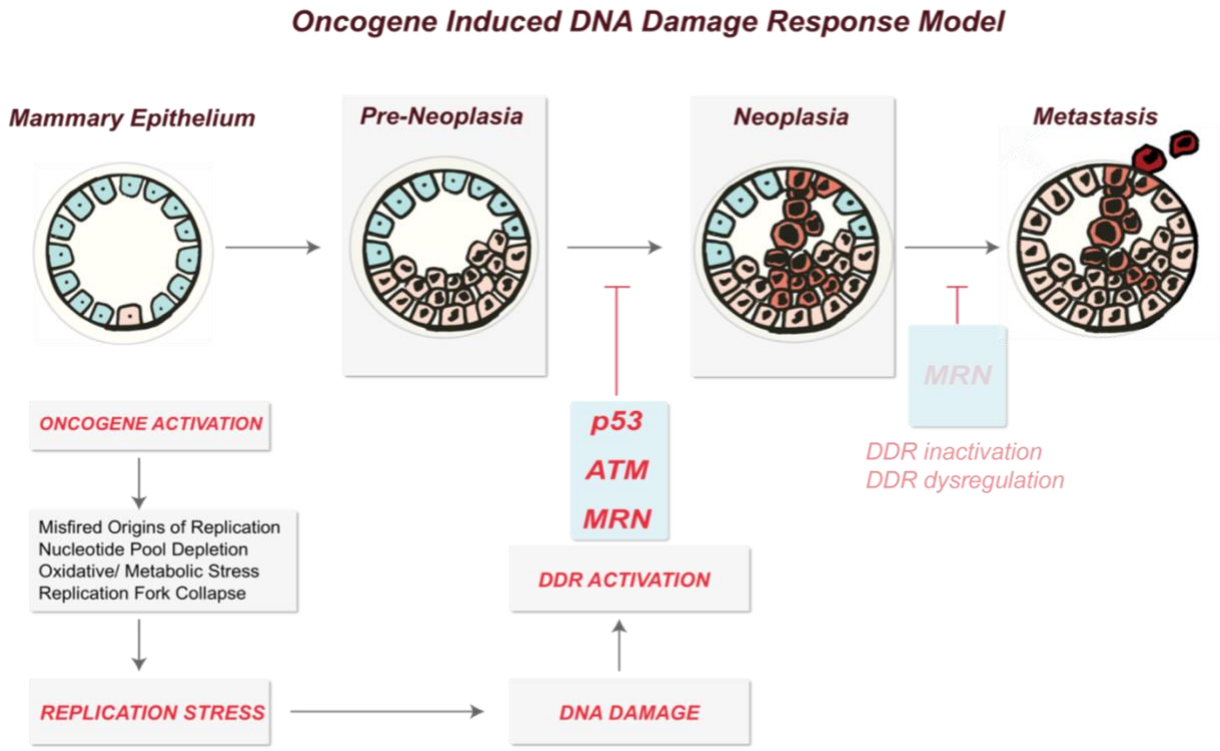

Figure 1.2 : Oncogene Induced DNA damage response (DDR) model. Mammary neoplasia is used as a model cancer to indicate how the DDR restrains early pre-neoplastic lesions in response to oncogenic activation and accumulating DNA damage. DNA DSBs are sensed by the Mre11-Rad50-Nbs1 (MRN) complex which in turn activates master kinase Ataxia Telangiectasia Mutated (ATM) and downstream p53 signaling induces senescence or apoptosis. In late-stage neoplasia, the DDR is often inactivated or dysregulated, giving rise to chromosomally unstable, clinically aggressive cancers.

1.4.1. DDR Deficiency in Cancer

DDR deficiency in cancer can be due to rare germline mutations or more often due to somatic mutations in DDR genes. Pan-cancer analyses of The Cancer Genome Atlas

datasets highlight that DDR gene alterations are highly common in cancer[66]. In fact, one-third of all TCGA cancer types show somatic mutations in DDR genes in conjunction with high SCNAs and loss of heterozygosity[66,67]. Intriguingly, examining loss-of-function alterations within DDR pathways shows many co-occurring mutations in multiple pathways, highlighting the complexity of the DDR and its association with cancer[68]. Further, DDR alterations were also specifically correlated with higher mutational burden and diversity[66–68].

While these analyses speak to the DDR overall, alterations in the specific DSB repair pathways (HR, NHEJ, and TMEJ) are amongst the most common. In particular, HR pathway genes were altered in 40% of all cancers and in breast and ovarian carcinomas, HR alterations are ubiquitous[69]. Independent of HR alterations, in ovarian carcinoma, NHEJ defects were found in roughly 20 out of 47 patient primary cultures[70]. Moreover, mice with defects in Ligase IV, DNA-PKcs, Ku 80, or XRCC4 in a p53 deficient background all show accelerated tumor development[70]. Finally, TMEJ dysregulation in cancer has been the subject of several recent discoveries. Using microhomology based scar signatures to identify TMEJ repair sites, it was noted that up to 30% of TCGA cancers exhibit hyperactive Pol θ repair[41]. These lines of evidence showcase the importance of DDR dysfunction in tumor origination and maintenance.

1.4.2. Altered Responses for Therapeutic Sensitivity

Recent preclinical studies have provided evidence that DNA repair pathways should be viewed as a network[71–74]. When DNA repair pathways are dysregulated in cancer or if a patient is deficient for a key DNA repair protein, one or more pathways are simultaneously altered[5,71]. Studies have begun to explore the therapeutic potential of

exploiting DDR deficiencies. However, we limit ourselves if we only exploit synthetically lethal interactions between one or two target proteins within this vast network for therapeutic purposes. Synthetic lethality occurs when two or more combinations of gene expression deficiencies now result in cell-death whereas individual deficiencies are not sufficient for lethality[75]. For example, in HR deficient cells it is well known that inhibition of Poly-ADP-Ribose-Polymerase 1 (PARP) induces a synthetic lethality in the cells[76]. However, it is also known that in cells with HR deficiency, there is an increased dependence on NHEJ factors for resolution of endogenous DSBs[77]. This is further supported by the fact that dual knock-out of *Atm* and *Prkdc* (DNA-PKcs gene) results in embryonic lethality[78]. As a result, not only are HR deficient cells sensitive to inhibitors to PARP, they may also be sensitive to inhibitors of DNA-PKcs[77,79]. Moreover, they are likely to be highly sensitive to other inhibitors of NHEJ proteins and by extension; TMEJ[80].

Genetic evidence for this altered dependence is seen when we analyze “genomic scar patterns” of DDR defects. Signatures of Homologous Recombination Deficiency (HRD) may indicate upregulation of alternative end joining pathways that now contribute to DSB repair[41,66,81]. Analysis of Pol θ dependent TMEJ repair patterns shows many similarities to signatures that have previously been labeled as HRD signatures[41]. Furthermore, continued discrepancies between HRD signatures and HR deficiency as assessed by HR functional assays suggest that HRD signatures are not predictive of repair capacity[69,82–84]. In the most recent study of the comprehensive repertoire of mutational signatures in human cancer, in conjunction with the Pan Cancer Analysis of Whole Genomes (PCAWG) cohort, it was noted that many of the existing signatures overlap significantly[68]. This study concluded that few DNA repair “signatures” are unique

and many have strong associations with defective DNA-maintenance processes[68]. However, the biological processes by which these signatures arise are still unknown and remain to be categorized.

Thus, these studies highlight how these pathway deficiencies may result in altered DDR responses. By viewing the DDR as a network of pathways that can alter functional capacity of any individual pathway to adapt to a deficiency, we can begin to identify personal therapeutic approaches for patients with known DDR defects.

1.4.3. TP53 and the DNA Damage Response

TP53 is the most commonly mutated gene in human cancers. As a result, TP53 pathway deficiency is common in cancer and is associated with poor prognostic outcomes in many different cancer types[85]. The p53 protein is involved in numerous processes that respond to cellular stress[86]. As a tumor suppressor protein, p53 is also a downstream effector of the DDR, with involvement in DNA damage checkpoint functions and apoptotic activation[61]. In 80% of TP53 mutant cancers, both alleles are functionally impaired[85]. Despite substantial investigation into the physiological role of p53 and the long-standing observation that p53 deficiency leads to resistance to DNA damaging therapies, the DDR has not been systematically evaluated in a p53-deficient cell.

There are several important knowledge gaps that exist regarding p53-deficiency and the DDR. First, TCGA mutational studies have drawn attention to cancer patient samples with dual loss of function mutations in ATM master kinase and TP53[87,87–89]. Classical epistasis models in genetics suggest that mutations in two proteins in the same pathway are epistatic to each other, i.e. one mutation masks the phenotype of the other. Since ATM and p53 are in the same DDR pathway, p53 mutation should mask the effect

of the ATM mutation. In this case, it would not be evolutionarily advantageous to further mutate ATM. However, the prevalence of patients with double mutations suggest that there are p53-independent functions of ATM that are critical for restraining cancer progression. Thus, one important knowledge gap in the field is to assess the p53-independent functions of the DSB repair pathways. When the downstream effector is absent, what are the alternative mechanisms by which the MRN complex, ATM, and other components of the DSB repair pathway function to restrain tumorigenesis? Chapter 3 of this dissertation will investigate this specific question.

Second, p53-deficiency has been linked to radio- and chemo-resistance since the 1990's[90–93]. Yet the mechanisms of therapeutic resistance in p53-deficient cells and the possible involvement of DNA repair pathways remain to be characterized. Recent work in p53-signaling has demonstrated that epithelial cells with intact p53 have fluctuations in p53-signaling that dictate cell fate post DNA damage[62]. However, we have yet to fully uncover the modes by which cell fate decisions are made in cells lacking p53 altogether. As there are no personalized therapies for cancer patients with p53-deficiency, these studies aim to elucidate a clinically relevant mechanism that can be directly translated to meet this need.

1.4.4. DDR and the Immune System

The interplay between the immune system and the DDR is starting to become fully appreciated as studies reveal how the DDR activates components of the innate and adaptive immune responses during cancer progression and in response to cancer therapy. Tumor mutational burden is correlated to neoantigen load and activation of T cell responses against novel cancer antigens presented on cancer cells[94,95]. Defects in the

DDR increase tumor mutational burden and give rise to frequent chromosomal translocations that can result in novel fusion onco-proteins, mutated self-proteins, or aberrant protein expression[96]. All of these may trigger adaptive T cell immune responses. Moreover, DDR dysfunction can lead to the presence of nucleic acids in the cytoplasm which trigger innate immune cells[97,98]. Nuclear compartmentalization of nucleic acids is critical for protecting self-DNA and for discriminating between self-DNA and infectious DNA viruses[97]. Pattern recognition receptors (PRRs) are viral detectors that detect nucleic acids[99]. Cytoplasmic and membrane bound PRRs can activate Type 1 Interferon responses, which are critical for antiviral defense and recruitment of phagocytic cells[98]. Thus, cytoplasmic DNA sensors exist to protect the cell from viral infection and due to their binding of double stranded DNA (dsDNA). They can also alert the immune system of cells whose nucleic acid material is present in the cytoplasm, because they are able to bind dsDNA[98]. During the cell-cycle, nuclear envelope collapse is the only time when nucleic acid material is not compartmentalized. Outside of this physiological scenario, there exists several pathological reasons for the presence of dsDNA in the cytoplasm. Cells with DDR dysregulation accumulate unrepaired DSBs leading to chromosomal mis-segregation, which is known to increase dsDNA in the cytoplasm[97]. Intriguingly, dsDNA in the cytoplasm may be contained by a micronucleus (i.e. a portion of the nuclear membrane that now encloses the nucleic acid material)[97]. The DDR may also be involved in micronuclei formation[100]. However, micronuclei disintegration is common and often results in dsDNA entering the cytoplasm.

Mitotic progression of DNA DSBs has been implicated as the major mechanism of the abscopal response[101]. The abscopal response is a radiotherapy term that describes

reduction of tumor size of tumors outside of the field of irradiation due to systemic effects[102]. Evidence now shows that the abscopal response is in part mediated by DSB presence in the cytoplasm and activation of cyclic GMP-Synthase (cGAS) and Stimulator of Interferon Genes (STING) which results in innate immune activation[101]. The benefits of this activation are a widespread effect on tumor reduction in tissues that were not part of the initial focal therapy. Thus, DDR defects in checkpoint responses may also contribute to mitotic DSBs resulting in increased genomic fragmentation during mitosis. Finally, there are well-documented patient cases of germline mutations in DDR proteins and cytoplasmic DDR sensors resulting in auto-immune disorders that trigger excessive inflammatory cascades in humans[97,103]. Thus, an understanding of how DDR proteins may contribute to mitotic DSB entry, micronuclei formation and immune activation is key to elucidating the *in vivo* implications of DDR dysregulation and tumor clearance.

1.4.5. The Balance Between DDR and Genome Instability

How can the DDR serve as an anti-tumor barrier (i.e. tumor suppressor) and also be utilized as a tolerance mechanism for tumor propagation and maintenance? This question has been of critical importance in the past decade as whole-genome and single-cell sequencing have revealed the extent of the complexity found in a cancer cell's genomic landscape[67,104,105]. Seminal experiments conducted in cancer tissues from the pre-neoplastic to neoplastic stages have shown how DDR mutations are progressively accumulated during cancer evolution[106,107]. In breast cancer, ductal carcinoma in situ (DCIS) enables us to study the pre-neoplastic mutations found in DDR proteins[106]. Commonly, pre-neoplastic cells retain p53 and rarely have DDR mutations. The initial lesions are often activating oncogenic mutations or amplifications in genes such as c-Myc

or epidermal growth factors[108,109]. Oncogenic activation, as discussed previously in Figure 1.2, is an inducer of endogenous DNA damage which then activates the DDR. In early pre-neoplasia there are clear indicators of strong and sustained DDR activation. In late-stage neoplasia, this activation is impaired or dysregulated due to the long-standing selection pressure to mutate DDR proteins[13,63,106,107,110,111]. As cancer evolves, the frequency of mutations in ATM and TP53 increases, suggesting that the transition from pre-neoplasia to neoplasia is restrained heavily by the presence of an active DDR.

Simultaneously, as the DDR is inactivated, the cell experiences continuous endogenous DNA damage due to the persistence of oncogenic signaling. The cell is forced to repeatedly progress through the cell-cycle with endogenous DNA damage and in doing so, begins to depend on aspects of the DDR to avoid cell-death[111–114]. This results in unique DDR dependencies in late-stage neoplastic lesions as the DDR adapts to new cellular demands. These dependencies are evidenced by the existence chromosomally unstable cancers with highly variable sensitivity to DNA damaging agents[115–118]. Due to their ability to tolerate high levels of ongoing DNA damage, the addition of external clastogenic chemotherapies often may not induce cell-death. In these cells, we must elucidate the exact DDR pathways that become essential for cell survival to understand how these cells tolerate high levels of DNA damage.

In summary, this dissertation will touch upon two key projects that address knowledge gaps in the field of the DDR in cancer. First, how does p53-deficiency contribute to therapeutic resistance and how are DNA repair mechanisms altered in p53-deficient states? Second, what is the function of the MRN complex in a p53-deficient cancer, when the downstream effector of the cell-cycle checkpoint is no longer present?

How does MRN-activated DDR restrain tumor progression in early-stage neoplasia? Insights into these two topics will aid in our overall understanding of the complex role of the mammalian DDR and the therapeutic ramifications of DDR dysfunction in human cancers.

CHAPTER 2 – DUAL INHIBITION OF DNA-PK AND DNA POLYMERASE THETA OVERCOMES RADIATION RESISTANCE INDUCED BY P53 DEFICIENCY

2.1. Summary

TP53 deficiency in cancer is associated with poor patient outcomes and resistance to DNA damaging therapies. However, the mechanisms underlying treatment resistance in p53-deficient cells remain poorly characterized. Here, we show that p53-deficient cells exhibit hyperactive repair of therapy-induced DNA double strand breaks (DSBs), which is mediated by DNA-dependent protein kinase (DNA-PK). Single-cell analyses of DSB repair kinetics and cell cycle state transitions reveal an essential role for DNA-PK in suppressing S phase DNA damage and mitotic catastrophe in p53-deficient cells. Yet, a subset of p53-deficient cells exhibit intrinsic resistance to therapeutic DSBs due to a repair pathway that is not sensitive to DNA-PK inhibition. We show that p53 deficiency induces overexpression of DNA Polymerase Theta (Pol θ), which mediates an alternative end-joining repair pathway that becomes hyperactivated by DNA-PK inhibition. Combined inhibition of DNA-PK and Pol θ restores therapeutic DNA damage sensitivity in p53-deficient cells. Thus, our study reveals DNA-PK and Pol θ dependent end joining repair of S phase DSBs as critical determinants of response to DNA-damaging agents in p53-deficient cells. Inhibition of these targetable DSB end joining pathways may improve the efficacy of DNA-damaging therapies in p53-deficient cancers.

2.2. Introduction

TP53 is the most commonly mutated tumor suppressor gene[119]. p53 mediates pleiotropic tumor suppressive effects through regulation of cell cycle arrest, apoptosis, and cellular metabolism in response to cellular stress[86,120]. Beyond its role as a tumor suppressor, p53 deficiency is associated with poor prognostic outcomes across many different cancer types[85,121–123]. There is both clinical and preclinical evidence that p53-deficient cancers exhibit resistance to a variety of DNA damaging therapies[91–93,124–126].

Despite accumulating evidence that p53 deficiency in cancer is associated with poor clinical outcomes, the mechanisms for therapeutic resistance in p53-deficient cells remain poorly characterized. Several factors play into the ambiguity surrounding the role of p53 and radio-resistance. First, early work suggested a role for loss of p53-mediated apoptosis in enabling increased survival post-radiation[125,127]. However, in epithelial cancer cell models p53-induced cell cycle arrest, rather than apoptosis, has been associated with radiosensitization[128]. Yet, p53-mediated effects distinct from cell cycle arrest and apoptosis may also regulate radiosensitivity, as critical aspects of this relationship seem to be independent of p21 induction and the G1/S checkpoint[129–131]. Second, an important mechanism of cell death by DNA damaging therapy is mitotic catastrophe[54,132,133]. However, the determinants of therapy-induced mitotic catastrophe remain poorly understood. Third, further obscuring our limited understanding is a growing appreciation for the role of intratumoral heterogeneity as determinants of therapeutic response[134]. Single-cell analyses are thus likely to reveal new insights into the underpinnings of treatment response in p53-deficient cells. Unfortunately, lack of

progress in understanding the mechanistic bases of therapeutic resistance in p53-deficient cells has hampered efforts to better target p53-deficient cancers.

The advent of time-lapse microscopy enables longitudinal assessment of biosensors at the single cell level, which has yielded novel insights into mechanisms of therapeutic response and p53-dependent cellular fate decisions[61,135,136]. Recent evidence highlights the importance of p53-signaling waves in regulation of cellular fate decisions of quiescence versus cell cycle re-entry after DNA damage [62,137,138]. However, the mechanisms that determine such cell fate decisions upon DNA damage induction in p53-deficient epithelial cells, which are prevalent in cancers, have not been established, and may lead to novel strategies to restore treatment sensitivity.

In this study, we use time-lapse microscopy of cell cycle and DNA damage biosensors to investigate the relationship between therapeutic DNA damage and cell fate at the single-cell level. We find that p53-deficient cells exhibit hyperactive repair and accelerated resolution of DNA damage foci, particularly in S phase of the cell cycle. We show that the accelerated resolution of therapeutic DNA damage in p53-deficient cells is dependent on DNA-PK, a critical serine/threonine kinase in the non-homologous end joining (NHEJ) pathway[139]. Inhibition of DNA-PK using the small molecule inhibitor NU7441 partially restores sensitivity to DSB inducing agents in p53-deficient cells. We further demonstrate a role for Polymerase Theta (Pol θ) mediated end joining (TMEJ), an alternative therapeutic resistance pathway in p53-deficient cells. Thus, our work provides critical insight into a clinically-relevant mechanism for why p53-deficient cells are resistant to DNA damaging therapies.

2.3. Results

2.3.1. P53-Deficient Cells Exhibit Radioresistance and Accelerated Resolution of DNA DSBs

We first established an isogenic cell system to investigate determinants of treatment-induced cell fate in p53-deficient cells. In order to minimize potential contributions of accessory mutations on phenotypes observed in cancer cell line models, we used CRISPR/Cas9 to disrupt *TP53* in the p53-proficient immortalized epithelial cell line model hTert-RPE1 ("RPE1"), which has also been a preferred model for investigating p53-dependent cell fate[138,140,141]. Two independent CRISPR/Cas9-targeted *TP53*$^{-/-}$ RPE1 clones were selected for further study after confirming cells were deficient for p53 protein and lacked p53-dependent transcriptional induction of p21 in response to ionizing radiation (IR) (Figure 2.1A-C).

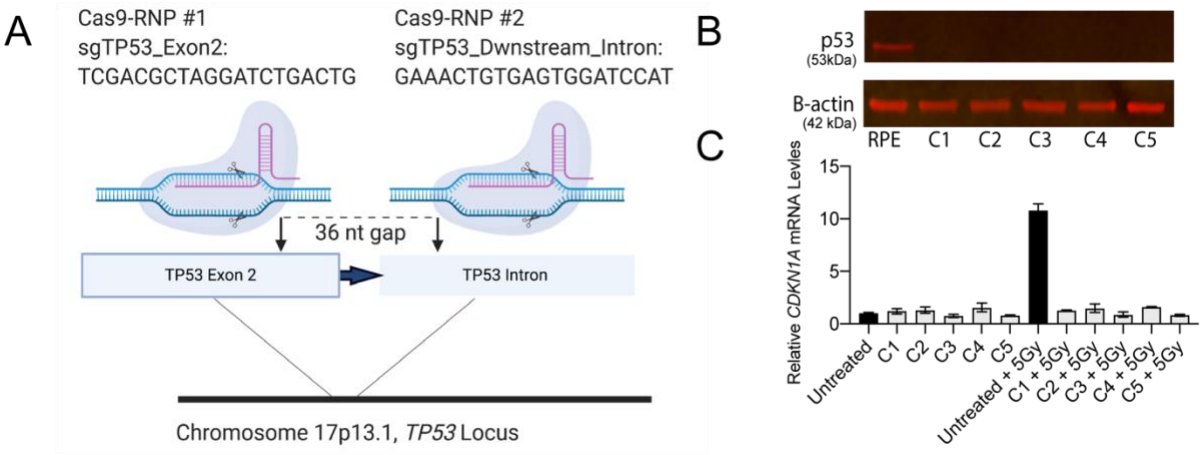

Figure 2.1 : Isogenic model of TP53 Deficiency in RPE1 cells. A, Schematic of CRISPR target locus in human TP53 gene. Two sgRNAs were designed to target sites in the terminal region of exon 2 (which encodes the p53 transactivating domain) and a site in the downstream intron with a 36 nucleotide (nt) gap. sgRNAs were complexed with Cas9 in the RNP system and electroporated into RPE1 cells. B, Western Blot of 5 selected single-cell clones that were profiled for p53 protein. C, Functional assay evaluating p53-

dependent CDKN1A transcriptional responses to treatment of 5Gy IR. RNA from cells exposed to IR were harvested 6 hrs post treatment.

To assess whether p53 deficiency confers a proliferative advantage when treated with ionizing radiation, we performed a mixed competition assay. We took mCherry labelled RPE1 and mixed them with equal numbers of unlabeled *TP53*$^{-/-}$ RPE1 or p53-proficient RPE1 (control) (Figure 2.2A). We quantified the relative abundance of the unlabeled cells after to exposure to IR (0 – 6Gy), normalized to untreated samples at each timepoint. RPE1 labeled and unlabeled cells maintained stable representation across time and treatment conditions (Figure 2.2B). Additionally, p53-deficient cells did not demonstrate a proliferation advantage in the absence of IR. However, treatment with IR at any dose level led to substantial positive selection for p53-deficient cells (Figure 2.2C,D). We also observed that p53 deficiency induced resistance to the radiomimetic clastogen Neocarzinostatin (NCS) by colony forming assay (Figure 2.2E-I). Thus, p53 deficiency in this isogenic model is sufficient to induce radioresistance.

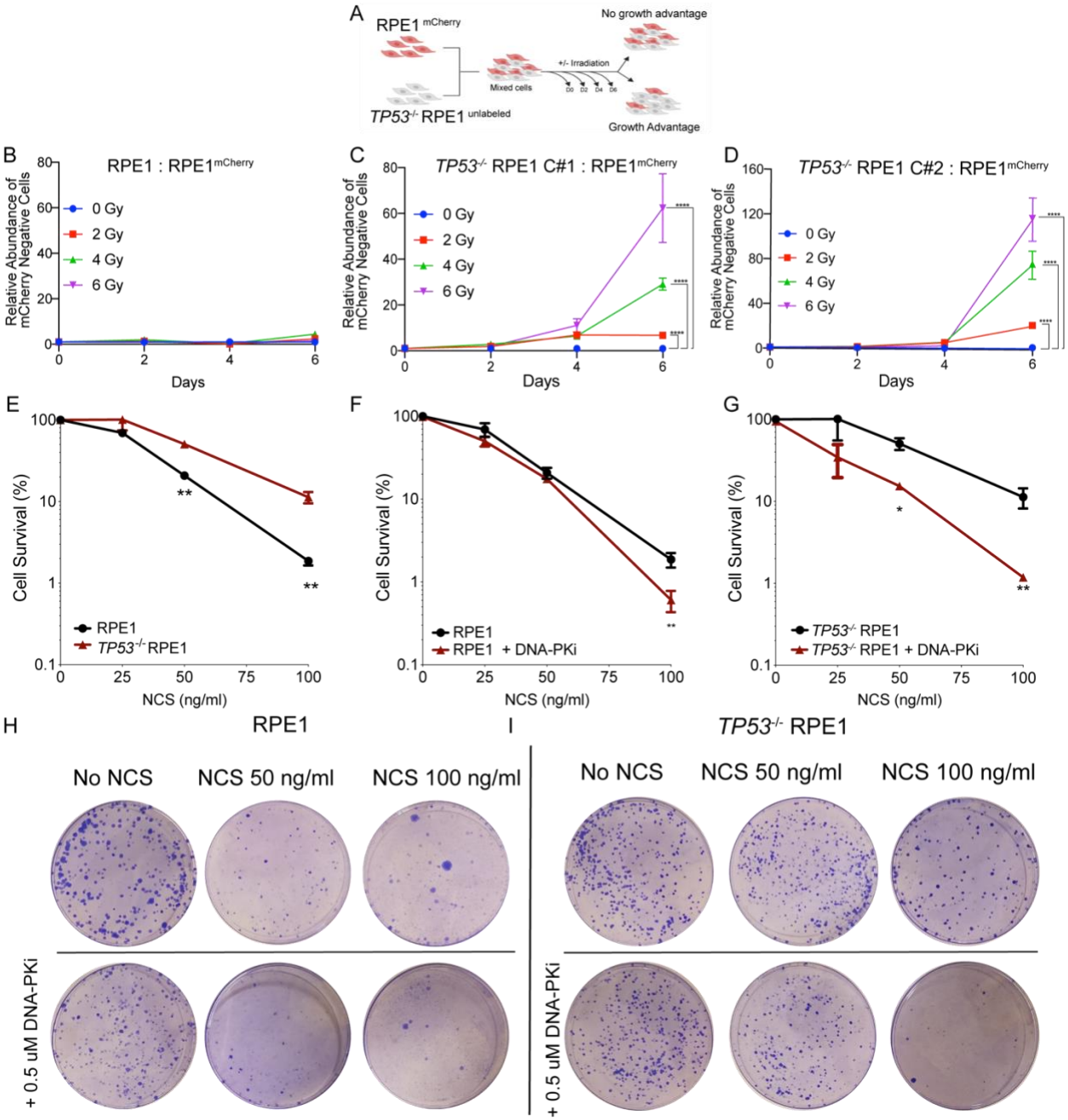

Figure 2.2 : TP53 Deficiency Confers Radioresistance. A, Live cell imaging procedure. Cells transfected with 10 nM si-control or si-TP53 for 48 h prior to imaging. 18 h into imaging, cells are treated with NCS (100 nM), DNA-PKi (.5 uM) or both and imaged for 72 total hours.B, Relative abundance of unlabeled RPE1unlabelled over RPE1mCherry measured by Intellicyte high-throughput cytometry +/- SEM (n=6) is shown, normalized to the untreated (0Gy) cohort at each time point. C,D Relative abundance of unlabeled TP53 -/- Clone#1/ #2 measured by Intellicyte high-throughput cytometry SEM (n=6) is shown, normalized to the untreated (0Gy) cohort at each time point. E, Clonogenic survival assays performed in RPE1 vs TP53-/- RPE1 cells exposed to NCS. F,

Clonogenic survival assays of RPE1 treated NCS +/- 0.5 uM DNA-PKi. Reported values are mean of n = 3 replicates, and survival fraction was calculated by first calculating plating efficiency and normalizing it to the untreated samples. G, TP53-/- RPE1 cells were treated with NCS +/- 0.5 uM DNA-PKi. H,I Representative colony forming plates for e and f at NCS doses of 0, 50 and 100 ng/ mL +/- 0.5 uM DNA-PKi. Cell numbers for each conditions plated are the following: UT (500), NCS 50 ng/ ml (2000), NCS 100 ng/ ml (6000).

Unrepaired DSBs can suppress proliferation through the engagement of DNA damage-induced cell cycle checkpoints. We examined kinetics of DSB repair by performing immunofluorescence for 53BP1 and γH2AX after treatment of p53 WT and *TP53*$^{-/-}$ cells with 5Gy IR (Figure 2.3). We observed a reduction in the number of 53BP1 damage foci in *TP53*$^{-/-}$ cells as early as 30 minutes after treatment, that became even more pronounced by 4 hours post-treatment (Figure 2.3A,B). Similar patterns of reduced foci formation were also apparent with γH2AX staining at early timepoints (Figure 2.3C,D). Quantification of IR-induced DSBs by neutral COMET assay revealed an equivalent DSB burden induced immediately after 5Gy IR, irrespective of p53 status (Figure 2.4A,B). However, by 4 hours post-treatment, tail DNA percent was significantly reduced in the *TP53*$^{-/-}$ cells while remaining elevated in p53-proficient RPE1 (Figure 2.4A,B). Thus, p53 deficiency is sufficient to induce radioresistance and accelerated DSB repair in an isogenic model.

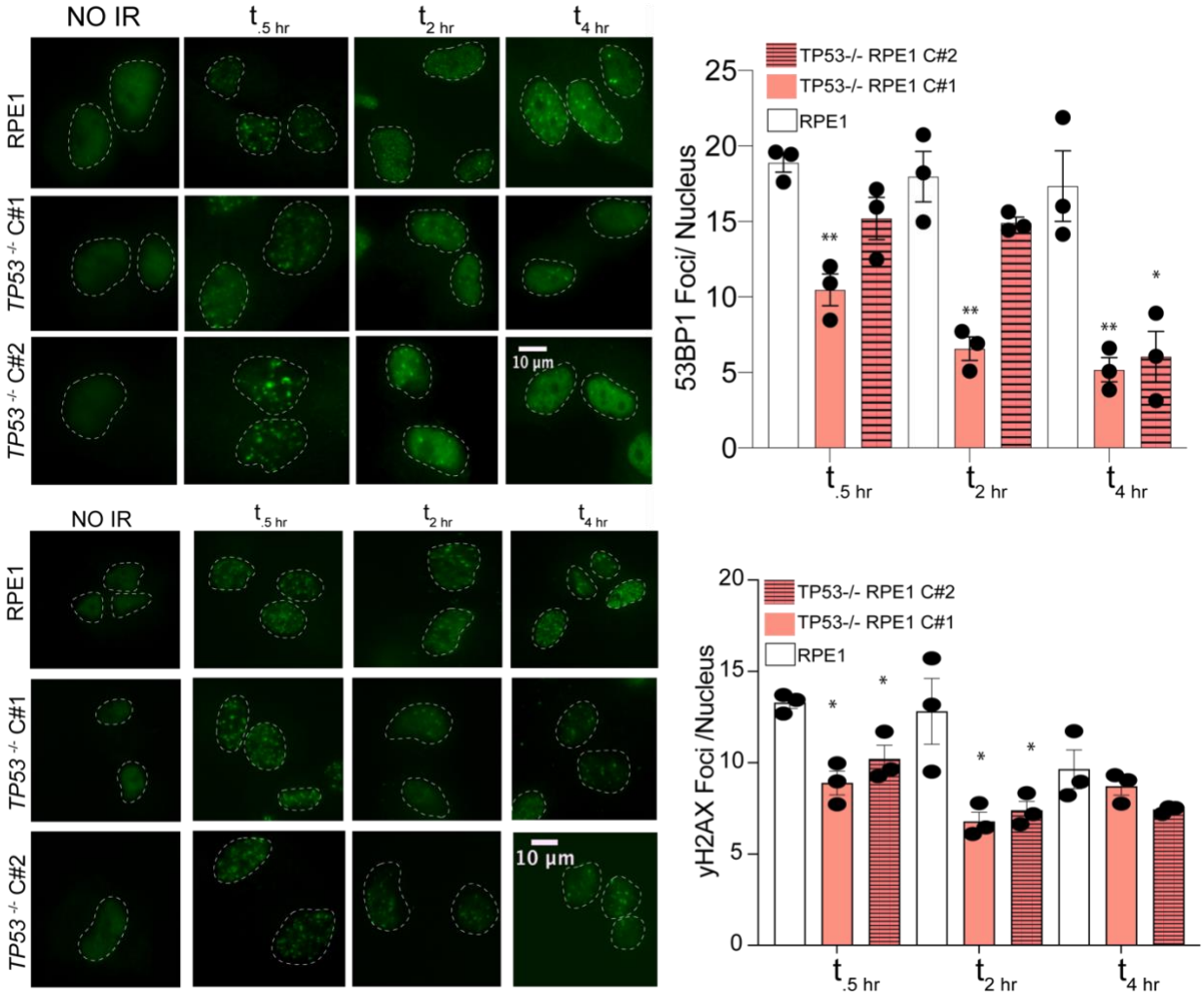

Figure 2.3 : Accelerated Repair of DNA Damage Foci in TP53 Deficient Cells. A, Representative immunofluorescence images of 53BP1 foci in cells with indicated genotypes untreated (no IR) or treated with IR (5Gy) and collected at .5, 2, and 4 h after irradiation. B, Quantification of 53BP1 foci. Data shown are mean (n=50 cells per treatment condition) SEM (n=3), and are consistent across two independent biological replicates. *$p < 0.05$; **$p < 0.01$; by two-tailed Student's t-test. C, Representative immunofluorescence images of yH2AX foci in cells with indicated genotypes untreated (no IR) or treated with IR (5Gy) and collected at .5, 2, and 4 h after irradiation. D, Quantification of yH2AX foci. Data shown are mean (n= 50 cells per treatment condition) +/- SEM (n=3), and are consistent across two independent biological replicates. *$p < 0.05$ by two-tailed Student's t-test.

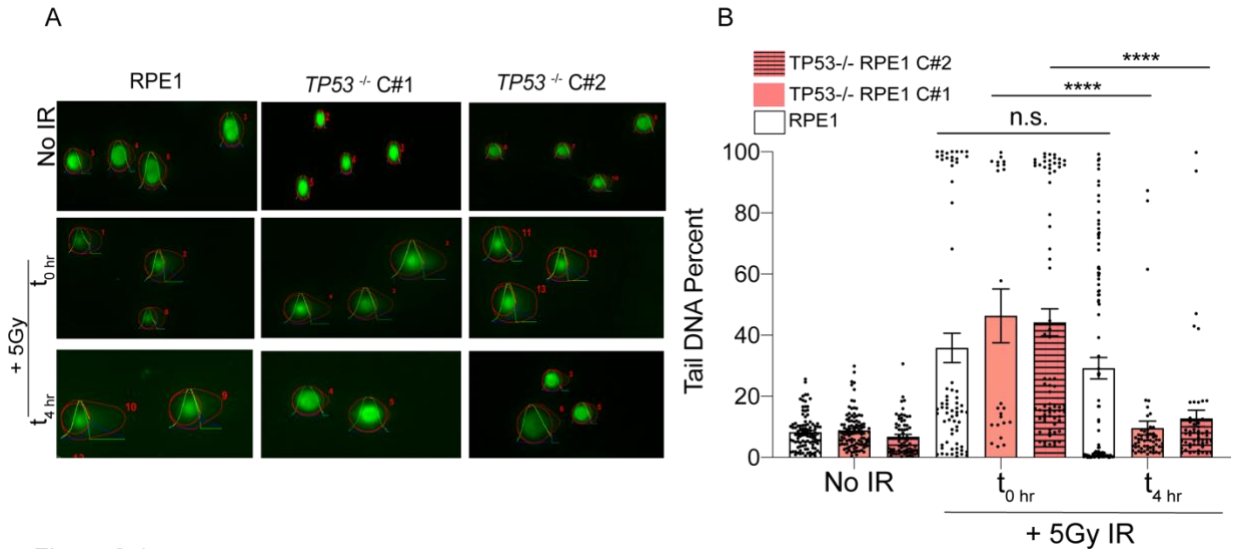

Figure 2.4 : Total DNA Damage Burden Assessment in TP53 Deficient cells. A, Representative Neutral COMET fluorescence staining for DNA tails in cells with indicated genotypes treated with or without 5Gy IR. For irradiated cells, 2 timepoints are shown: immediately after and 4 hours post IR. COMET tails and heads are denoted by OpenComet software analysis. B, Quantification of DNA DSBs via Neutral COMET assay reported as tail DNA percent at 0 and 4 hours post IR in RPE1 and two TP53-/- RPE1 cell lines. Data shown are mean (n= 50-150 cells per treatment condition) +/- SEM, and are consistent across three independent biological replicates. *$p < 0.05$; **$p < 0.01$; ****$p < 0.0001$ by two-tailed Student's t-test.

2.3.2. Inhibition of DNA-PK Restores DNA Damage Foci Burden

To directly assess the relationship between DSB repair kinetics, cell cycle status, and cell fate at the single cell level, we established a live cell imaging platform (Figure 2.5A). RPE1 cells were dually labeled with PCNA-mCherry (to monitor cell cycle state transitions) and 53BP1-mVenus (to monitor DSB foci kinetics) (Figure 2.5B)[49,60]. To concurrently measure DSBs in real-time, 53BP1 is the preferred reporter for live-cell imaging. γH2AX requires phosphorylation to become a marker for DNA DSBs and is therefore not compatible with live-cell reporter systems to assess DNA damage. These dual labeled cells were treated with scrambled siRNA (si-Control) or siRNA targeting *TP53* (si-*TP53*), the latter of which resulted in >90% knockdown of *TP53* transcript and elimination of p53-dependent *CDKN1A* transcription in response to IR (Figure 2.5C). 48

hours after siRNA treatment, RPE1 cells were imaged for a total of 72 hours every 10 minutes, and 18 hours into imaging, the DSB inducing agent was added (Figure 2.5A). To minimize time from radiation exposure to image capture and to induce equivalent DSBs in each population of cells, we utilized 100 ng/ml of Neocarzinostatin (NCS), a well-known radio-mimetic. NCS has been previously utilized in studies evaluating DNA DSB repair in conjunction with live-cell imaging and has been shown to induce peak DSBs within 10 minutes of drug addition[142,143]. This experimental design allowed us to determine the cell cycle status of each cell within the asynchronous cell population at the time of NCS exposure. After NCS treatment, single-cell analyses for DSB repair foci kinetics and cell cycle outcomes were performed. As anticipated from the mixed-competition assays, analysis of global proliferation by live-cell imaging revealed significantly greater proliferation of p53-deficient RPE1 cells relative to controls after NCS treatment (Figure 2.5D,E).

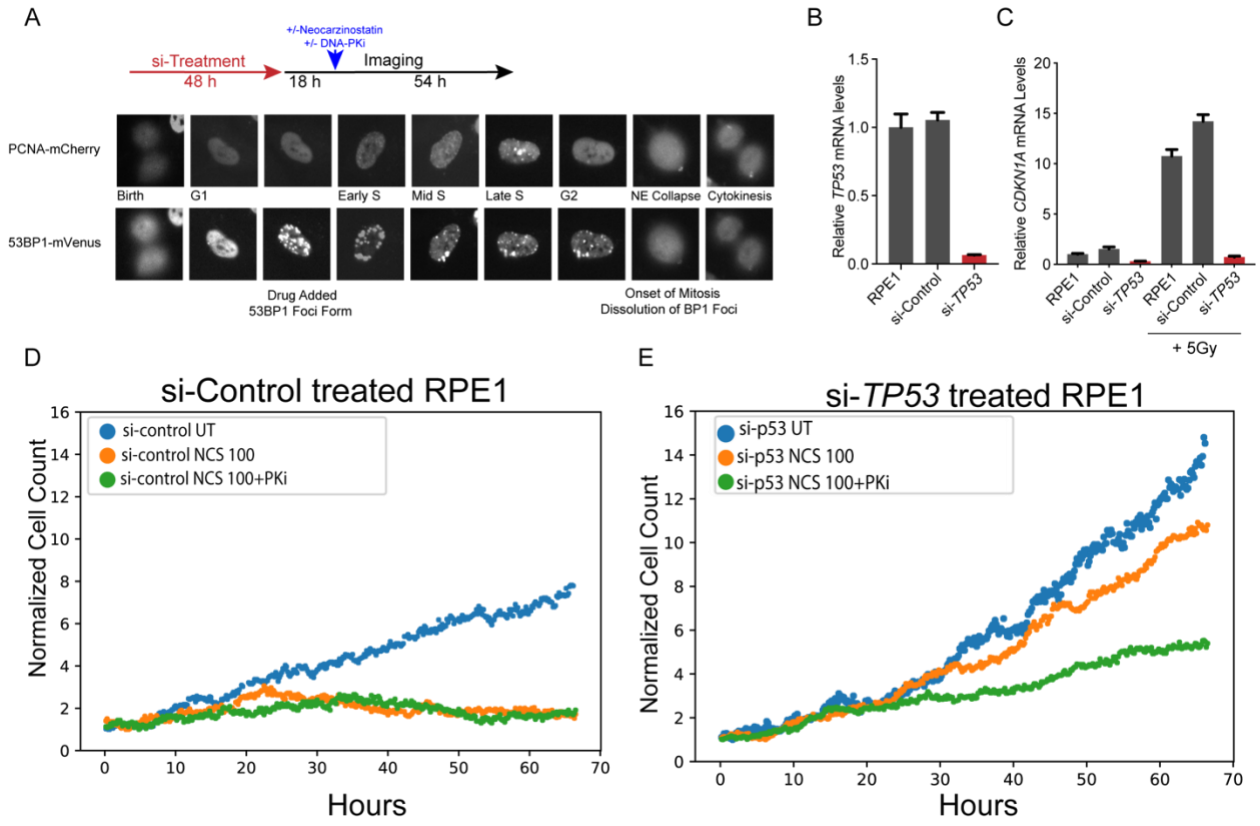

Figure 2.5 : Overview of Live-Cell Imaging Platform A, Live cell imaging procedure. Cells transfected with 10 nM si-control or si-TP53 for 48 h prior to imaging. 18 h into imaging, cells are treated with NCS (100 nM), DNA-PKi (.5 uM) or both and imaged for 72 total hours. B, RPE1 cell expressing the PCNA-mCherry and 53BP1-mVenus reporters. Cell cycle phases delineated by PCNA foci and DNA DSBs are marked by 53BP1 foci. C, RT-qPCR for TP53 mRNA levels (left) and CDKN1A mRNA levels (right) in si-control treated vs. si-TP53 treated cells. To induce CDKN1A expression, cells irradiated at 5Gy and mRNA harvested 3 hrs post IR. D, Quantification of cell proliferation from live-cell imaging experiments for si-Control treated RPE1. Cell counts were normalized to cell numbers at start of imaging. Here we show one representative imaging beacon for each treatment condition (untreated, NCS 100 ng/ ml at 18 hours, and NCS 100 ng/ml + 0.5 uM DNA-PKi at 18 hours). E, Cell proliferation counts for si-TP53 treated RPE1 over live-cell imaging.

To analyze DSB repair kinetics in cells exposed to NCS, we tracked and quantified 53BP1 foci in single cells and plotted heatmaps of damage foci burden over time from cell birth to mitosis (Figure 2.6A). Our results indicate that cells with functional p53 sustain high levels of damage foci in a prolonged manner after NCS exposure. In contrast, p53-deficient cells on average developed a lower peak burden of 53BP1 foci after NCS treatment, with accelerated resolution of damage foci to baseline levels (Figure 2.6B). Moreover, p53-deficient cells also exhibited greater variance in 53BP1 foci burden and kinetics. Given the rapidity with which 53BP1 foci were being resolved, we hypothesized that hyperactive NHEJ may be contributing. We thus performed the same experiment in the presence of an inhibitor of DNA-dependent Protein Kinase (DNA-PKi, NU7441 0.5μM), which targets the central kinase in the NHEJ pathway[144–146]. Strikingly, DNA-PKi qualitatively abolished the difference in 53BP1 kinetics after NCS treatment between p53-deficient and proficient cells (Figure 2.6B). To quantitatively assess the magnitude in damage burden, we calculated peak maximum 53BP1 foci values for each cell represented in the heatmap (Figure 2.6C). Consistent with the heatmap representation, the median peak foci count after NCS treatment was 40% lower in si-*TP53* treated cells relative to controls (Figure 2.6C, $p<0.0001$). Notably, DNA-PKi treatment resulted in a >2-fold increase in peak 53BP1 foci levels in the p53-deficient cells, whereas there was no comparable effect in control cells (Figure 2.6C). These results indicate that DNA-PK activity is required for accelerated resolution of clastogen-induced DNA damage foci in p53-deficient cells.

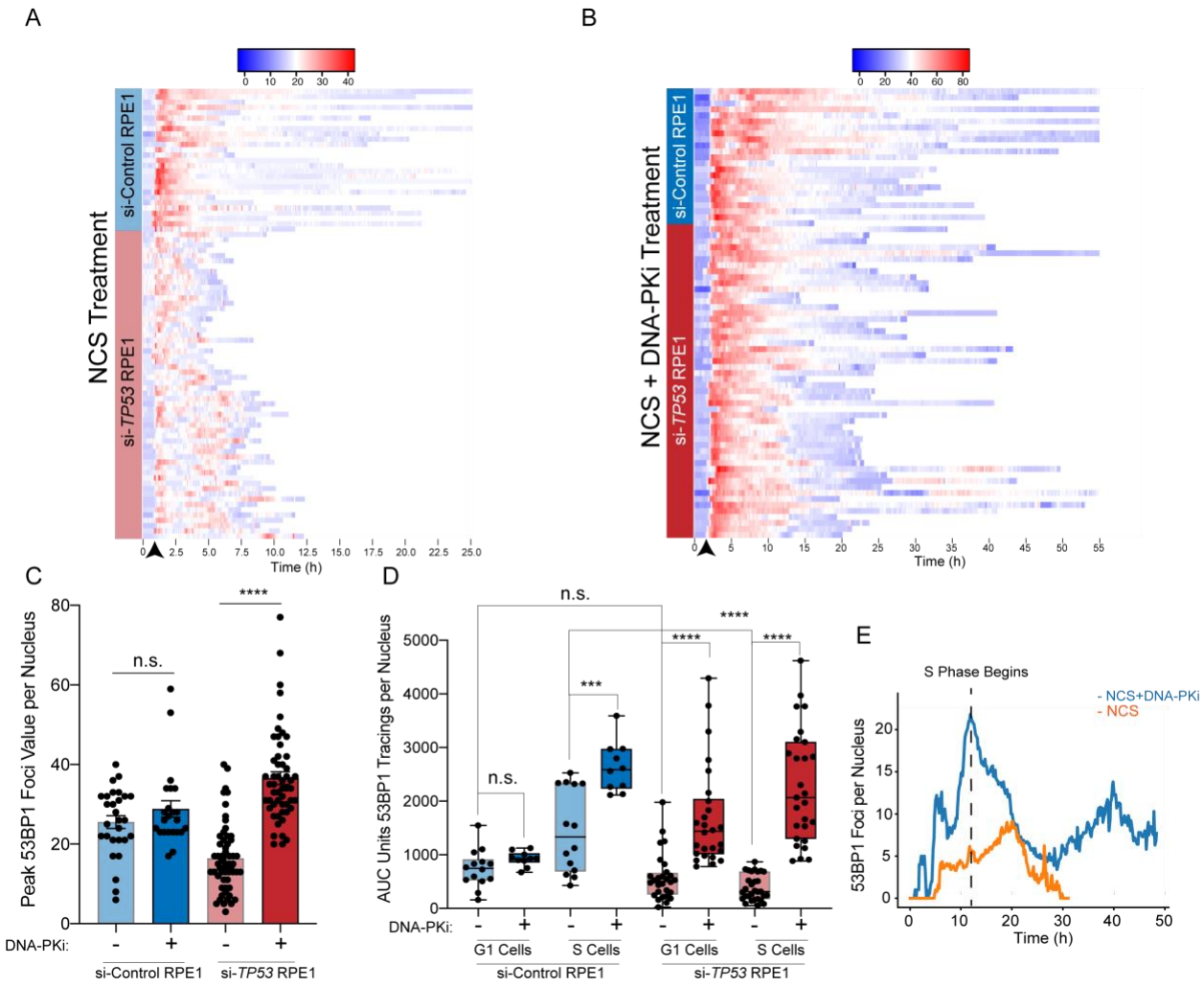

Figure 2.6 : Inhibition of DNA-PK Restores DNA Damage Foci Burden in TP53 Deficient Cells A, Heatmap of 53BP1 foci tracings for single cells tracked from birth to mitosis or end of imaging. For si-control (n = 30 cells) and si-TP53 treated RPE1 (n = 60 cells) treated with NCS 100 ng/ml. For visualization, cells are aligned to 10 frames prior to drug addition (black arrow). B, Heatmap of 53BP1 foci tracings for si-control (n = 25 cells) and si-TP53 treated RPE1 cells (n = 55 cells) treated with 100 ng/ml NCS + 0.5 uM DNA-PKi. C, Peak 53BP1 foci counts for cells treated with 100 ng/ml NCS or NCS+0.5 uM DNA-PKi. Significance determined using two-tailed t-test. D, Area under the curve (AUC) analysis of 53BP1 burden showing integral DNA damage for cells treated with NCS vs. NCS and DNA-PKi. Cells are segregated into two groups: cells exposed to drug in G1 vs. S phase (n = 25-30 G1or S cells for si-TP53 cohort, n = 10-15 G1 or S cells for si-control cohort). Significance determined by two-tailed t-test. ****p < 0.0001, ***p < 0.001, n.s. = non-significant. E, 53BP1 foci burden in G1 phase p53-deficient RPE1 upon exposure to NCS and DNA-PKi. Dashed line = S phase onset, blue line = mean 53BP1 foci burden for all cells in G1 with NCS and DNA-PKi addition, orange line = mean foci value for cells in G1 with NCS treatment alone, (n = 30 cells for each condition).

Following this analysis, we studied the effects of DNA-PKi in different phases of the cell cycle during drug exposure. We used PCNA live-cell imaging to resolve cell cycle phase transitions in cells tracked for 53BP1 foci kinetics. We performed area under the curve (AUC) analyses in single cells to estimate total DNA damage burden during G1 and S phase after NCS exposure (Figure 2.6D). This analysis revealed that the diminished 53BP1 foci burden observed in p53-deficient cells was most pronounced during S phase relative to control cells (Figure 2.6D). DNA-PKi treatment significantly increased S phase 53BP1 burden in both si-Control and si-*TP53* treated RPE1 cells (Figure 2.6D). While si-*TP53* treated cells in G1 were also affected to a lesser degree, we were curious to examine if the effect was in part due to loss of the p53-dependent G1/S checkpoint resulting in propagation of unrepaired DNA damage into S phase. Indeed, we found that DNA-PKi induced a drastic increase in 53BP1 foci as p53-deficient cells transitioned from G1 to S phase, which subsequently diminished over time (Figure 2.6E, $p<0.00001$ at t = start of S phase). Thus, DNA-PK is required for hyperactive resolution of clastogen-induced DSB foci in p53-deficient cells, and most prominently during S phase.

2.3.3. Checkpoint Responses Halt P53-Proficient Cells

To investigate the association between DNA damage and activation of cell cycle checkpoints, we quantified cell cycle phase durations for all treatment conditions (Figure 2.7A,B). Time-lapse microscopy of live cells expressing the PCNA biosensor enables us to deconvolute biological effects in different cell cycle stages without the use of any synchronization agents. Specifically, we separately evaluated the effect of NCS treatment on cells that were either in G1 or S phase at the time of drug addition. p53-proficient G1 cells exposed to NCS induced a significant prolongation of G1, indicative of G1/S

checkpoint activation, with a substantial proportion of cells remaining arrested for the duration of imaging (Figure 2.7C). Similarly, cells exposed to NCS in S phase exhibited a G2-M checkpoint (Figure 2.7D). p53-deficient cells exhibited no prolongation of G1 duration after NCS, consistent with the notion that G1/S checkpoint activation is p53-dependent (Figure 2.7E)[53,147]. DNA-PK inhibition did not alter G1 duration in either p53-proficient or p53-deficient cells (Figure 2.7C,E). In contrast, DNA-PKi increased the duration of G2-M checkpoints irrespective of p53 status (Figure 2.7D,F). These observations suggest that increased levels of S phase DNA damage induced by DNA-PKi and NCS treatment (see Figure 2.6D,E) result in activation of a G2/M checkpoint that is, at least partially, p53-independent. However, the duration of G2/M checkpoint activation differed by p53 status. While p53-proficient cells frequently remained arrested for the entire duration of imaging (open circles, Figure 2.7C,D), p53-deficient cells experienced a more transient prolongation of G2 duration followed by progression into mitosis (Figure 2.7E,F).

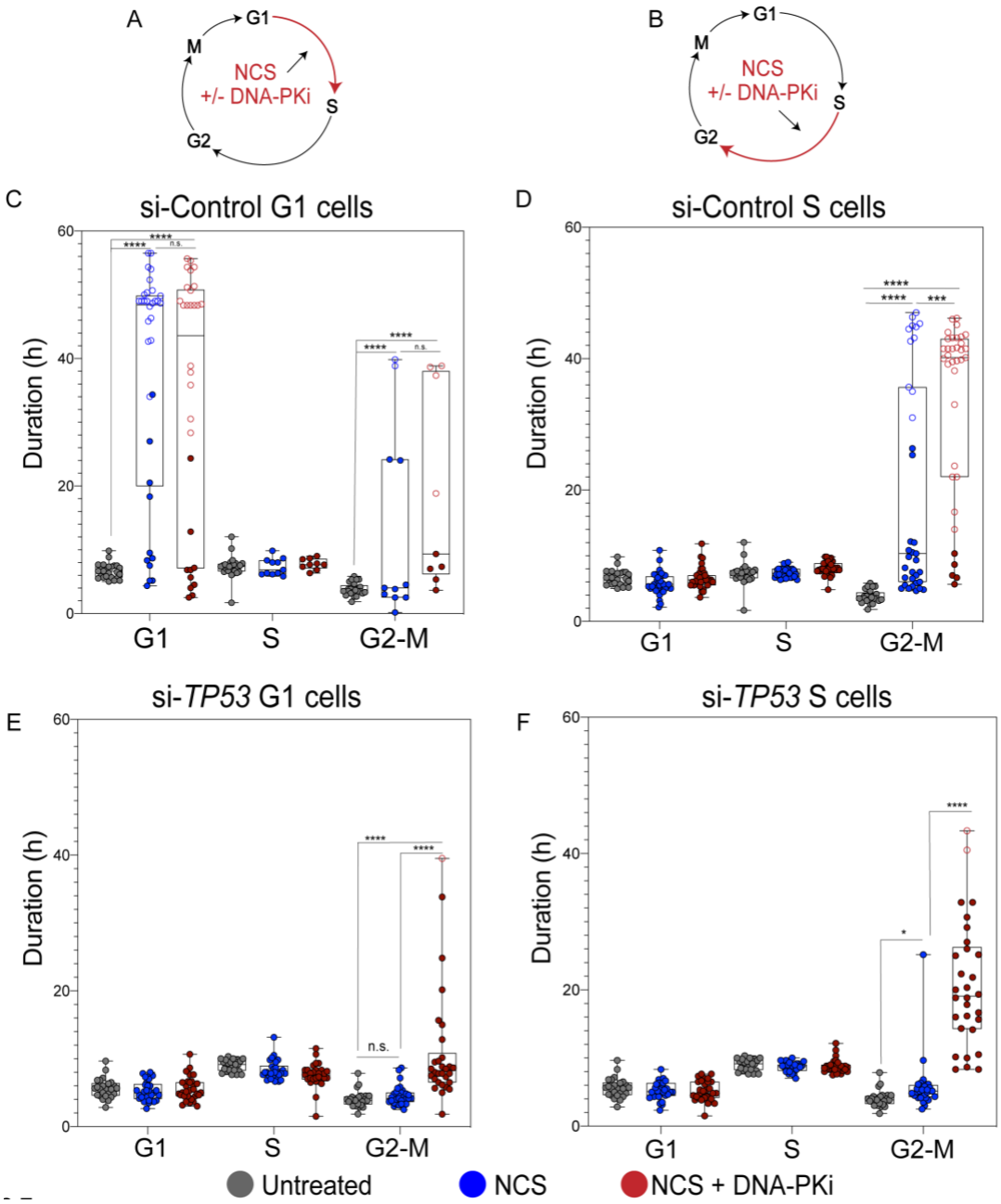

Figure 2.7 : Cell Cycle Checkpoint Responses are Altered in TP53 Deficient Cells with DNA-PKi Treatment. A, Schematic depicting NCS treatment (50 ng/ml + 100 ng/ml for si-control and 100 ng/ml for si-TP53 RPE1) and/or NCS + 0.5 uM DNA-PKi treatment, and phase of the cell cycle cells are exposed to drug (G1). B, Schematic of drug treatment for S phase cells. C, Distribution of cell cycle phase lengths, each colored dot is an individual cell with untreated cells (no NCS) shown in black, NCS treated cells shown in blue, and NCS+ 0.5uM DNA-PKi treated cells shown in red for si-control RPE1 in G1 phase. n = 20 untreated and n = 30 treated cells (for each treatment cohort). Statistical significance was determined by comparing untreated and treated groups at each phase. ****p < 0.0001, n.s. = non-significant. Open circles indicate arrested cells that did not enter

the subsequent phase of cell cycle for remainder of imaging. D, Distribution of cell cycle phase lengths for si-control treated RPE1 in S phase, ***p < 0.001, ****p < 0.0001, n.s. = non-significant as evaluated by two-tailed t-test. E, Distribution of cell cycle phase lengths for si-TP53 treated RPE1 in G1 phase, ****p < 0.0001, n.s. = non-significant as evaluated by two-tailed t-test. F, Distribution of cell cycle phase lengths for si-TP53 treated RPE1 in S phase, ****p < 0.0001, n.s. = non-significant as evaluated by two-tailed t-test.

2.3.4. Inhibition Of DNA-PK Induces Catastrophic Mitoses in P53-Deficient Cells

We next used a heatmap representation to track the fate of individual cells from birth until mitosis (Figure 2.8). Red bars indicate a mitotic catastrophe or apoptosis event (Figure 2.8A,B). The median cell cycle time for both untreated p53-proficient and p53-deficient cells was approximately 22-24 hours. NCS treatment is indicated as a dashed line at the 18 hour timepoint. Individual cells are ordered according to cell cycle phase at the time of NCS treatment (G1 versus S) and eventual cell fate (viable, G1 arrest, G2 arrest, or mitotic catastrophe/apoptosis). The majority (70%) of p53-proficient (si-Control) G1 cells exposed to NCS activated a G1 checkpoint that was maintained for the remainder of imaging (Figure 2.8A). 26% of these cells underwent G2 arrest or mitotic catastrophe, whereas only 3% retained their proliferative capacity (Figure 2.8A). Control cells exposed to NCS in S phase exhibited more diverse cell fates: 40% G2 arrest, 17% mitotic catastrophe, and 43% that retained proliferative capacity. These observations, made using single-cell tracking of asynchronous cell populations, are consistent with observations of intrinsic radioresistance of S phase cells using cell synchronization methods[90]. In contrast, the majority of p53-deficient (i.e., si-*TP53* treated) cells in G1 or S at the time of NCS treatment remained viable without perceptible engagement of any cell cycle checkpoints (Figure 2.8B, 80% and 87%, respectively). Consistent with prior 53BP1 analyses, S phase cells are most sensitized to DNA-PKi as the addition of the

inhibitor increased G2 arrest frequency in control cells (40% to 91%), and increased mitotic catastrophe in p53-deficient cells (13% to 47%, Figure 2.8B, Figure 2.9). In total, the percentage of viable p53-deficient cells after NCS decreased from 87% to 47% when treated in S phase with DNA-PK inhibition ($p<0.0001$, Fisher's exact test, Figure 2.8B).

Despite the significant increase in mitotic catastrophe induced by combined treatment with DNA-PKi and NCS, 47% of p53-deficient cells exhibit intrinsic resistance to therapy with retained proliferative viability (Figure 2.8B). We hypothesized that levels of unrepaired DNA damage may be determinants of viable (*i.e.*, resistant) versus non-viable (*i.e.*, sensitive) cell fates. To evaluate this hypothesis, we quantified integral DNA damage burden in p53-deficient RPE1 with viable versus non-viable mitotic outcomes (Figure 2.9C,D). The mean integral DNA damage burden was approximately 2-fold higher in non-viable cells, relative to cells that viably completed mitosis (Figure 2.9D, $p<0.0001$). Further analysis revealed that integral DNA damage burden in S phase was most highly associated with cell viability after drug treatment (Figures 2.9C). In addition, we traced the average 53BP1 foci burden over time for these two cohorts (Figure 2.9E). Our results indicate that cells with non-viable mitotic outcomes have an increased peak value of DNA damage after treatment with DNA-PKi and NCS, which remains elevated over time ($p<0.0001$ at $t=20$ hrs, Figure 2.9E). Conversely, these findings indicate that p53-deficient cells that exhibit intrinsic therapeutic resistance may be utilizing compensatory DSB repair pathways to counteract the effects of NCS and DNA-PKi prior to mitotic entry.

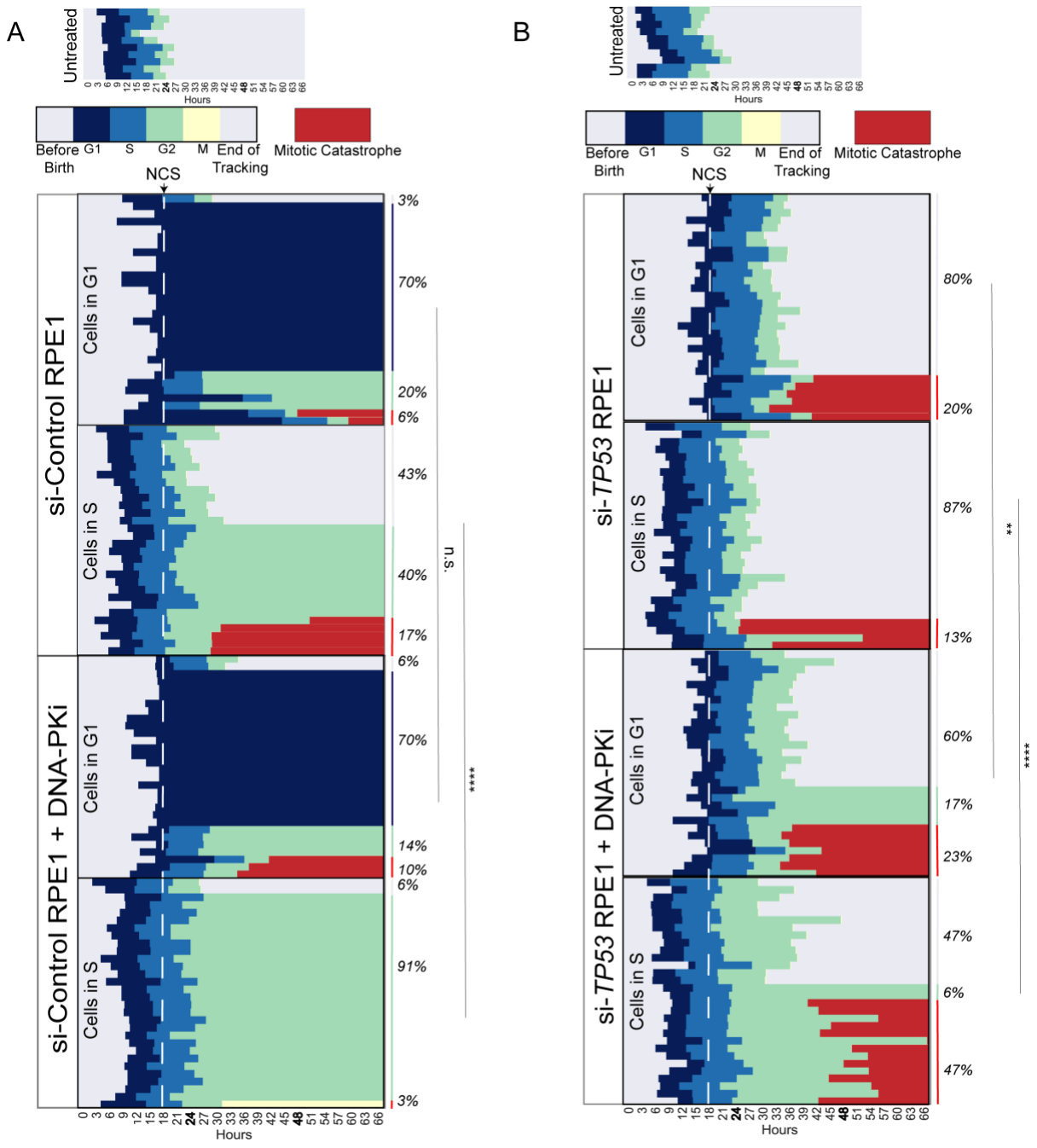

Figure 2.8 : Inhibition of DNA-PK in TP53 Deficient Cells Induces Mitotic Catastrophe. , A, Cell cycle outcome analyses for si-control treated RPE1, dashed white line indicates drug addition, each row is an individual cell (n = 60 cells for NCS and n=60 cells for NCS+DNA-PKi treatment). Colored bars indicate different phases of the cell cycle, legend shown with no treatment control for comparison. Cells with red bars at the end of mitosis indicate terminal cell cycle event (mitotic catastrophe or apoptosis). Event frequency is reported as a percentage on the right. Cells exposed in G1 vs. S cells are

treated as separate cohorts. Fisher's exact test was performed between -/+ DNA-PKi cohorts using 2 outcome groups (viable, vs. non-viable (arrested cells + terminal outcomes). ****$p < 0.0001$, n.s. =non-significant B, Cell cycle outcome analyses for si-TP53 treated RPE1, dashed line indicates drug addition, each row is an individual cell (n = 60 cells for NCS and n=60 cells for NCS+DNA-PKi treatment).

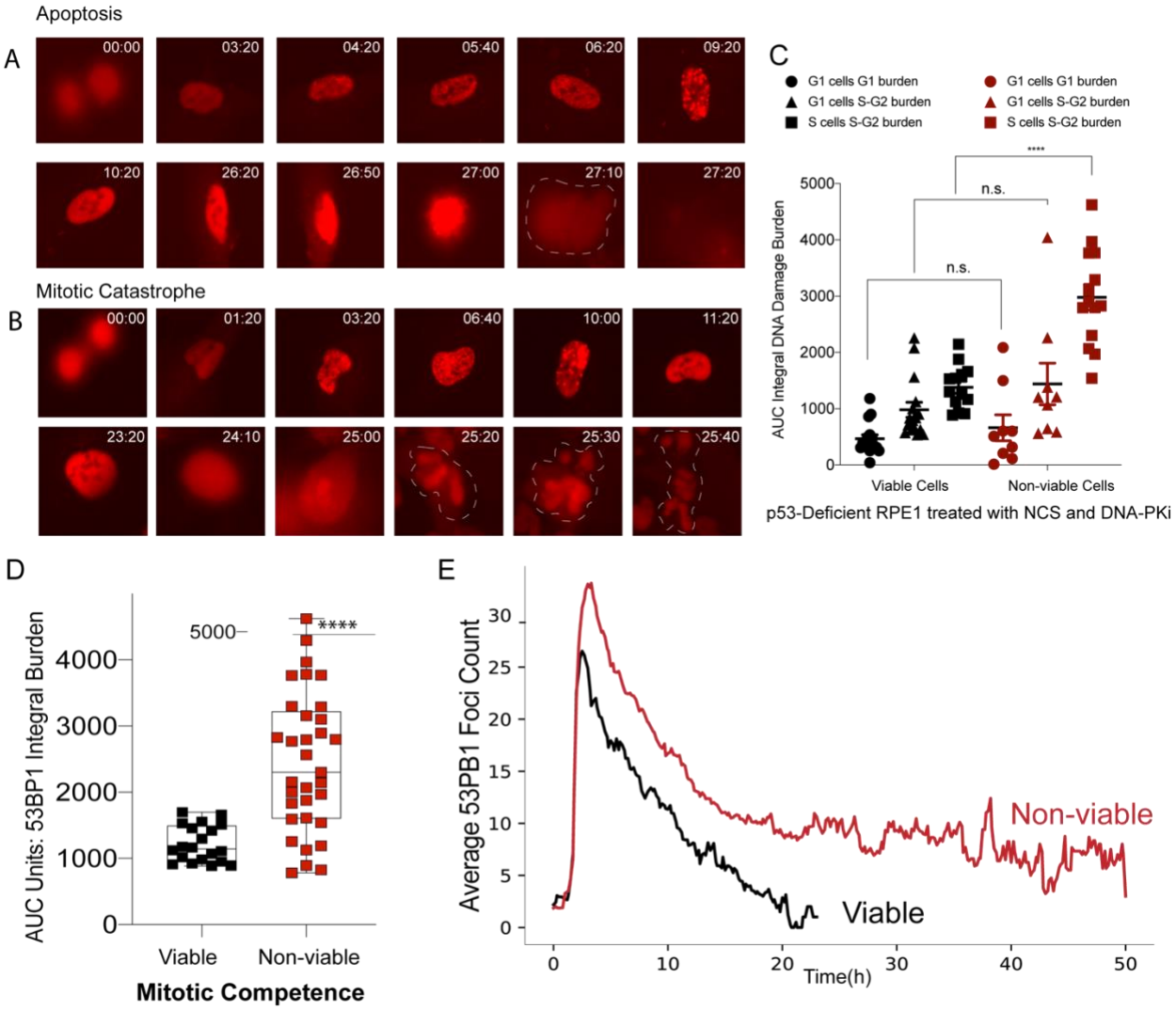

Figure 2.9 : Peak DNA Damage Burden Directly Correlates to Induction of Mitotic Catastrophe. A, Time stamped image sequence of apoptotic cell (PCNA channel shown). Cells that experienced nuclear degradation during cell cycle prior to mitosis were categorized as "apoptotic cells." In this sequence a cell in G2 experiences cell death at 27 hours post birth, with indication of mitotic attempt, with nuclear envelope collapse or presence of any daughter cells. B, Time stamped image sequence of cell that experienced mitotic catastrophe (PCNA channel shown). Cell undergoes nuclear envelope collapse (24:10), and attempts mitosis, in subsequent images fragmentation of nucleus is clearly visible with no viable daughter cells present. Cell non-viability during mitosis was defined as mitotic catastrophe. C, Integral DNA damage burden for p53-deficient cells treated with NCS (100 ng/ml) and DNA-PKi (.5 uM) are calculated and

segregated by viable (black) vs. non-viable outcomes (red). Legend indicates which phase of cell cycle the cells are in during drug exposure, followed by the phase for which the burden is calculated. Ex: G1 cells G1 burden = cells in G1 during drug exposure and total damage burden in G1. Area under the curve (AUC) analysis was performed by plotting 53BP1 foci counts over time for each cell and integrating burden over time. Statistical significance was determined using two-tailed Student's t-test. D, AUC analysis of 53BP1 damage burden in viable vs. non-viable p53-deficient cells that were treated with NCS and DNA-PKi. Statistical significance was calculated using a Mann-Whitney test comparing ranks. ****$p < 0.0001$ E, Dynamics of 53BP1 foci burden p53-deficient RPE1 segregated by mitotic viability. The red line corresponds to mean 53BP1 foci burden for all p53-deficient cells treated with NCS and DNA-PKi that undergo catastrophic mitoses, black line indicates mean foci value for p53-deficient cells with NCS and DNA-PKi treatment that are viable post mitosis, (n = 20 viable cells and n = 33 non-viable cells).

2.3.5. P53-Deficient Cells Utilize Alternative End-Joining Pathways

Prior studies have demonstrated that cells with NHEJ deficiency exhibit a compensatory increase in alternative end-joining repair mediated by DNA polymerase theta (Pol θ, gene *POLQ*)[40,41,148]. Polymerase theta dependent end joining (TMEJ) of DNA DSBs is characterized by deletions and templated insertions that are flanked by short tracts of sequence identity, or microhomology (MH)[148]. We found that *POLQ* expression was 10- to 20-fold higher in two independent *TP53*$^{-/-}$ RPE1 clones, relative to parental *TP53* wild-type cells (Figure 2.10A). *POLQ* is also overexpressed in TCGA breast, lung, bladder, colorectal, gastric, glioblastoma, pancreatic, prostate, melanoma, and uterine cancers with *TP53* mutation, relative to their *TP53* wild-type counterparts (Figure 2.10B).

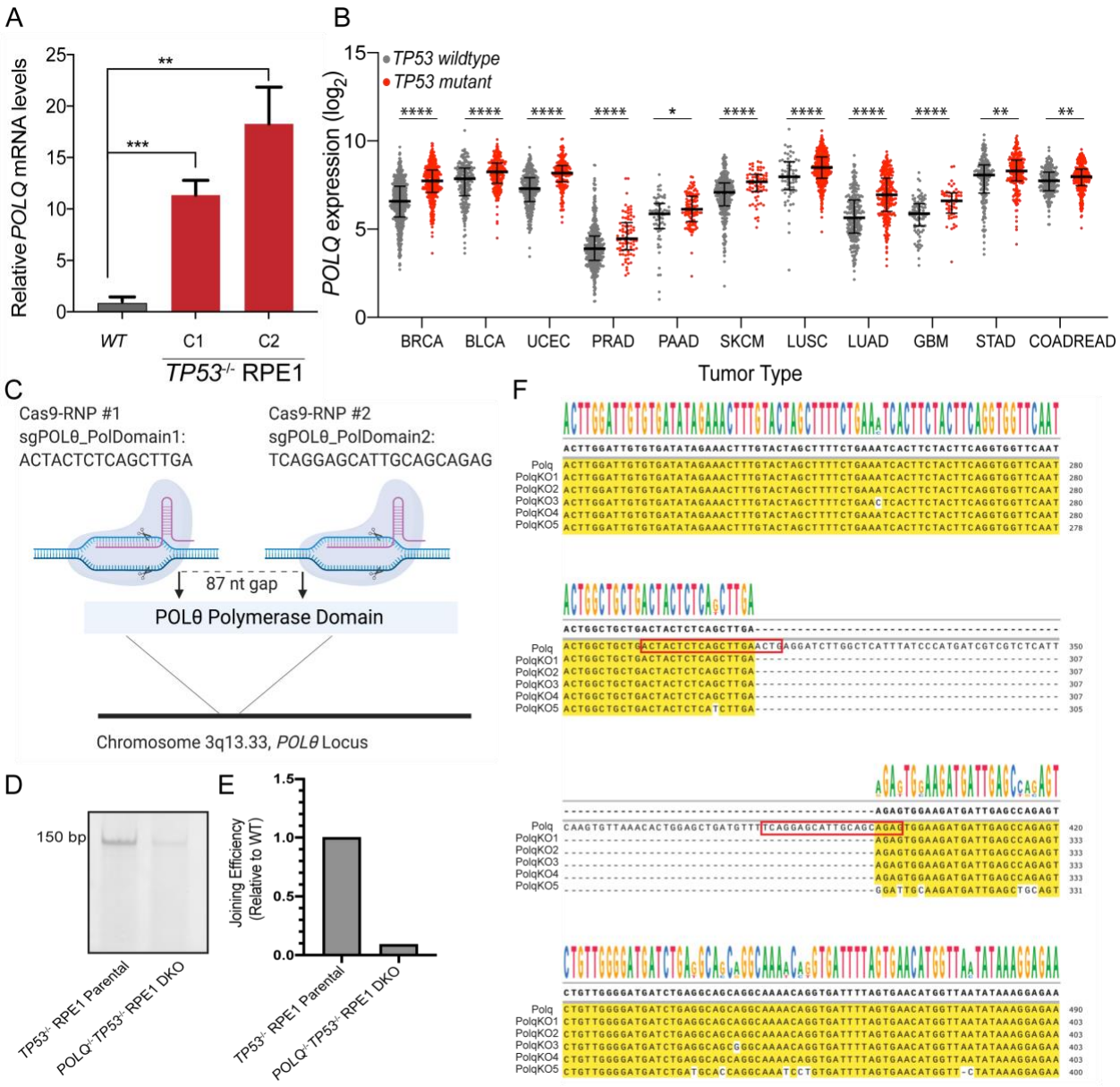

Figure 2.10 : POL Theta Expression is Upregulated in TP53 Deficient Cells and Cancers. A, RT-qPCR for POLQ mRNA levels in 2 TP53-/-RPE1 clones compared to WT RPE1. Significance was determined using two-tailed t-test. ****$p < 0.0001$, **$p < 0.01$. B, POLQ gene expression depicted as log2 values of TP53 wild-type vs. mutant cancers across a subset of TCGA tumor types. Tumor labels follow TCGA labeling format. BRCA: breast cancer, BLCA: B-cell lymphoma, UCEC: uterine cancer, PRAD: Prostate cancer, PAAD: pancreatic cancer, SKCM: melanoma, LUSC: lung squamous cell cancer, LUAD: lung adenocarcinoma, GBM: glioblastoma multiforme, STAD: stomach cancer, and COADREAD: colorectal cancer. ****$p < 0.0001$, ***$p < 0.001$, **$p < 0.01$, *$p<0.05$, as calculated by one-way ANOVA. C, Schematic of CRISPR target locus in human POLQ gene. Two sgRNAs were designed to target sites in the polymerase domain, with an 87 nucleotide (nt) gap. sgRNAs were complexed with Cas9 in RNP system and

electroporated into RPE1 cells with a TP53-/- background to create double knockout cell line. D,E POLQ specific substrates were introduced into the TP53 -/- vs. POLQ-/-TP53-/- DKO cells to assess repair efficiency. Products were amplified and characterized by electrophoresis and end joining efficiency was normalized to RPE1 with POLQ expression. F, Sanger sequencing analysis of CRISPR edited locus in POLQ-/- TP53-/- RPE1 clones. The locus of interest was PCR-amplified and cloned into a TOPO vector for sequencing analyses. Each line of sequence shown was derived from a different TOPO clone and aligned to show differences. The POLQ-/-TP53-/- clone has 87bp deletion resulting in frameshift mutations. Red boxes indicated sgRNAs used for the CRIPSR.

To assess whether hyperactive TMEJ contributes to therapeutic resistance of *TP53*$^{-/-}$ RPE1 cells to NCS and DNA-PKi, we sought to inhibit Pol θ. As pharmacological inhibitors of Pol θ are not yet commercially available, we created a double knockout *POLQ*$^{-/-}$*TP53*$^{-/-}$ RPE1 line (Figure 2.10C). Bi-allelic frameshift mutations in *POLQ* were confirmed by Sanger sequencing and functional deficiency was established using an extrachromosomal TMEJ repair assay (Figure 2.10D-F)[148].

To directly assess whether TMEJ repair is increased after DNA-PKi treatment, we analyzed chromosomal break repair patterns at a site-specific DSB in p53-deficient RPE1 cells. Cells were transfected with Cas9 ribonucleoprotein (RNP) complexes that target the *LBR* locus, with or without DNA-PKi[149]. Genomic DNA was harvested 60 hours later and analyzed for break repair patterns using next generation sequencing (NGS) (Figure 2.11A). Target amplification and TIDE analyses confirmed high rates of target site cleavage in all samples transfected with a full complement of Cas9-RNP[150]. We applied a bioinformatic algorithm (ScarMapper, see methods) to characterize the spectrum of repair products with at least 0.1% prevalence, classified according to the size of left deletion (LD), right deletion (RD), insertion (Ins), and microhomology (MH) (ScarMapper Methods). Indels <5bp were categorized as NHEJ, with the predominant repair product

being a +A 1bp insertion[149]. TMEJ was defined as repair products whose frequency was diminished by at least 2-fold in *POLQ*$^{-/-}$ cells. All other repair products were categorized as "Unclassified." DNA-PK inhibition in *TP53*$^{-/-}$ RPE1 cells results in a substantial reduction in NHEJ repair, with a compensatory increase in TMEJ to nearly 45% of all DSB repair (Figure 2.11B,C). In contrast, DNA-PK inhibition in *POLQ*$^{-/-}$*TP53*$^{-/-}$ RPE1 cells did not result in a substantial increase TMEJ signature repair (Figure 2.11D,E). However, a higher proportion of Unclassified repair products were detected (Figure 2.11D,E). A limitation of NGS analysis of DSB break repair is that non-amplifiable target loci are not measured. Thus, we used digital PCR to quantify the *LBR* locus detection rate, relative to a control locus, upon inhibition of DNA-PK and/or Pol θ (Figure 2.11F). *LBR* locus detection rates were most reduced upon inhibition of DNA-PK and Pol θ, indicating an increase in unrepaired DSBs upon inhibition of both DSB repair pathways (Figure 2.11G). These observations confirm an essential role for TMEJ in compensatory repair of chromosomal DSBs upon pharmacologic inhibition of DNA-PK.

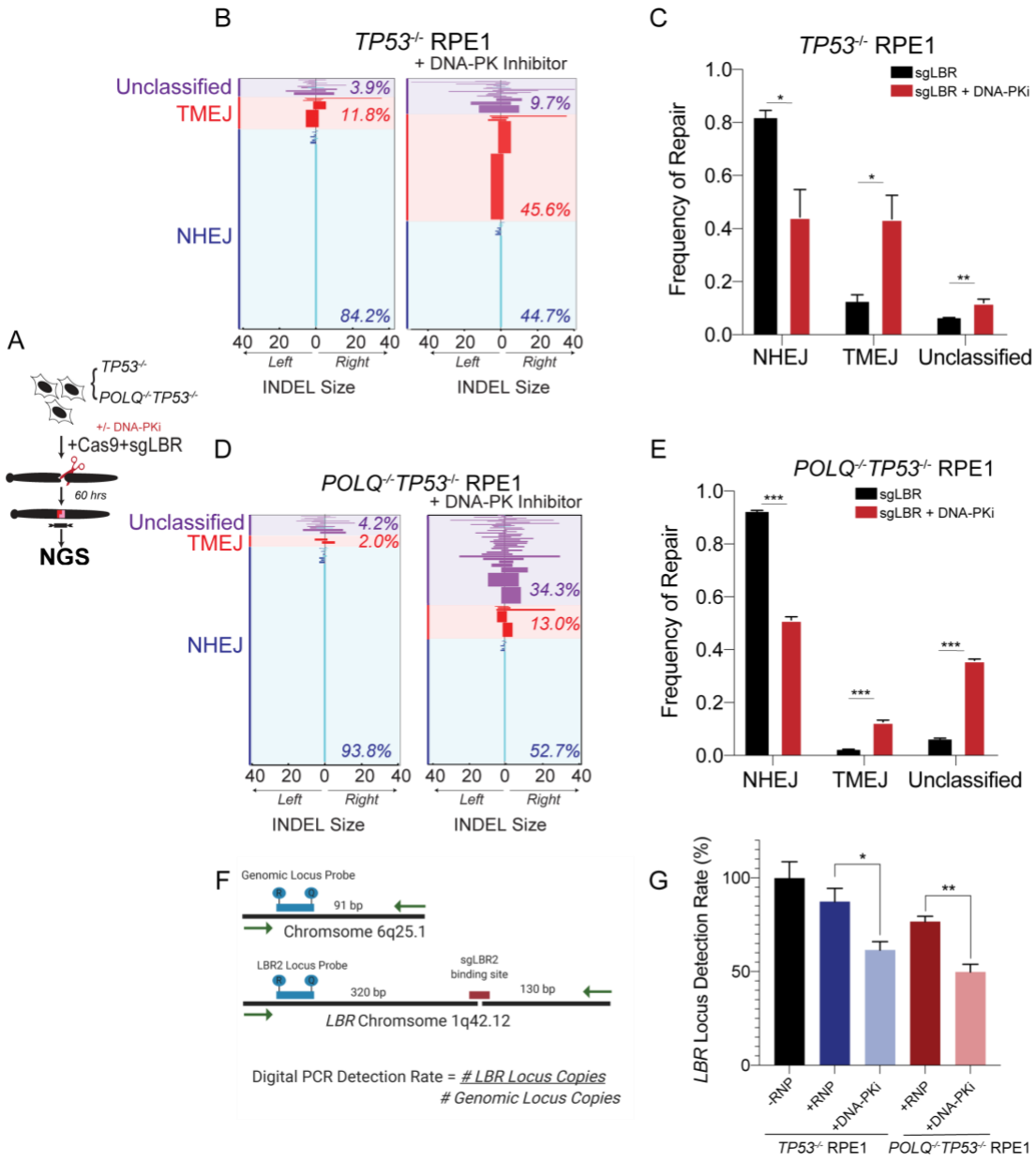

Figure 2.11 : TP53 Deficient Cells Utilize Alternative End Joining in the Absence of Active DNA-PK. A, Schematic depicting chromosomal break repair assay. TP53-/- , and POLQ-/-TP53-/- RPE1 are segregated into 2 cohorts (+/- 3 uM DNA-PKi). Cells are electroporated using Cas9-RNP-sgRNA-LBR and evaluated by next generation sequencing for break repair products at target locus. B, Horizontal bar chart representation of individual break repair products at LBR locus in TP53-/- RPE1 by NGS. Position 0 denotes LBR locus cut site, with left and right positions denoting final INDEL size and orientation. Results are reported as average with SEM of n=3 independent biological replicates. C, Histogram of overall frequency of repair of NHEJ, TMEJ, and Unclassified products in TP53-/- RPE1 with or without DNA-PKi treatment. D, Horizontal bar chart representation of individual break repair products at LBR locus in POLQ-/-TP53-/- RPE1 by NGS. Position 0 denotes LBR locus cut site, with left and right positions

denoting final INDEL size and orientation. Results are reported as average with SEM of n=3 independent biological replicates. E, Histogram of overall frequency of repair of NHEJ, TMEJ, and Unclassified products in TP53-/- RPE1 with or without DNA-PKi treatment. RPE1, TP53-/-, and POLQ-/-TP53-/- RPE1 cutting efficiency, all three cell lines have comparable levels of cutting efficiency with sgLBR. F, Schematic depicting digital PCR method for assessing LBR detection rate. G, Results of digital PCR assay on TP53 -/- vs. POLQ-/-TP53-/- cells with -/+RNP and subsequently -/+ DNA-PKi (3uM). Average of 3 independent biological replicates are shown with SEM. Statistical significance was calculated using Multiple-t tests. *p<0.05, **p<0.01.

To determine the impact of *POLQ* inhibition on cellular viability, we performed clonogenic survival assays in the parental *TP53*$^{-/-}$ and *POLQ*$^{-/-}$*TP53*$^{-/-}$ RPE1 lines treated with NCS with or without DNA-PKi. Genetic deficiency in *POLQ* resulted in significantly reduced viability after NCS treatment, both without or with concomitant inhibition of DNA-PK (Figure 2.12A). Thus, TMEJ represents an independent repair pathway that mediates resistance of p53-deficient cells to DSB-inducing therapy. Notably, *TP53*$^{-/-}$ RPE1 cells with inhibition of both TMEJ and NHEJ repair pathways had comparable clonogenic survival to p53-proficient RPE1 cells. Collectively, these findings indicate that hyperactive end joining repair via NHEJ and TMEJ mediate resistance to DNA damaging therapy induced by p53 deficiency (Figure 2.12B).

2.4. Discussion

These results recognize enhanced DNA DSB end joining repair capacity as a novel component of therapeutic resistance induced by p53 deficiency, and that loss of functional p53 alone is sufficient to increase hyperactive repair. Concomitant analyses of DSB and cell cycle biosensors in live cells reveal mitotic catastrophe as the primary mode of therapy-induced cell death in p53-deficient cells, and DNA damage burden in the preceding S phase as a key determinant of this outcome. Our findings indicate that DSB end joining hyperactivity is critical for suppressing S phase DNA damage burden, and

thereby the likelihood of mitotic catastrophe (Figure 2.12B). These mechanisms are particularly relevant in p53-deficient cells, where the DNA damage-induced G1/S checkpoint is lost, and DSBs incurred in G1 phase are efficiently propagated into S phase (see Figures 2.6-8).

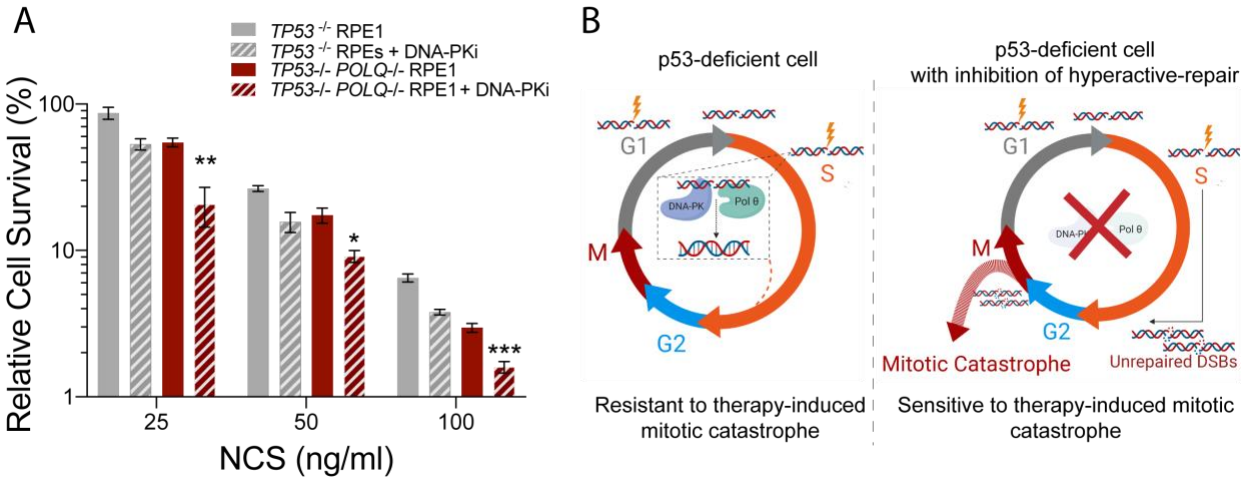

Figure 2.12 : Graphical Summary. A, Colony forming efficiency assay evaluating TP53-/- and POLQ-/-TP53-/- RPE1 after treatment with NCS (at 25 ng/ml, 50 ng/ml, and 100 ng/ml) with or without .5 uM DNA-PKi, data shown are mean +/- SEM (n= 3). Statistical significance assessed with student's two-tail test. ***$p < 0.001$, **$p < 0.01$, * $p<0.05$. in comparison to the survival curve of TP53 -/- + DNA-PKi. All individual data from each cell line are first normalized to no NCS and no DNA-PKi treatment (i.e. the plating efficiency). B, Graphical summary, hyperactive DNA-PK and Pol Theta enable accelerated repair of S phase DNA DSBs in p53-deficient cells (left panel), thereby preventing adverse DSBs from entering mitosis. This mechanism decreases the risk of terminal mitotic catastrophe which occurs when un-repaired DSBs enter mitosis (right panel).

Although NHEJ Is conventionally considered to be most critical for repair in G1, we observed a relatively greater impact of DNA-PK inhibition on the fate of S phase cells after treatment with a radiomimetic. There are several potential explanations for this unanticipated observation. First, recent findings suggest that DNA-PK may be dispensable for synapsis formation during NHEJ[151]. Accordingly, repair of "simple" DSBs in G1 phase may have a reduced reliance on DNA-PK, whereas repair of more "complex"

DSBs in S phase may require DNA-PK, possibly in partnership with the nuclease Artemis[152–154]. Second, it is possible that DNA-PK inhibition may be more impactful in S phase due to trapping of Ku proteins at DSBs, which inhibits the activation of homologous recombination pathways[155]. Third, DNA-PK may be particularly important in early S phase, when sister chromatids are not broadly present. Notably, we observed a prominent peak of unrepaired DSBs just as p53-deficient cells transitioned from G1 to S phase. Our observation that DSB end joining hyperactivity in p53-deficient cells is highly sensitive to DNA-PK inhibition warrants further mechanistic investigation. Recently, CYREN (cell cycle regulator of NHEJ) has been proposed to be a cell-cycle phase specific inhibitor of the Ku70/80 heterodimer that is critical for restricting NHEJ to G1[156]. It is therefore possible that p53-deficiency may transcriptionally reprogram cell cycle-inhibitors of NHEJ to enable hyperactive repair, though that is beyond the scope of this study.

Regulatory mechanisms that confer TMEJ hyperactivity in cancer are just beginning to be investigated, although transcriptional overexpression of *POLQ* has also been observed in breast and ovarian cancers with *BRCA1*/*BRCA2* deficiency or mutations in other genes that confer Pol θ synthetic lethality[41,157]. Recent work examining integrated pathway analysis of *TP53* deficiency noted *POLQ* to be frequently overexpressed in *TP53* pathway deficient cancers[85]. Our findings, in an isogenic p53-deficient cell line model, indicate that this relationship may be causal. The mechanism for p53-dependent suppression of *POLQ* expression remains to be elucidated, and may entail the regulation of non-coding RNAs[158]. Pol θ is an error-prone DNA repair polymerase and therefore it is also possible that wild-type p53 suppresses *POLQ*

expression as part of its role in maintaining genome stability. In particular, recent work has shown that depletion of p53 enhances hijacking of stalled S phase replication forks by Pol θ and increases TMEJ activity at damage sites in p53-null cells compared to p53-proficient cells[159]. The increased use of TMEJ can also be explained by the potential creation of more complex DSBs upon NHEJ suppression that serve as poor substrates for homologous recombination (HR). Indeed, the molecular mechanisms of NHEJ and TMEJ hyperactivity induced by p53 deficiency warrant further investigation.

Clinically, a wide range of *TP53* mutations in cancer are observed, some of which may potentially exert gain-of-function activity[124,160]. The current study demonstrates the effect of p53 deficiency on hyperactive DSB end joining repair and resistance to therapeutic DNA damage. However, whether these findings are also applicable to cells expressing *TP53* missense mutations remains unclear. Evaluating the effects of different p53 mutations on DSB repair mechanisms and therapeutic responses remains an important topic for future investigation.

Radiotherapy and other forms of DNA damaging therapy are employed in the vast majority of cancer patients[161]. Resistance to DNA damaging therapy may thus explain the adverse clinical outcomes associated with *TP53* mutations in many different cancer types[85]. Our study supports the investigation of DNA-PK inhibitors administered in combination with DNA damaging therapy (including radiotherapy) in patients with p53-deficient cancers. Additionally, as inhibitors of Pol θ are currently in development[162], our study suggests that combined inhibition of both DNA-PK and Pol θ represents a promising strategy to reverse the therapeutic DNA damage resistance in p53-deficient cancers.

2.5. Materials and Methods

2.5.1. Key Reagents

All key reagents can additionally be found with catalog number and identifiers in Table 2.1. Table also includes detailed information on software used for analyses and algorithms available for image processing.

Table 2.1 Key Reagents Table

REAGENT or RESOURCE	SOURCE	IDENTIFIER
Antibodies		
F(ab)2-Goat anti-Rabbit IgG (H+L) Cross-Adsorbed Secondary Antibody, Alexa Fluor 633 (1:10,000 for IF)	Thermo Fisher Scientific	Cat# A-21072, RRID:AB_2535733
Chicken anti-Mouse IgG (H+L) Cross-Adsorbed Secondary Antibody, Alexa Fluor 488, (1:10,000 for IF)	Thermo Fisher Scientific	Cat# A-21200, RRID:AB_2535786
Mouse Anti-beta-Actin Monoclonal Antibody, Unconjugated, Clone AC-15 (1:10,000 for WB)	Sigma-Aldrich	Cat# A1978, RRID:AB_476692
Rabbit Anti-53BP1 Polyclonal Antibody (1:500 for IF)	Bethyl	Cat# A300-272A, RRID:AB_185520
Mouse Anti-p53 (1C12) mAb Antibody (1:1000 for WB)	Cell Signaling Technology	Cat# 2524, RRID:AB_331743
Rabbit Anti-phosphorylated Histone H2AX (γ-H2AX) Polyclonal Antibody (1:500 for IF)	Trevigen	Cat# 4418-APC-100
Chemicals, Peptides, and Recombinant Proteins		
DNA-PKi	SelleckChemicals	NU7441 (KU-57788)

Neocarzinostatin (NCS)	SigmaAldrich	N9162-100UG
Trypsin EDTA	Gibco	25200-056
Polyethylenimine, Linear (MW 25,000)	Polysciences	23966
Bovine Serum Albumin	Fisher Scientific	BP9706-160
Corning® Cell-Tak™ and Tissue Adhesive	Corning	354240
RNAiMax	ThermoFisher	13778100
Critical Commercial Assays		
PlasmoTest	Invitrogen	REP-PT1
RNAeasy Plus Mini Kit	Qiagen	74136
Comet Assay Kit	Trevigen	4250-050-K
Q5® Hot Start High-Fidelity 2X Master Mix	NEB	M0494S
NEBuilder® HiFi DNA Assembly Master Mix	NEB	E2621L
TOPO® TA Cloning® Kit for Sequencing	Invitrogen	450030
T4 DNA Ligase	NEB	M0202S
EdU-Click 594	baseclick	BCK-Edu594
NEON Electroporation Kit	ThermoFisher	MPK1025
Cas9 Protein and TracrRNA for Alt-R Electroporation	IDT	Cas9 (s.p. high fidelity) #1081060 TracrRNA #1072532
Experimental Models: Cell Lines		
hTERT-RPE1-Tricolor Reporter (PCNA-mCherry, 53BP1-mVenus, H2B-mTurquoise)	Gift from Dr. Jeremy Purvis	(See Citations)
hTERT-RPE1	ATCC	ATCC® CRL-4000™
hTERT-RPE1-*TP53-/-*	This paper	
hTERT-RPE1-*TP53-/-POLQ-/-*	This paper	
Oligonucleotides (sgRNAs and Primers)		
sgLBR	GCCGATGGTGAAGTGGTAAG	Synthesized at: IDT
sgTP53_Exon2	TCGACGCTAGGATCTGACTG	IDT
sgTP53_Dwnstream_Intron	GAAACTGTGAGTGGATCCAT	IDT
sgPOLQ_1	ACTACTCTCAGCTTGA	IDT

sgPOLQ_2	TCAGGAGCATTGCAGCAGAG	IDT
LBR_Fwd	AAATGGCTGTCTTTCCCAGTAA	EtonBio
LBR_Rev	ACGCAGTGGCTAAATCATCC	EtonBio
TP53 RTqPCR Primer Fwd	GAGGTTGGCTCTGACTGTACC	EtonBio
TP53 RTqPCR Primer Rev	TCCGTCCCAGTAGATTACCAC	EtonBio
CDKN1A RTqPCR Primer Fwd	TCACTGTCTTGTACCCTTGTGCTT	EtonBio
CDKN1A RTqPCR Primer Rev	AGAAATCTGTCATGCTGGTCTGCC	EtonBio
ONTARGET plus Human TP53 Si-RNA SMARTPOOL	Horizon Discovery (previously Dharmacon)	L-003329-00-0010
ONTARGET plus NON-TARGETTING control siRNAs SMARTPOOL	Horizon Discovery (previously Dharmacon)	D-001810-10-05
ESR1 Genomic Locus Fwd Primer	ATCTGTACAGCATGAAGTGCAAGA	EtionBio
ESR1 Genomic Locus Rev Primer	CTAGTGGGCGCATGTAGGC	EtonBio
ESR1 Genomic Locus Probe	T+C+T +AT+G +A+CC TG (Locked nucleic acid probe with HEX)	IDT (LNA : Locked Nucleic Acid Probe)
LBR Locus Probe	TGAGATTGAATGTAGCCTTTCTGGCCCTAA (with FAM)	

LBR Nested Sequencing Primers

Purple -> Binds genomic DNA
Green -> Phasing portion of primer
chr1:225423928-225424162
Size: 235 base pairs
Forward Primer: 114 base pairs left of cut
Reverse Primer: 123 base pairs right of cut
Rcomp = reverse complimentary

TCAATTCAAGCTCTGTTCCATCTTTATACTTCACAGTGTAAAGCTGGGAGGTGCTG
TCGTGGCTCAGAATTTCTACTTCATAATAAAGTGAACTCCCAGGCCATCGA**CCT***CT*
TA*CCACTTCACCATCGGC*AAATTTCCTACTTGGCATTTTCTATAATTAACCTGAATA
GTTTTAAAGAAAAAAATTTGAGTCAATACATACACATTTATGTATTCGTCTTTTTCCA
CAGGCTGA

Primer Name	Orientation	Location	Sequence
LBR2.1 F0	Forward	chr1:225423928-225423949	CGACGCTCTTCCGATCTTCAATTCAAGCTCTGTTCCATC
LBR2.1 F1	Forward	chr1:225423927-225423949	CGACGCTCTTCCGATCTTTCAATTCAAGCTCTGTTCCATC
LBR2.1 F2	Forward	chr1:225423927-225423949	CGACGCTCTTCCGATCTCTTCAATTCAAGCTCTGTTCCATC
LBR2.1 F3	Forward	chr1:225423927-225423949	CGACGCTCTTCCGATCTACTTCAATTCAAGCTCTGTTCCATC
LBR2.1 F4	Forward	chr1:225423927-225423949	CGACGCTCTTCCGATCTGACTTCAATTCAAGCTCTGTTCCATC
LBR2.1 F5	Forward	chr1:225423927-225423949	CGACGCTCTTCCGATCTAGACTTCAATTCAAGCTCTGTTCCATC
LBR2.1 R0	Rcomp	chr1:225424162-225424143	CGTGTGCTCTTCCGATCTTCAGCCTGTGGAAAAAGACG
LBR2.1 R1	Rcomp	chr1:225424163-225424143	CGTGTGCTCTTCCGATCTATCAGCCTGTGGAAAAAGACG
LBR2.1 R2	Rcomp	chr1:225424164-225424143	CGTGTGCTCTTCCGATCTGATCAGCCTGTGGAAAAAGACG
LBR2.1 R3	Rcomp	chr1:225424165-225424143	CGTGTGCTCTTCCGATCTTGATCAGCCTGTGGAAAAAGACG
LBR2.1 R4	Rcomp	chr1:225424166-225424143	CGTGTGCTCTTCCGATCTCTGATCAGCCTGTGGAAAAAGACG
LBR2.1 R5	Rcomp	chr1:225424167-225424143	CGTGTGCTCTTCCGATCTAC

Software and Algorithms		
Python ≥v3.5	*G. van Rossum*, *Python tutorial*, *Technical Report CS-R9526*, *Centrum voor Wiskunde* en *Informatica* (CWI), *Amsterdam*, May *1995*	https://www.python.org/
Flow Jo	*FlowJo™ Software (Mac) [proliferation assay analysis] Becton, Dickinson and Company; 2019.*	https://www.flowjo.com/
Graphpad Prism v8	N.A.	https://www.graphpad.com/
Fiji	*Schindelin, J.; Arganda-Carreras, I. & Frise, E. et al. (2012), "Fiji: an open-source platform for biological-image analysis", Nature methods **9(7)**:*	https://imagej.net/Fiji#Downloads

	676-682, PMID 22743772, doi:10.1038/nmeth.2019 (on Google Scholar).	
CellProfiler	*CellProfiler Program Citation:* McQuin C, Goodman A, Chernyshev V, Kamentsky L, Cimini BA, Karhohs KW, Doan M, Ding L, Rafelski SM, Thirstrup D, Wiegraebe W, Singh S, Becker T, Caicedo JC, Carpenter AE (2018). CellProfiler 3.0: Next-generation image processing for biology. PloS Biol. 16(7):e2005970 / doi. PMID: 29969450 (Research article) *Analyst Software Citation:* Jones TR, Kang IH, Wheeler DB, Lindquist RA, Papallo A, Sabatini DM, Golland P, Carpenter AE (2008) CellProfiler Analyst: data exploration and analysis software for complex image-based screens. BMC Bioinformatics 9(1):482/doi: 10.1186/1471-2105-9-482. PMID: 19014601 PMCID: PMC2614436	www.cellprofiler.org
NIS Elements AR software		https://www.nikon.com/products/microscope-solutions/lineup/img_soft/nis-elements/
SnapGene software v4 .3.4	GSL Biotech	https://www.snapgene.com
Open Comet v1.3.1	BM Gyori, G Venkatachalam, PS Thiagarajan, D Hsu and MV Clement. “OpenComet: An automated tool for comet assay image analysis”, Redox Biology, 2:457-465, 2014.	http://www.cometbio.org
ScarMapper		https://github.com/pkMyt1/ScarMapper.git

Additional Image Analysis Scripts	Code EV1 Supplementary and Code Availability (MATLAB scripts)	PMID: 30886052 PMID: 29102360
Other		
Genes	www.Ensembl.org	Ensembl v91

2.5.2. Cell Culture

TP53$^{+/+}$*, Fusion-Reporter (TP53*$^{+/+,}$*PCNA-mCherry, 53BP1-mVenus), TP53*$^{-/-}$*,* and *TP53*$^{-/-}$*POLQ*$^{-/-}$ cells are hTERT immortalized RPE1. The fusion-reporter cell line was gifted by Dr. Jeremy Purvis and originally created utilizing lentiviral transduction of the dual reporters into RPE1 followed by single-clone selection for stably expressing cells. Cells were maintained in Dulbecco's modified Eagle's medium (DMEM), with 10% Fetal Bovine Serum (Hyclone FBS) and 2mM L-glutamine (ThermoFisher). All cells were maintained at 37°C in an atmosphere of 5% CO2. Cells were routinely tested for mycoplasma contamination using PlasmoTest (Invivogen).

2.5.3. Establishment Of Stable Cell Lines

To create the *TP53* and *POLQ* deficient cell lines, we used the Alt-R-CRISPR-Cas9 system (IDT). We performed Neon transfection (Invitrogen) and followed the manufacturer's protocol with Alt-R HiFi Cas9 nuclease, crRNA and tracrRNA purchased from IDT. crRNA was designed using MIT CRISPR (http://crispr.mit.edu) to target Exon 2 of the *TP53* gene to create the *TP53*$^{-/-}$ cell line and the polymerase domain of the *POLQ* gene to create the *TP53*$^{-/-}$*POLQ*$^{-/-}$ cell line (Supplementary Figs 1,5). Forty-eight hours after transfection, cells were seeded for single clone selection. Restriction enzyme screening, western blots, PCR screening, and Sanger sequencing confirmed gene targeting, post which we performed functional tests.

2.5.4. Immunofluorescence

Cells were fixed with 3% Paraformaldehyde for 15 min at room temperature, followed by permeabilization with 0.25% TritonX-100 in PBS. Cells were subsequently processed for immunostaining experiments using the antibodies listed below. Nuclei were visualized by staining with DAPI. The primary antibodies used were: γH2AX (1:500, Trevigen, 4418-APC-100), and 53BP1 (1:500 for immunofluorescence, Bethyl, #A300-272A). The secondary antibodies were: FITC Goat Anti-Mouse IgG (H + L) (1:500, Jackson ImmunoResearch, 115-095-003) and FITC Goat Anti Rabbit IgG (H + L) (1:500, Jackson ImmunoResearch, 111-095-144). Images were acquired using the GE IN CELL 2200 high through-put imaging system at 40x magnification.

2.5.5. SI-RNA Treatment

WT Fusion-Reporter RPE cells were passaged twice after -80 °C thaw and plated on 12 well plates at a density of 100,000 cells/ well for siRNA treatment. Twenty-four hours post plating, cells were exposed to 10nM / well si-TP53 (SMART pool from Dharmacon), and si-Control (Non-targetting SMART pool from Dharmacon), in OPTIMEM with RNA-iMAX (ThermoFisher) as a transfection reagent. As a no-treatment control, cells were exposed to RNA-iMAX and OPTIMEM without siRNA. 48 hours post transfection, cells were transferred onto 12 well Cell-Tak coated glass plates (Cellvis), at a concentration of 50,000 cells/well for imaging. Prior to imaging and at the end of imaging, samples were taken for RT-qPCR analysis of p53 mRNA to confirm si-RNA knockdown.

2.5.6. Mixed Competition Assay - Flow Cytometry

mCherry labelled and unlabeled hTERT-RPE1 cell lines were plated on 96 well plates at a 1:1 ratio (1500 cells each for a total of 3000 cells per well), and irradiated post

plating at 0, 2, 4, or 6 Gy, and left to grow. Irradiation was performed after cell plating to ensure time for cell adherence for both RPE1 and TP53 $^{-/-}$ RPE1. Cells were fully adherent at time of radiation (4h post-plating). At indicated timepoints cells were harvested by trypsinizing and quenching with PBS with 5% BSA. Cells were fixed with 2% PFA and subsequently transferred to V-bottom plates (ThermoFisher, #249570). Cells were quantified by flow cytometry using the Intellicyt iQue at a volume of 100 µL/ sample, collecting all events per well. For each condition, 6 biological replicates were collected.

2.5.7. Time-Lapse Imaging Microscopy

Cells stably expressing Proliferating Cell Nuclear Antigen (PCNA)-mCherry and Tumor Suppressor p53 Binding Protein 1 (53BP1) – mVenus were treated with si-RNA for 48 hours prior to imaging. PCNA-mCherry and 53BP1-mVenus fusion reporter is a gift from Dr. Jeremy Purvis and Hui Chao Xiao. Cells were plated on Cell-Tak (Corning) coated glass-bottom 12-well plates (Cellvis) with Phenol-free DMEM (Invitrogen) supplemented with 10% FBS, and L-glutamine. Twenty-four hours post plating, cells were image captured every 10 min for 72 h in the mCherry and mVenus fluorescence channels. 18 hours into imaging, DNA-PK inhibitor (DNA-PKi, NU7441) was added at a concentration of 0.5 µM / well, and/or Neocarzinostatin (NCS, Sigma-Aldrich) at a concentration of 100ng/ mL/ well. We commenced imaging every 10 minutes in both channels for another 48 hours. Fluorescence images were obtained using a Nikon Ti Eclipse inverted microscope with a 40x objective and Nikon Perfect Focus (PFS) system to maintain focus during acquisition period. Cells were maintained at constant temperature (37 °C) and atmosphere (5% CO_2). Nikon, NIS Elements AR software was

utilized for image acquisition. Image analysis was performed on ImageJ – Fiji and Cell Profiler.

2.5.8. Colony Forming Assays

Cells lines used in the assay are indicated in the figures. Cells were treated with NCS and/ or DNA-PKi for twenty-four hours, after which we performed a media change. For all colony forming assays, cells were incubated for 10 days at 37 °C to allow colony formation. Colonies were stained by Coomassie blue and counted on day 10.

2.5.9. Digital PCR

Primers and 5' hydrolysis probes were designed to specifically detect the copies of *LBR* locus. *ESR1* locus was used as genomic control. Each reaction assay contained 10 µLof 2x dPCR Supermix for Probes (No dUTP), 0.9 µmol/L of respective primers, 0.25 µmol/L of respective probes, and 10 ng of DNA in a final volume of 20 µL. Droplets were generated using automated droplet generator (Bio-Rad catalog #186-4101) following manufacturer's protocol. PCR parameters for *LBR* locus were 10 sec at 95 °C, then 40 cycles of 94 °C for 30 sec, 60 °C for 30 sec, and 72°C for 2 min followed by 98°C for 10 min with a ramping of 2 °C/sec at all steps. The PCR cycling parameters for *ESR1* genomic locus were 10 sec at 95 °C, then 40 cycles of 94 °C for 30 sec and 60 °C for 1 min followed by 98°C for 10 min with a ramping of 2 °C/sec at all steps. After PCR amplification, droplet reader (Bio-Rad QX200™ Droplet Reader Catalog #1864003) was used to measure the end-point fluorescence signal in droplets as per the manufacturer's protocol. The recorded data was subsequently analyzed with QuantaSoft software version 1.7.4.0917 (Bio-Rad). Each Taqman probe was evaluated for sensitivity and specificity.

2.5.10. DNA Repair Assay

Cell lines used in the assay are indicated in the figure. 5×10^5 cells were transfected with sgLBR2 and TracrRNA complexed Cas9 protein at final concentrations of sgRNA:tracrRNA duplex: 22 pmol and Cas9 : 18 pmol per reaction, with Neon transfection kit (Invitrogen) using 2 1350 V, 30 ms pulses in a 10 µL chamber. 60 hours post transfection, cells were harvested for genomic DNA extraction (Nucleospin). Part of the gDNA was utilized for Sanger Sequencing and TIDE analysis post amplification of the genomic LBR2 locus. For analysis of INDELs, 100 ng of gDNA was amplified using phased primers. These libraries were indexed with the Illumina unique dual combinatorial indices. Following pooling, 2 x 150 cycle sequencing was done on an Illumina iSeq™. INDELs were identified by comparing the target reference sequence to the resulting sequence reads in the FASTQ files via a 10-nucleotide sliding window using the ScarMapper program.

CHAPTER 3 – MRE11 MEDIATES A P53- INDEPENDENT G2/M CHECKPOINT RESPONSE TO ONCOGENIC ACTIVATION

3.1. Summary

The DNA Damage Response (DDR) is a critical anti-tumor barrier during tumorigenesis. Defects in the DDR give rise to clinically aggressive breast cancers with high levels of genome instability. In this study, we perform a CRISPR based in-vivo murine DDR screen that identifies Mre11 as the most crucial DDR gene that restrains tumor proliferation. Prior work on the Mre11 protein, an apical double-strand-break sensor in the DDR, has revealed that Mre11 deficiency gives rise to uncontrolled proliferation and genome instability in murine models of triple negative breast cancer. However, the mechanism by which Mre11 regulates these two processes remains unknown. We then utilize live-cell imaging in conjunction with an in-vitro primary murine mammary epithelial cell system to show that Mre11 mediates a potent p53-independent G2/M checkpoint response during oncogenic induction. The absence of Mre11 enables cells to increase entry into mitosis and remain viable post- mitosis with ongoing genome instability. We characterize a unique nuclear phenotype associated with Mre11 deficiency: aberrant micronuclei formation. Mre11 deficient mouse embryonic fibroblasts lack ability to form micronuclei in response to irradiation and are further characterized by a functional defect in interferon signaling in response to micronucleus formation. These results highlight the importance of Mre11 in early checkpoint responses in pre-neoplasia and indicate potential roles for Mre11 in innate immune signaling to clear senescent cells *in-vivo.* Clinically, 10%

of triple negative breast cancers show Mre11 deficiency and increased sensitivity to chemotherapy. Recent work has also implicated ATR signaling kinase as a critical mediation of mitotic entry post-S phase; treatment with inhibitors to ATR have previously shown great potency in Mre11-deficient cancers. These results pave the way for potential utilization of ATR inhibitors in Mre11 deficient cancers with translational implications in human breast cancer.

3.2. Introduction

The DNA damage response (DDR) is activated in early pre-neoplasia and becomes dysregulated over tumorigenesis[106,163–165]. Several important discoveries highlight how the DNA damage response may be activated in early pre-neoplastic lesions; however, the DDR is composed of a vast network of proteins and the most critical genes essential for the anti-tumor functions and the exact mechanisms by which they operate to restrain tumor proliferation remain poorly characterized.

To this end, we performed an *in vivo* murine DDR CRISPR screen to systematically evaluate which DDR genes are most critical for restraining tumor formation in a mouse-model of *c-Myc* driven Triple Negative Breast Cancer (TNBC). Oncogene-induced DNA replication stress is the primary mechanism for DDR activation in the early stages of cancer and the *c-Myc* driven TNBC model has previously been utilized to study *in-vitro* effects of oncogenic induction on DNA damage and emerging chromosomal instability (CIN)[166–170] Here, we report Mre11 as the top candidate from the *in vivo* screen with 12/40 murine mammary tumors having significant enrichment for Mre11 small guide RNAs (sgMre11) compared to internal controls.

Mre11 is part of the trimeric Mre11-Rad50-Nbs1 (MRN) complex that primarily detects DNA double strand breaks (DSBs) in eukaryotic cells[16]. The MRN complex is often denoted as the “first responder” to DNA DSBs and its position in the apex of the DDR is well-warranted[16,32]. Genetically, Mre11 and Rad50 are evolutionarily conserved across all three domains of life, emphasizing their importance as the core catalytic components of the complex[31]. Germline mutations in the MRN complex give rise to a series of genetic syndromes collectively termed: Genome Instability Syndromes[171]. These syndromes predispose patients to having developmental abnormalities, cerebellar dysfunction, and a high incidence of cancers[31,171]. Furthermore, all members of the MRN complex are encoded by essential genes and knockdown of any of the three proteins results in embryonic lethality, highlighting the importance of MRN for eukaryotic viability and maintenance of genomic integrity[31].

Somatic point mutations in MRN complex proteins, particularly the scaffolding protein Mre11, are rare in cancer[172–174]. Additionally, gene alterations via deep-deletion, insertions or fusions, are also infrequent[172–174]. However, protein-based expression studies evaluating the presence of the complex have highlighted that MRN complex members are significantly depleted in up to 10% of Triple Negative Breast Cancers (TNBCs)[170]. Tissue microarrays evaluating MRN expression in epithelial ovarian cancer (EOC) have shown that MRN complex is undetectable in 41% of low-grade and 19% of high-grade EOC’s[175]. In contrast to patterns of MRN deficiency in ovarian and breast carcinomas, over-expression of MRN has been detected in clinically aggressive colorectal cancers[176,177]. While it is unclear how MRN deficiency is induced, it may be that post-transcriptional regulatory mechanisms may contribute to the patterns of MRN deficiency

seen, these recurrent observations of MRN deficiency in cancer along with the results of the *in-vivo* screen highlight the importance of this complex in restraining tumorigenesis.

To understand the role of the double strand break sensors in cancer, it is critical to review the role that the MRN complex may serve as an anti-tumor barrier. During oncogenic activation in early pre-neoplastic lesions, cells experience tremendous replication stress. Endogenous replication stress is defined as the deregulation of DNA replication resulting in increased replication fork collapse and subsequent DNA damage. Replication fork collapse can lead to DSBs and/ or long stretches of single-stranded DNA (ssDNA). Recent work from our lab has shown the Mre11 is critical for prevention of replication fork collapse when oncogene-induced misfiring of origins increase replication-transcription collisions[170]. Moreover, prior work has also shown that Mre11 deficiency increases tumor hyper-proliferation and genome instability[170]. These previously reported phenotypes of Mre11 are both p53 and ATM-independent[170]. ATM is a member of the Phosphatidylinositol-3-kinase-like Kinase family (PIKK) and is a serine master kinase with numerous target proteins including ATR and p53[144]. ATR is a sister kinase of ATM and binds to ssDNA that has been coated with RPA; and it is well-known that ATM and ATR have the ability to cross-talk[17]. ATM directly phosphorylates p53 and canonical depictions of the DDR pathway often portray p53 as a downstream effector with respect to regulation of the G1/S checkpoint and apoptotic responses to DNA damage[46]. However, in many cancers p53 is mutated, absent, or suppressed by over-expression of MDM2[66]. In these situations, the role of the MRN complex becomes unclear because the downstream effector is functionally absent.

The goal of this study was to investigate the role of DDR proteins in serving as an anti-tumor barrier in pre-neoplastic lesions and to define the mechanisms by which the top candidate in our screen, Mre11, regulates tumor proliferation and genome instability. We use an *in vivo* DDR CRISPR screen and derive 40 mammary tumors to evaluate loss of which DDR proteins is most conducive to mammary tumor formation. We use live-cell imaging to first characterize the effect of Mre11 dysfunction in tumor proliferation. We characterize a p53-independent G2-M checkpoint function that is mediated by Mre11 to prevent mitotic entry of DNA damage and to subsequently eliminate cells with CIN. MRN deficiency also promotes ongoing genome instability in early G1 of daughter cells, highlighting transmission of under-replicated DNA through mitosis. Finally, we showcase an exciting role for Mre11 in mediating innate immune signaling via micronucleus formation. These results provide a mechanistic understanding for Mre11 and how it functions as a critical anti-tumor barrier.

3.3. Results and Discussion

To investigate the principal DDR genes involved in restraining tumorigenesis, we performed the *in-vivo* CRISPR DDR library screen utilizing a Cre-inducible mouse model of Triple Negative Breast Cancer (TNBC) (Figure 3.1A). TNBC is characterized by near universal p53 loss and a high incidence of co-occurring *c-Myc* overexpression (OE). Thus, p53 deletion and *c-Myc*^{OE} are 2 major drivers of TNBC, a cancer sub-type known for its complex genomic instability and oncogenic replication stress. Moreover, DDR dysregulation and mutations in core DDR genes have previously been reported in human TNBCs. To generate this model, we first crossed Rosa26$^{Cas9/Cas9}$ to Rosa26$^{MycOE\text{-}CD2/MycOE\text{-}CD2}$ (OE = overexpression) to make Rosa26$^{Cas9/MycOE\text{-}CD2}$ mice capable of over-

expressing a *c-Myc* cassette under a Cre-dependent locus. We then bred the Rosa26$^{Cas9/MycOE-CD2}$ to Trp53$^{fl/fl}$ mice (a gift from Dr.Perou) to generate the target mouse line with both inducible p53 deficiency and *c-Myc* overexpression: Rosa26$^{Cas9/MycOE-CD2}$Trp53$^{fl/fl}$ (Figure 3.1B). In addition, expression of CRISPR Cas9 endonuclease enables editing of multiple mouse genes upon exposure to short-guide RNAs for *in vivo* or *in vitro* experiments.

The DDR CRISPR library is a custom, previously published pooled resource of sgRNAs that target 309 murine DDR genes (10 guides per gene) and also contains 834 non-targeting sgRNA controls[41]. The DDR library was cloned into a Lenti-CRISPR-Cre-V2-Lumifluor plasmid (see methods) and introduced to murine mammary glands via lentiviral intraductal injections (Figure 3.1A). The benefits of this model include spontaneous tumor generation post Cas9 mutation of targeted DDR genes and the presence of an immunocompetent landscape that more closely aligns to the human mammary tissue. The lentivirus with Cre-recombinase activates Cas9-GFP expression, removes a stop codon in front of a *c-Myc* cassette, and introduces deletion of Trp53 exon 2 (Figure 3.1B).

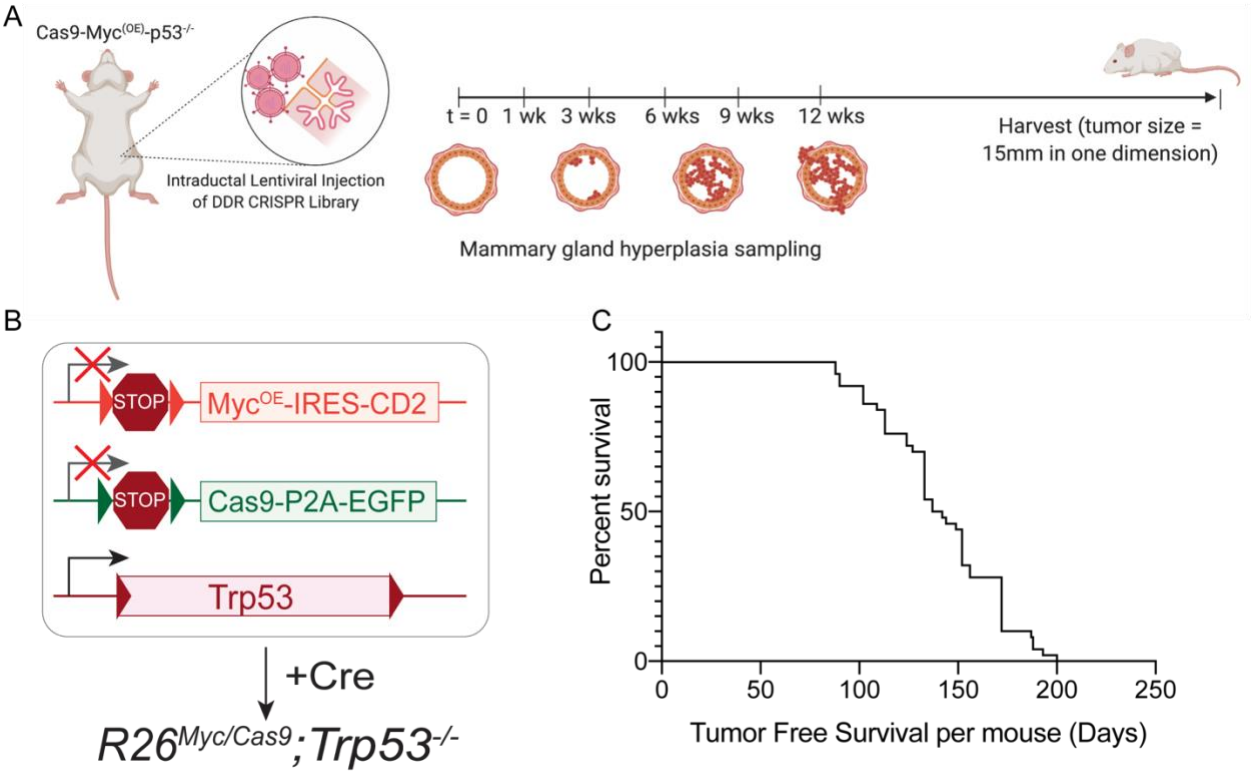

Figure 3.1 In-Vivo DDR Library Screen. A, Schematic depicting the in-vivo DDR CRISPR library screen. Female mice aged 6-10 weeks were bilaterally injected with lentivirus containing 3090 targetting sgRNAs, 834 non-targetting controls and Cre-recombinase. 2 mice were sacrificed each at weeks 1,3,6,9 and 12 for hyperplastic gland sampling. B, Depiction of the Cre-recombinase activated genotypic changes in mouse model of TNBC. Myc-Overexpression (OE), Cas9-GFP expression, and Trp53 deletion were Cre-recombinase dependent. C, Survival curve indicating the tumor free survival per mouse. Tumor free survival was calculated by bi-lateral palpation of mice weekly. Data represents the first day palpable tumor was recorded. All mice in the study barring the 10 sacrificed for hyperplastic sampling at early time-points, developed tumors.

3.3.1. IN-VIVO DDR Library Screen Reveals Key Genetic Targets In Mammary Tumor Formation

At the start of the study, 40 female mice from 6-10 weeks of age were bilaterally injected with the DDR-CRISPR lentiviral library at a multiplicity of infection of 1 to ensure that each mammary epithelial cell would only receive 1 sgRNA and then compete during tumorigenesis (Figure 3.1A,C). The tumor free survival curve is shown per mouse in

Figure 3.1C. These mice were followed post-injection until tumor growth equaled 15 mm in either of the right or left mammary glands, at which point tumors were harvested and stable cell lines generated. At the end of the study, which spanned 200 days, 43 total tumors were harvested from the cohort. 40 of these tumors met the tissue size requirement for sequencing analysis (Figure 3.1C and see methods). Several mice had multiple discrete tumors per gland resulting in the final number of tumors exceeding the total mice in the study. Post tumor-DNA extraction, we sequenced each sample to determine abundance of DDR sgRNAs in each tumor (gland z-Score) compared to the original DDR library plasmid (Plasmid z-Score) that was sequenced to calculate fold enrichment (Figure 3.2A-C). sgRNA enrichment in each tumor cohort was used to determine which DDR genes were most essential for mammary tumor formation starting from the hyperplastic lesions (shown as Days 7 and 21 in Figure 3.2A,B) to neoplastic lesions (mammary tumors, Figure 3.2C). Our results show the sgRNA with highest abundance across the most tumors (12/40) is sgMre11a which targets the Mre11 gene (Figure 3.2D).

sgMre11a was detected as the singular sgRNA in 2/12 tumors and in 10/12 was found with other sgRNAs targeting the following DDR genes: *Trp53bp1* and *Lmo4.* These genes encode the p53-Binding Protein 1 (53BP1) and the Lim domain transcription factor 4 (Lmo4) respectively. Of these, 53BP1 binding protein is a well-known DSB binding protein and marker of DNA damage. Intriguingly, other MRN complex members (Rad50 and Nbs1) were not major hits in the screen, suggesting that Mre11 is the most critical member of the trimeric complex. These results also highlight potential synergistic pathways that may act to inhibit proliferation together. The results of the screen also

highlight Mre11a deficiency as a critical mediator of tumorigenesis compared to other DDR genes. Moreover, evolving work in the field of Mre11 has recently highlighted the critical roles of Mre11 in replication fork protection, fork rescue, genome maintenance, and proliferation in response to replicative stress. Thus, we decided to further evaluate the mechanistic role of Mre11 with respect to proliferation and genome stability.

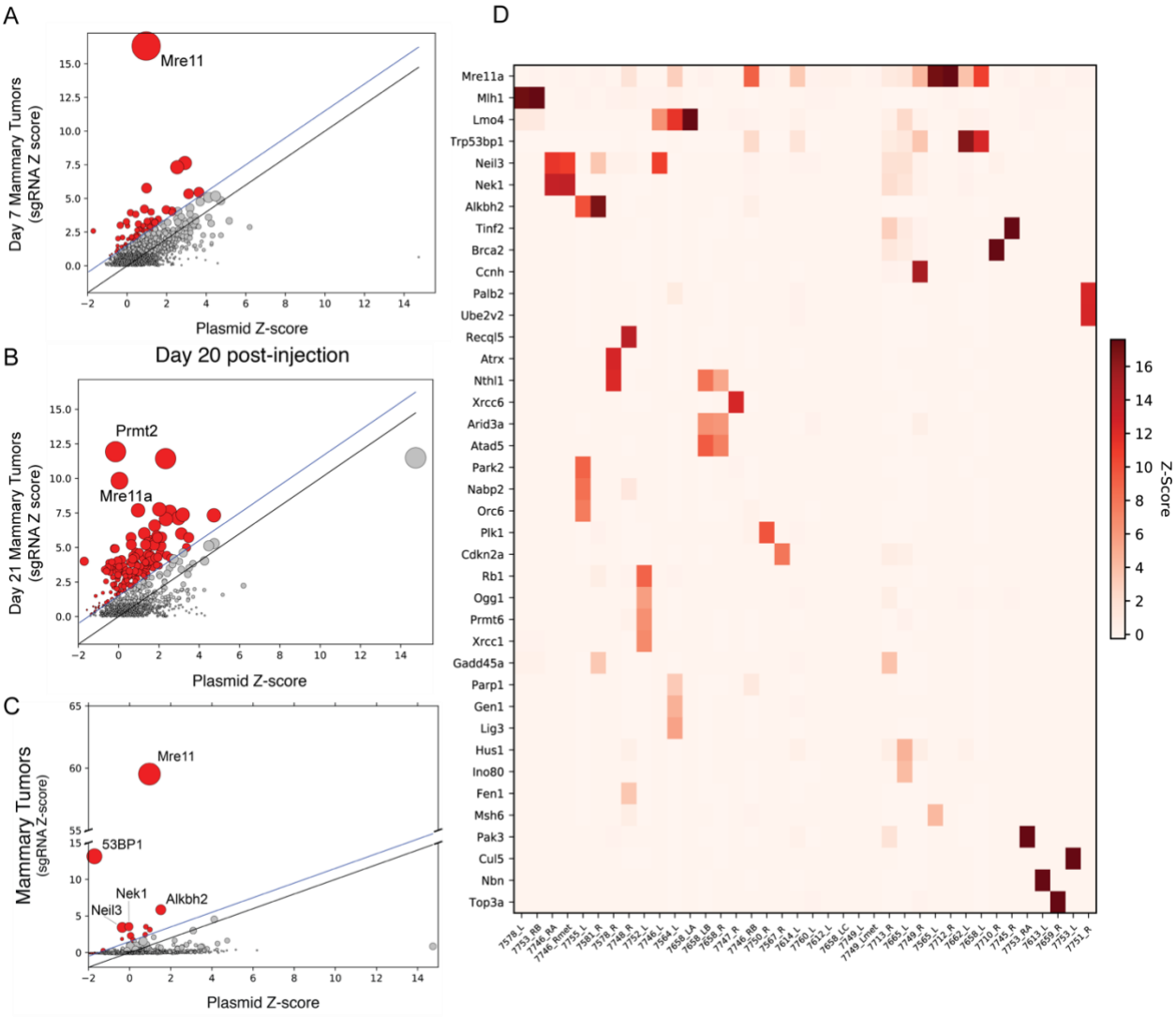

Figure 3.2 : DDR Screen Results. A, Shows DNA sequencing results from a hyperplastic mammary glands (n=4) harvested day 7 post-intraductal injection. The Plasmid Z score is determined by sequencing the individual sgRNA frequencies found by sequencing the pooled DDR library plasmid utilized for lentiviral generation. The sgRNA Z score was calculated by determing the frequency of sgRNA reads specific for each DDR gene

sequenced from the hyperplastic sample. Upward deviation from the mid-line indicates increased abundance in tumor (as shown by red circles), whereas negative deviation indicates depletion in the tumor (gray circles not essential for tumor formation). B, sgRNA abundance in day 21 hyperplastic glands (n=4) where the top sgRNA was Protein Arginine Methyltransferase (Prmt2). Mre11a is also indicated in this graph. C, Sequencing results indicate sgRNA abundance across all mammary tumors (n=40). sgMre11a was found in abundance in 12 total tumors, making it the most frequent sgRNA that was present across all mammary tumors in the study. In 2/12 tumors sgMre11a was the single most abundant sgRNA detected.

3.3.2. Cell Cycle Profiles Of MRE11 Deficient Cells

In order to clarify the role of MRN complex in restraining proliferation during cancer progression, we utilized the same mouse model in a series of *in-vitro* studies evaluating Mre11 in the context of cell-cycle regulation. Previously, MRN complex has been studied utilizing exogenous DNA damage; specifically, damage induced by ionizing radiation (IR). Using IR, others have shown that MRN complex is important for G2 checkpoint responses that are ATM dependent. However, as most of these experiments were performed in the presence of high levels of genotoxic DSBs; it is unclear how Mre11 responds to endogenous replicative stress. Prior results from our lab have also shown that the proliferative advantage conferred by Mre11 deficiency is not recapitulated by treatment with inhibitors against ATM or by deleting p53. This raises the exciting possibility that the proliferation advantage we are observing is both an ATM and p53-independent function of Mre11. Given the previous findings regarding Mre11 complex and its role in activating DNA damage checkpoints, we then proceeded to assess presence or absence of checkpoint responses in a primary murine mammary epithelial cell system (pMMECs, Figure 3.3A).

The pMMEC *in-vitro* model system enables extraction of primary murine mammary epithelial cells, viral transduction to induce the same genotypic drivers utilized in the

screen, and downstream analysis of the initial cell-cycles post-oncogenic induction. To induce Mre11 deficiency in the pMMEC system, we utilized the same sgMre11 used in the CRISPR screen, a previously published sequence[170,178]. sgMre11 recapitulates a patient-derived Ataxia-Telangiectasia Like Disease (*ATLD1)* mutation in the C terminus of Mre11 to destabilize the transcript, and thereby the entire protein complex resulting in functional deficiency of the MRN complex in cells of interest (Figure 3.3B). Taking advantage of the large protein domain similarities between murine and human Mre11, sgMre11 targets the scaffolding region of Mre11 that docks to Rad50 to create the complex. To introduce the *ATLD1* mutation, we created a short-guide (sg) RNA against amino acid R611, to induce a small deletion using CRISPR-Cas9 resulting in a premature stop codon and truncated protein product in murine cells (Figure 3.3B). This particular Mre11 mutant retains the endonuclease domain that is essential for cellular viability but lacks the scaffolding domain that is critical for MRN complex formation. The Mre11-ATLD mutant does not have the ability to localize to DNA DSBs and does not form a complex with Rad50 and Nbs1, thereby making it functionally DDR deficient.

To evaluate cell-cycle profiles we combined the pMMEC system with live-cell imaging (Figure 3.3A). We co-infected pMMECs of interest with a lentivirus for Proliferating-Cell Nuclear Antigen (PCNA) fused to the mCherry reporter. PCNA is part of the replication ring clamp that slides along with the mobile replication fork during S phase, resulting in discrete formation of PCNA foci in S phase of the cell cycle. When combined with live-cell imaging, this reporter can be utilized to reliably evaluate various phases of the cell cycle, nuclear morphology, and checkpoint function of single-cells and populations.

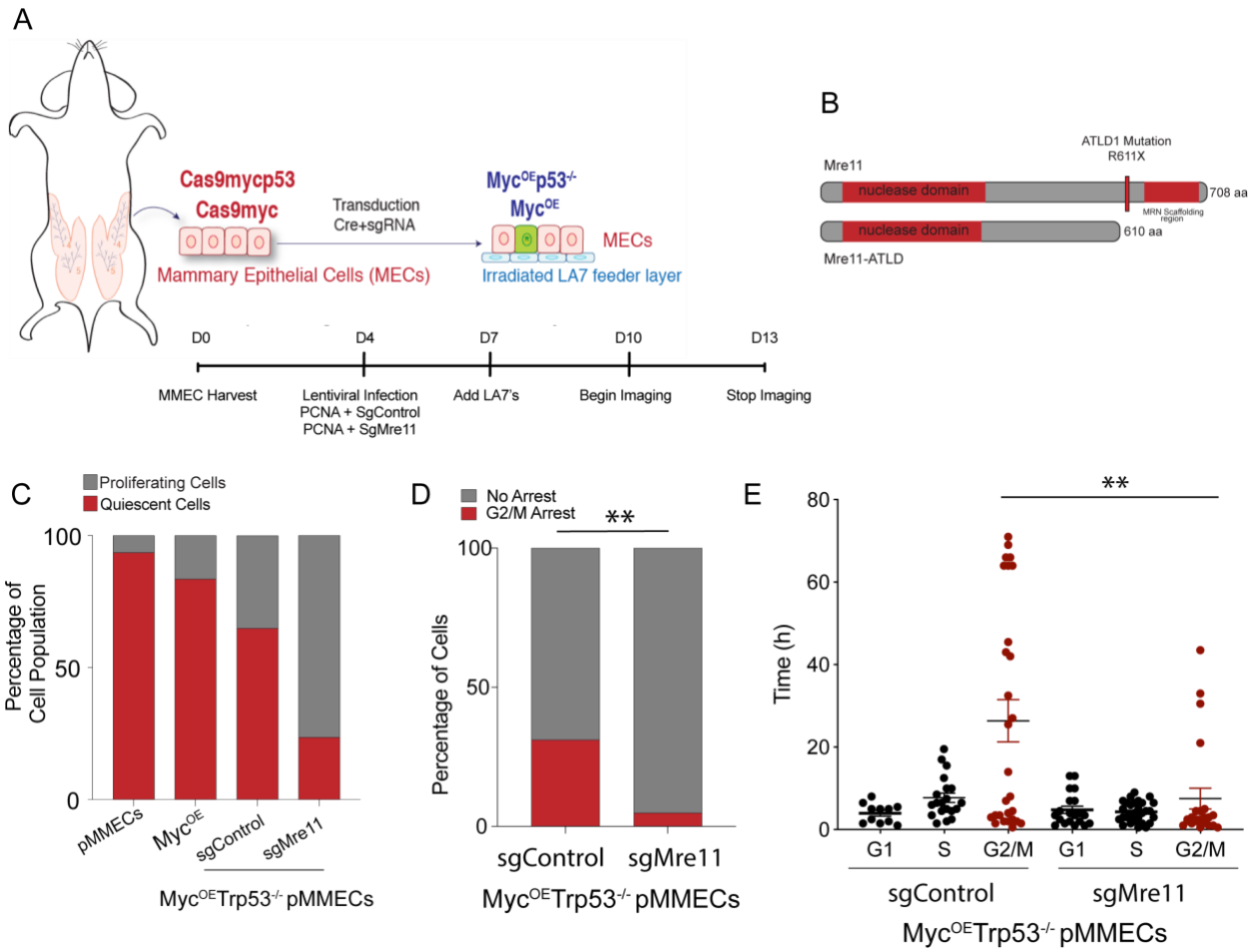

Figure 3.3 : Live-Cell Imaging of pMMECs. A, Schematic of the in-vitro pMMEC system utilized in conjuction with live-cell imaging. The two mouse genotypes from which pMMECs were harvested are listed along with the timeline leading up to imaging. Cells were transduced once daily for two days with Lentivirus (LV)-sgRNA+Cre and LV-PCNA-mCherry. Imaging was performed for 72 hours with image acquisition in the GFP (Cas9 activation) and mCherry channels every 20 min. B, Representation of the ATLD mutation induced by sgMre11. The scaffolding region int he C-terminus of Mre11 for the Mre11-Rad50-Nbs1 (MRN) complex is lost in the ATLD1 mutant, which is a truncated protein of 610 amino acids (aa). C, Prolfierating cell fraction as quantified by a cell experiencing either S phase or mitosis in the 72 hour imaging period, OE = over-expression. n=185, 235, 128, and 102 cells total per condition (left to right) respectively. D, Quantification of frequency of G2/M arrest in cells that completed S phase in sgControl vs. sgMre11 treated cohort (n=45 sgControl and n=62 sgMre11 cells). $p<0.01$ = ** as evaluated by Fisher's exact test. E, Individual length of different cell-cycle phases for sgControl vs. sgMre11 treated cells. $p<0.01$ = ** as evaluated by Student's t-test for the G2/M length, SEM is reported.

3.3.3. Proliferation Phenotypes In Mammary Epithelial Cells

Due to the genetic complexity of late-stage neoplastic lesions, we decided to sequentially mutate mammary epithelial cells (MECs) that were harvested from mice to study Mre11 through tumor progression. The genetic manipulations in these pMMECs were performed utilizing lentiviral co-infection with lentiviral-sgMre11-Cre or lentiviral-sgControl-Cre to induce *c-Myc*-activation and/or p53 deficiency in cells from 2 different mouse genotypes (Figure 3.3A). To evaluate pMMECs via live-cell imaging required the pMMECs to be propagated on glass with Cell-Tak (see methods). We established a protocol where pMMECs can be co-cultured on a selective feeder layer of rat-derived LA7 fibroblast cells that mimic the stromal environment of breast tissue. These LA7 feeder cells can further be irradiated at 70Gy to prevent proliferation. To differentiate between feeder cells and pMMECs on imaging we utilized double positive (eGFP+, mCherry+) cells for our analysis. This ensured selective analysis of cells with Cre-inducible Cas9 expression that had been infected by our lentiviral Cre along with the PCNA reporter (Figure 3.3A). Thus, our studies first established the feasibility of performing live-cell imaging in primary MMECs that had not been immortalized.

Cells were imaged every 20 minutes for a total duration of 72 hours (Figure 3.3A). We first imaged unperturbed pMMECs derived from Rosa26$^{Cas9/Cas9}$ mice that received Cre with no sgRNA to assess cell cycle lengths and general attributes of these pMMECs. We assessed infection efficacy and found at minimum 67-70% of the pMMECs were double-positive for eGFP and mCherry. In many of our studies, the transduction efficacy was high enough to enable analysis of >90% of all cells within the field of view. Our initial analysis of these Cas9 expressing pMMECs resulted in the observation that the majority of the cells harvested are quiescent, undergoing no cell cycle activity for the duration of

imaging (Figure 3.3C). We also clarified that co-transduction with the PCNA-mCherry promoter alone did not confer any discernible increases in proliferation capacity. To perform this analysis, we analyzed cells that remained within the field of view for the entire duration of imaging and recorded all observable cell cycle events. Cells that did not have any replication, birth, or mitotic events for the entirety of imaging were labelled as quiescent. In this manner we were able to evaluate the proliferation index of each imaging cohort.

Next, we assessed the proliferation index of pMMECs with Myc^{OE}, $Myc^{OE}Mre11^{ATLD/ATLD}$, $Myc^{OE}Trp53^{-/-}$, and $Myc^{OE}Trp53^{-/-}Mre11^{ATLD/ATLD}$ pMMECs (Figure 3.3C). With each manipulation we noticed a substantial increase in the proliferation index. Intriguingly, while the other alterations increased the proliferation index nominally, loss of Mre11 induced the most significant increase in proliferative capacity (Figure 3.3C). This proliferation index, in essence, converted what was essentially a largely quiescent population of cells into cells that were rapidly dividing. These results indicated that p53 loss and MRN deficiency were not epistatic to each other, and that MRN complex may have a separate critical function other that downstream p53 activation that may be contributing to this phenotype.

3.3.4. MRE11 Mediates A P53-Independent G2/M DNA Damage Checkpoint

To further understand what may be contributing to the difference in proliferation, we next decided to directly compare the $Myc^{OE}Trp53^{-/-}$ vs. $Myc^{OE}Trp53^{-/-}Mre11^{ATLD/ATLD}$ pMMECs. Due to prior observations of Mre11 mediating the radiation-induced G2 checkpoint, we evaluated the frequency of G2/M arrest in each cohort, and defined arrest as entry into G2 proceeded by a lack of mitotic cytokinesis or anaphase for at least ½ of

the imaging time (36 hours). These cells were more likely to be in permanent G2/M arrest rather than transient G2 delay. In this manner, we discovered that G2/M arrest frequency was 31% in cells with Mre11, whereas in pMMECs where Mre11 deficiency was established, the G2/M frequency was significantly lower at 4.8% ($p<0.01$, Fisher's Exact Test, Figure 3.3D).

To evaluate this further, we plotted the individual phase lengths of sgControl vs. sgMre11 pMMECs that were within the field of view for the entire duration of imaging (Figure 3.3E). Consistent with the observations of increased frequency of G2/M arrest, the length of G2 was significantly prolonged in the $Myc^{OE}Trp53^{-/-}$ pMMECs, and the mean G2 length was ~20 hours, whereas $Myc^{OE}Trp53^{-/-}Mre11^{ATLD/ATLD}$ cells entered G2 and completed mitosis within 10 hours, or roughly half the time (Figure 3.3E, $p<0.01$ by Student's t-test).

3.3.5. Mitotic Fates In MRE11 Deficiency

Due to the complexity of the imaging dataset and the diversity in mitotic outcomes seen, we sought to characterize the mitotic patterns observed. We sorted the events into 5 main categories: mitosis, aberrant mitosis, re-replication, G2 arrest, and mitotic catastrophe (Figure 3.4A). Of these, the last two categories are non-viable events that force cells to exit cell-cycle with no observable re-entry into cell cycle during imaging. The first three categories enable continuation of cell cycle with daughter cells that continue to exhibit cell cycle activity (Figure 3.4A). Aberrant mitosis was characterized by asymmetrical mitotic events with binucleated cells or multi-nucleated cells undergoing cytokinesis to give rise to viable daughters capable of entering S phase in the next cell-cycle (Figure 3.4A). Re-replication was particularly striking, in normal somatic cells

replication is contained to one contiguous period of time in which PCNA foci appear. However, in cells with re-replication, there are two or more periods of PCNA foci formation that are interspersed between periods of resolution which indicate entry into G2 phase (Figure 3.4A).

In the 2000's, the phenomenon of re-replication was thought to be primarily attributed to mis-licensing or mis-regulation of cellular replicasome complexes at origins, in large part due to aberrant Cyclin E activity[179]. However, in the past decade, extensive re-replication has been overserved in tumor cell lines with disruption of mammalian Cdt1 via over-expression[180]. Cdt1 is loaded onto chromatin in the absence of Cyclin E and is progressively destroyed during S phase to prevent re-replication. Fascinatingly, while over-expression of Cdt1 causes significant re-replication in tumor lines, it does not have the same effect in primary cells. Cimprich, Cortez, Vaziri, and Liu have shown in a series of critical papers that this is inability of Cdt1 over-expression to cause re-replication in primary cells is due to the presence of p53-, ATM- and ATR-dependent checkpoint responses[181–184]. Primary cells will inhibit re-replication even in the context of mis-regulation of licensing factors if the DNA damage response is activated and master kinases are engaged by long stretches of ssDNA that accumulate in under-replicated cells[182]. However, it is unknown whether these same mechanisms curtail re-replication during activation of oncogenes at early stages of neoplasia and additionally, it remains unclear if this checkpoint response is entirely p53-dependent or may have alternative activators in the absence of p53 in cancers.

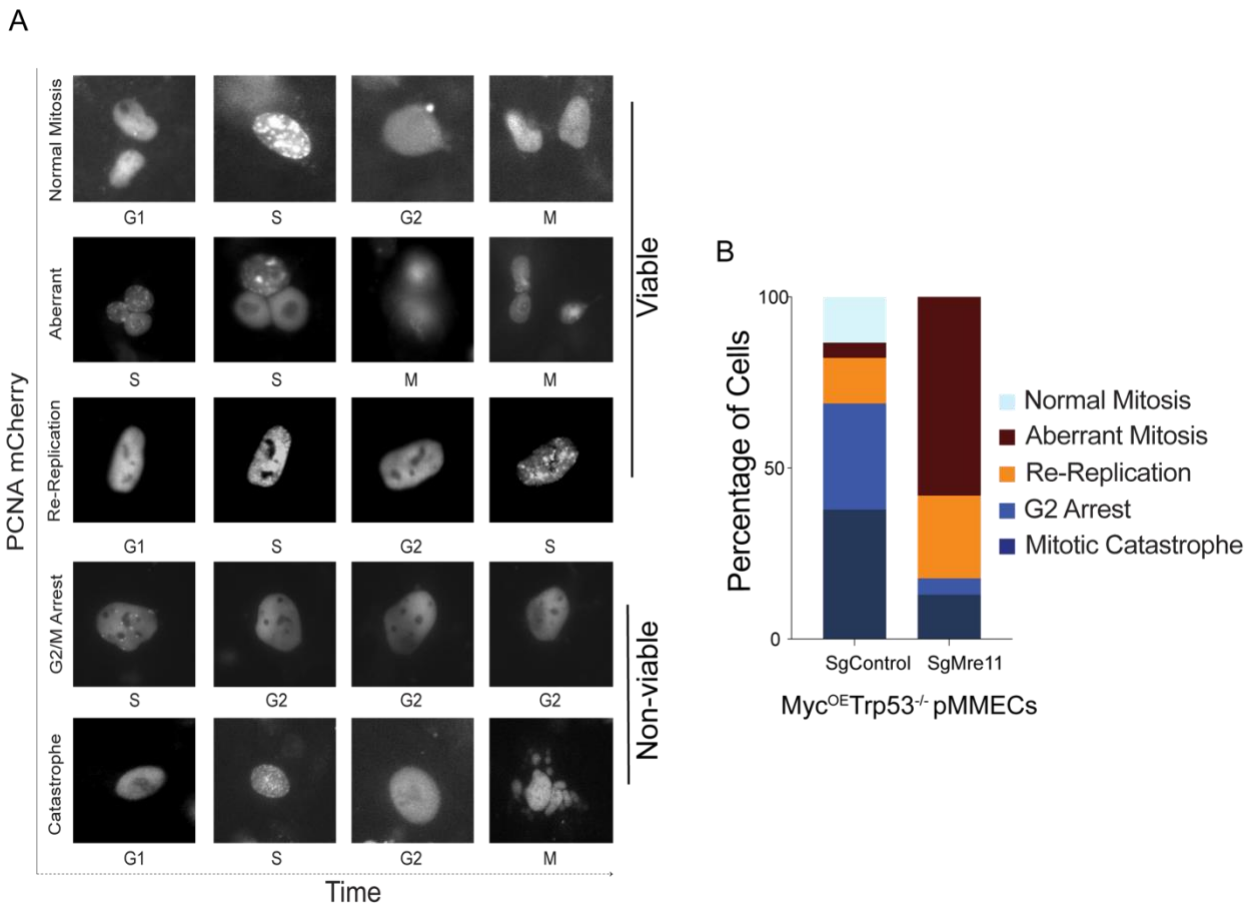

Figure 3.4 Mitotic Characterization of Mre11 Deficient pMMECs. A, Representation of 5 different mitotic cell fates that were utilized to characterize cells. The top three outcomes are viable outcomes that enable cells to continue to cell-cycle. The final two outcomes are terminal events such as permanent G2 arrest or mitotic catastrophe which induces cell death and nuclear degradation. B, Percentage of cells in each mitotic outcome. Normal mitosis was defined as mononuclear cells giving rise to 2 daughter cells post cytokinesis. Aberrant mitosis was characterized by asynchronous cell division or cytokinetic failure. Re-replication was defined as cells that re-entered S phase (induction of 2nd round of PCNA foci) post G2. G2/M arrest was quantified as entry into G2 >36 hours with no mitotic event. Mitotic catastrophe was characterized as mitosis with nuclear fragmentation and no subsequent cell-cycle activity (S phase or Mitosis) in daughter cell fragments. sgControl treated cell percentages are the following: 13.3% (normal mitosis), 4.4% (aberrant mitosis) 13.3%(Re-replication, 31.1% (G2 arrest), and 37.8% (mitotic catastrophe). sgMre11 treated cell percentages are the following: 0% (normal mitosis), 58.6% (aberrant mitosis) 24.2%(Re-replication, 4.8% (G2 arrest), and 12.9% (mitotic catastrophe).

Lastly, there are two non-viable cell cycle outcomes in our categorization scheme: extended G2 arrest and mitotic catastrophe (MC) (Figure 3.4A). G2 arrest has been previously described. MC has been defined in cell-cycle literature as an onco-suppressive, evolutionary strategy for eliminating mitosis-incompetent cells[185]. The ability to trigger MC in epithelial cells has also been a therapeutic endpoint for many anti-cancer drugs as it is an effective way to eliminate unstable cancer cells[54,132]. Therefore, the ability to undergo MC is a critical fail-safe against cancer progression and is thought to be distinct from anti-proliferation cascades such as senescence and apoptosis. The current consensus is that there are three broad manners in which MC occurs: (1) cells die without exiting mitosis by arresting interminably in mitosis (i.e. in Anaphase or metaphase), (2) reach G1 and fail to undergo replication (no sign of S phase foci), and undergo cell death immediately in the new daughter cell, and (3) *exit mitosis* and undergo senescence[185]. Utilizing these frameworks, we were visually able to accurately categorize cells that underwent MC (Figure 3.4A).

We quantitatively assessed what fraction of each of the $Myc^{OE}Trp53^{-/-}$ vs. $Myc^{OE}Trp53^{-/-}Mre11^{ATLD/ATLD}$ pMMECs underwent each of the 5 outcomes. The most prominent observation was that cells with MRN deficiency evaded mitotic catastrophe 3x more often and 82% of the population of cells viably continued to cell-cycle by aberrant means (Figure 3.4B). In contrast to this, in $Myc^{OE}Trp53^{-/-}$ cells, up to 70% of the population was eliminated via terminal cell-cycle events, in particular by mitotic catastrophe (Figure 3.4B). Of note, in cells with MRN deficiency, normal mitotic events were completely absent for all of the cells that were evaluated, indicating a high level of cell cycle and checkpoint de-regulation.

In summation, these analyses reveal a role for Mre11 in protecting against mitotic entry or triggering mitotic failure if the G2-checkpoint fails. Mitotic catastrophes in sgControl cells are likely to be triggered by the presence of under-replicated DNA entering mitosis. However, the abundance of aberrant mitoses in sgMre11 cells also indicate increased DNA damage and aneuploidy entering mitosis, but this damage is ineffectively transduced into mitotic elimination of the abnormal cells (Figure 3.4B).

3.3.6. MRE11 Deficiency Promotes Accelerated Mitotic Entry

The results of our previous experiments revealed Mre11 as a mediator of G2-M checkpoint and as a critical player in elimination of cells via mitotic catastrophe in early pre-neoplastic lesions. We wanted to understand how this regulation of mitotic entry related to genome stability in late-stage neoplasia. Moreover, we further wanted to quantify the exact magnitude of effect Mre11 had on mitotic progression and damage sustained in newly created daughter cells. TNBC is characterized by rampant genome instability, and we hypothesized that long-standing MRN deficiency promotes accelerated mitotic entry which then may lead to ongoing genome instability in these tumors. To study this, we utilized Mre11 deficient tumor lines derived from Cas9-Myc^{OE}-p53$^{-/-}$ mice (Figure 3.5A). The survival curves of this tumor induction study are still being collated and thus are not shown in this figure. We were able to utilize the first set of tumors formed to derive (2) Mre11 proficient and (3) Mre11 deficient tumor cell lines for the following studies (Figure 3.5B).

Using quantitative image-based cytometry (QIBC), we first quantified rate of mitotic entry via a S-M progression assay (Figure 3.5C). QIBC is a high-throughput platform for immunofluorescence (IF) based staining of cells to evaluate cell-cycle profiles en masse.

Cells are pulsed with EdU (to label S phase cells) for 30 minutes and then released into the mitotic synchronizing agent Nocodazole (NCD) or a DMSO control for up to 12 hours. At serial timepoints, cells are fixed and stained for nuclear content (DAPI), EdU (using Base-Click assay, see methods), and the mitotic marker H3-pS10 (phosphorylation of histone 3). Cells dually positive for the S phase and the mitotic markers at time of analysis are cells that have recently "progressed" from S phase to M phase (Figure 3.5C). We quantified the mitotic progression index at 0,3,6 and 12 h for Mre11 deficient vs. proficient cells in Figure 3.5D. Our results indicate that the rate of mitotic entry for Mre11 deficient cells is 5x greater than that of Mre11 deficient cells (Figure 3.5D, $p<0.0001$).These results highlight that this alone could account for the proliferation phenotype observed with Mre11 deficiency in prior studies.

Next, to link mitotic entry to genome instability, we assessed inherited DNA damage in daughter cells in the Mre11 deficient cohort. Recently, under-replicated DNA (UR-DNA) that has entered mitosis has been shown to be packaged into 53BP1 nuclear bodies that emerge in early G1 of next cell-cycle[114,186]. These nuclear bodies contain the UR-DNA and enable replication attempts to fix the UR-DNA or to separate it from the nuclear genome during the next replication phase[186]. Thus, 53BP1 nuclear bodies are an established marker for UR-DNA that is a result of DNA damage entering mitosis in replication stress induced cells. We synchronized our Mre11 deficient vs. proficient tumor cells in mitosis and performed an NCD shake-off to harvest mitotic cells and re-plate them. We then allowed these newly re-plated cells to enter mitosis over the next 2 hours and harvested these cells for QIBC analysis of 53BP1 bodies (Figure 3.5F). To eliminate cells that have already entered the next S phase, we used an EdU pulse at time of harvest.

This ensured that the cells analyzed would only have 53BP1 nuclear bodies due to UR-DNA and that we would not be detecting replication stress associated damage that was not inherited. To quantify these nuclear bodies, we plotted a frequency histogram of percent of cells with n number of 53BP1 bodies per nucleus (Figure 3.5G). Our results show that 10% of newly generated daughter cells without Mre11 have at least 1 nuclear body (Figure 3.5G). In comparison, ~1% of cells with Mre11 have any 53BP1 bodies (Figure 3.5G). Strikingly, only Mre11 deficient cells were found to harbor >1 53BP1 nuclear body per nucleus, an indicator of high levels of UR-DNA (Figure 3.5G).

These results implicate Mre11 deficiency as a promoter of ongoing genome instability in tumors and link the checkpoint functions of Mre11 directly to its role in genome maintenance. Two recent publications have implicated that ATR-inhibitors accelerate mitotic entry[112,187]. It is likely that Mre11 is upstream of ATR kinase activation and may mediate this mitotic checkpoint through ATR and its downstream targets. As a result, future directions of this project should evaluate ATR-inhibitors and assess whether Mre11 deficient cells are sensitive to inhibitor treatment.

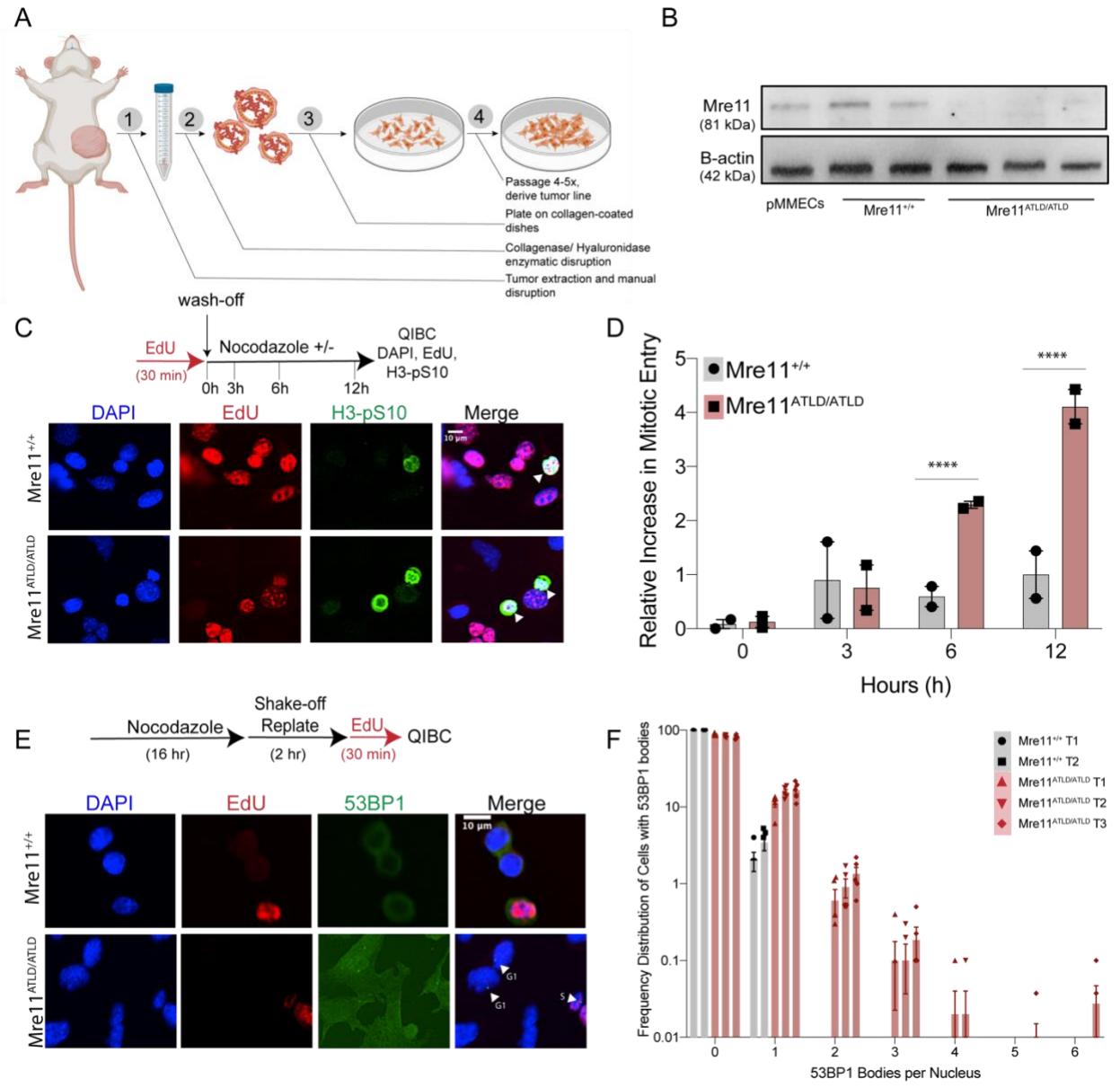

Figure 3.5 : Mre11 Deficiency Promotes Ongoing Genome Instability in Daughters. A, Stable cell line generation of murine mammary tumors. B, Western blot of 2 Mre11+/+ mammary tumors, and 3 Mre11 deficient mammary tumors. As a positive control, lysate from pMMECs was used. C, Quantitative Image Based Cytometry (QIBC) assay for assessment of S-M Progression of cells. Tumor cells were pulsed with 10uM EdU for 30 minutes and washed with PBS. 100ng/ ml Nocodazole (NCD) was added to the treatment cohort. Cells were harvested immediately after wash-off, 3h, 6h, and 12 h post release into NCD or DMSO control and fixed with 2% Paraformaldehyde for staining. Cells were stained with DAPI (DNA content), Alexa-Fluor 637 (BaseClick assay for EdU detection of S phase cells) or H3-pS10 (mitotic marker). Cells dually positive for EdU and H3-pS10 are cells that have recently entered mitosis after completing S phase. D, Quantification of the QIBC S-M progression assay, each datapoint is 5000 cells and an independent biological replicate. Relative increase in mitotic entry was normalized to %Edu and H3-

ps10 dual positive cells in the Mre11+/+ cohort at 12 hours. p<0.0001=**** E, 53BP1 Nuclear Body Assay for detection of transmission of under-replicated (UR-DNA) through mitosis into early G1 of daughter cells. Cells were treated with NCD for 16 hours and mitotic cells shaken-off and replaced for 2 hours to encourage entry into G1. Cells were pulsed with EdU to eliminate S phase cells in analysis, and stained for 53BP1. F, Quantification of E, each datapoint is 500 (Mre11+/+ cells) and 1500 (Mre11ATLD/ATLD cells). Frequency of cells with 0-6 53BP1 bodies per cell were evaluated and shown in logarithmic scale.

3.3.7. Nuclear Aberrancies In MRE11 Deficient Cells

The benefit live-cell imaging in experimental studies is the rich nature of the visual dataset itself. One striking observation that occurred during the blinded analysis of the imaging datasets was the prevalence of Polyploid Giant Cancer Cells (PGCCs) in all imaging beacons monitoring Mre11 deficient pMMECs (Figure 3.6A vs. B). PGCCs have been observed in clinically aggressive, metastatic breast cancers on tissue pathology and are indicators of high levels of chromosomal instability[188]. In contrast to these PGCCs, the sgControl treated pMMECs were characterized by large factions of quiescent fragmented nuclei (no S phase foci observed) (Figure 3.6A). The polyploid nature of the cells with MRN deficiency was also specific to pMMECs with p53 deficiency, i.e. this was not observed in the pMMECs with Myc^{OE} alone. The PGCCs in our study were characterized by their ability to continue proliferating through cell cycle even with highly aberrant nuclear structures (in the Mre11 deficient cohort, Figure 3.6B). States of aneuploidy have previously been described in cells with p53 loss; however, it is unclear how PGCCs tolerate continued cellular survival with visible genome instability and nuclear abnormalities.

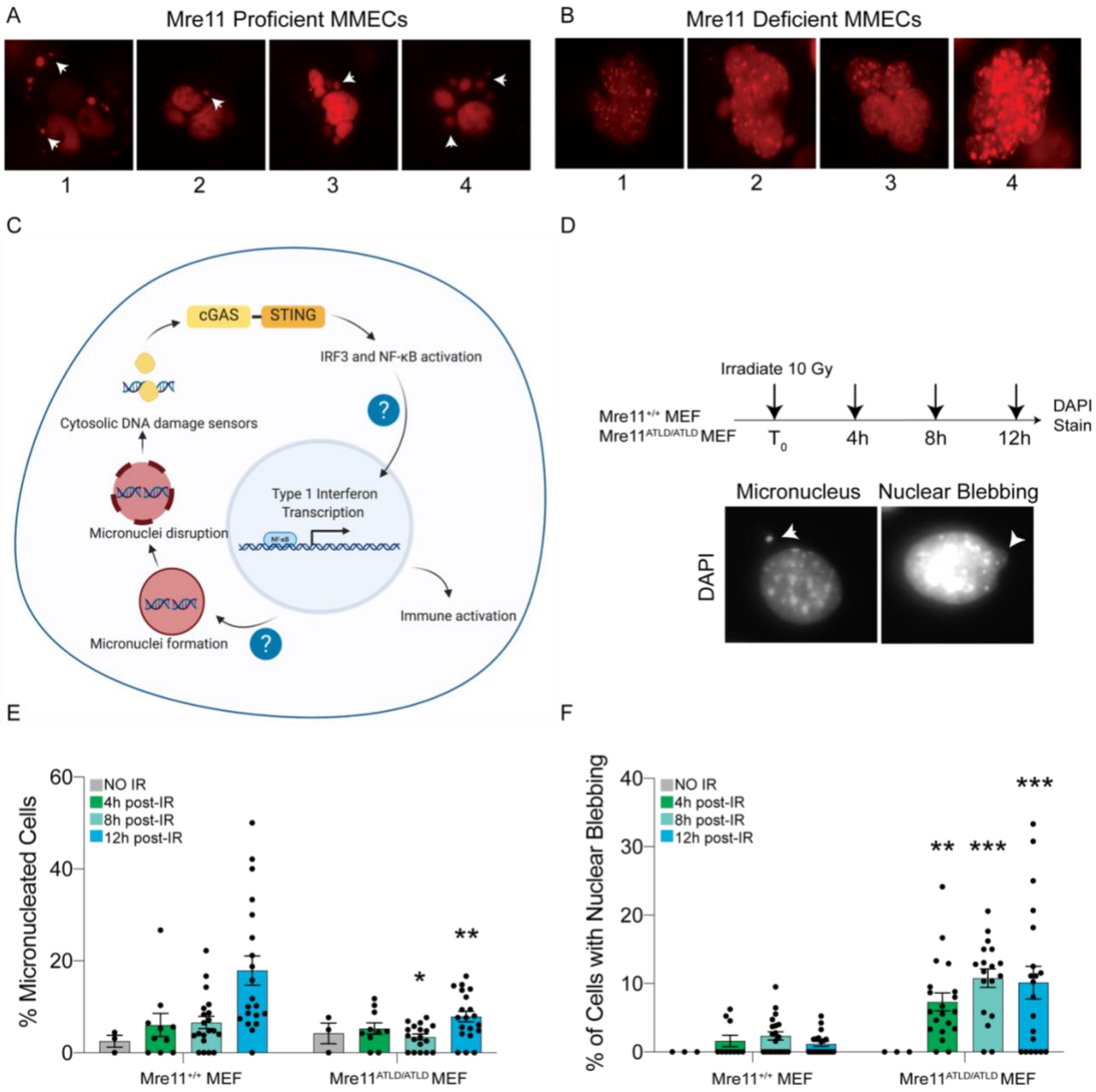

Figure 3.6 : Mre11 Deficiency Impairs Micronucleus Formation. A, sgControl MMECs from live-cell imaging, 4 examples of cells with micronuclei (arrows). B, sgMre11 MMECs from live-cell imaging, the foci indicate these are S phase cells, 4 examples shown. C, Diagramatic depiction of micronucleus mediated interferon signaling. The question marks indicate scientific unknowns regarding MN formation and IRF3 activated Type 1 interferon transcription in Mre11 proficient vs. deficient cells. D, Experimental set-up for the micronucleus formation assay. Mouse embroynic fibroblasts (MEFs) were irradiated at 10Gy and harvested immediately after, and up to 12 hours post irradiation, and stained with DAPI and imaged. Panels show examples of distinct micronucleus (left) and nuclear blebbing (right). E, Mre11 +/+ vs. ATLD/ATLD MEFs were evaluated for MN formation. Each datapoint is the average % micronucleated cells in an imaging beacon (n=25-50

cells/ beacon). Images from 3 different biological replicates per genotype were pooled for blinded analysis. $p<0.05$ = *, $p<0.01$ = **. F, Mre11 +/+ vs. ATLD/ATLD MEFs were evaluated for nuclear blebbing and nuclear membrane protrusions. Each datapoint is the average % cells with nuclear blebbing in an imaging beacon (n=25-50 cells/ beacon). Images from 3 different biological replicates per genotype were pooled for blinded analysis. $p<0.01$ = **, $p<0.001$=***.

To evaluate this, we studied the quiescent sgControl cells that are undergone MC and noted that these cells contained prominent, discrete cytoplasmic fragments of nuclear material. Micronuclei (MN) are nuclear segments that are present in the cytoplasm of cells, and often contain DSBs or other genomic fragments (white arrows, Figure 3.6A)[189]. How they are formed has become a topic of active investigation in the past five years. To begin, micronuclei have a close association with genome instability and chromosomal re-arrangements; particularly chromothripsis[190]. Chromothripsis is a type of genomic instability where cells undergo rapid genome re-rearrangements and chromosomal breakages within a matter of several cellular divisions, creating a punctuated model for cancer evolution. This type of genome chaos is advantageous as it offers cells the ability to accumulate a large mutational burden in a short amount of time. There are two main theories about the link between micronuclei and genome instability. One, during chromothripsis, large deletions or chromosomal fragments may be incurred by the cell which are then packaged as micronuclei. Two, genome fragments that are already present in micronuclei may undergo partial replication which are then re-integrated into the nuclear genome resulting in copy number abnormalities[190]. Both theories are not mutually exclusive and there is overall consensus that cells with high levels of genome instability are likely to have micronuclei and that MN formation can also be exogenously induced by irradiation.

In the pMMECs with Mre11 deficiency, the prevalence of micro-nucleated cells was rare, even though many of the cells were multi-nucleated (Figure 3.6B). We hypothesized that Mre11 complex formation may be required for micronuclei formation. To assess this, we used mouse-embryonic fibroblasts (MEFs) with Mre11-ATLD1 mutations to assess micronuclei formation and signaling (Figure 3.6C). These $Mre11^{ATLD/ATLD}$ MEFs were exposed to irradiation (a well-known inducer of MN) and their ability to form micronuclei was compared to WT (Mre11+/+) MEFs (Figure 3.6D). In our studies, $Mre11^{ATLD/ATLD}$ MEFs were unable to form micronuclei for up to 12 hours post radiation (Figure 3.6E). Furthermore, while micronuclei formation was reduced in the $Mre11^{ATLD/ATLD}$ MEFs, nuclear blebbing (where the nucleus protrudes due to loss of contiguous nuclear membrane against the nucleoplasm) was highly prevalent (Figure 3.6F). Nuclear membrane blebbing has also been described as a precursor step to micronuclei formation; however, here the $Mre11^{ATLD/ATLD}$ cells are unable to form micronuclei after this step. This supports the hypothesis that complex function is required for micronuclei formation.

3.3.8. MRE11 Mediates Micronucleus Formation in Response To Radiation

The presence of MN is often associated with senescence and elimination of chromosomally unstable cells by the innate immune system as MN often activate cytoplasmic damage sensors[189]. Cytosolic DNA has been a marker for cellular infection by viral pathogens. Thus, a host of inflammatory cytokines are activated by the presence of cytoplasmic dsDNA. Cytosolic sensors of DNA damage have recently come to attention due to their ability to enhance the effects of radiation in what is known as the “abscopal effect.” Simply defined, the abscopal effect is the observation that a tumor focus outside

of the field of irradiation is impacted by radiotherapy. Irradiation induces MN formation and thereby activates inflammatory cascades that produce chemokines which in turn trigger phagocytic innate immune cells[101] (Figure 3.6A). In this manner, the immune system is a key player in the abscopal effect. We performed several experiments to assess whether Mre11$^{ATLD/ATLD}$ MEF cells could trigger an interferon response to radiation. We hypothesized that Mre11$^{ATLD/ATLD}$ MEFs would mount a less robust interferon response to irradiation compared to WT MEFs.

3.3.9. MRE11 And Interferon Signaling

To assess whether Mre11$^{ATLD/ATLD}$ MEFs were able to induce an interferon (IFN) response, we performed RT-qPCR experiments evaluating transcription of IFNB1 and Interferon Stimulating Gene (ISG) post irradiation (Figure 3.7A). Our experiments indicate the Mre11$^{ATLD/ATLD}$ MEF cells are unable to mount a robust interferon response to irradiation in contrast to WT MEFs (Figure 3.7B). Subsequently we attempted to abrogate the WT MEF response with both a commercially available Mre11 inhibitor (Mirin) and an inhibitor to the downstream kinase ATM (ATMi) (Figure 3.7C,D). Treatment with Mirin did not reduce the interferon response in WT MEFs, suggesting that the Mre11 exonuclease inhibited by Mirin is not responsible for interferon responses (Figure 3.7C). Treatment with ATMi increased the interferon response noted in WT MEFs, suggesting that ATMi therapy may increase cytosolic dsDNA concentrations or further enable interferon signaling (Figure 3.7D). Further reconstitution experiments with various mutations of Mre11 will help delineate the exact function of Mre11 that is required for both micronucleus formation and subsequent interferon signaling.

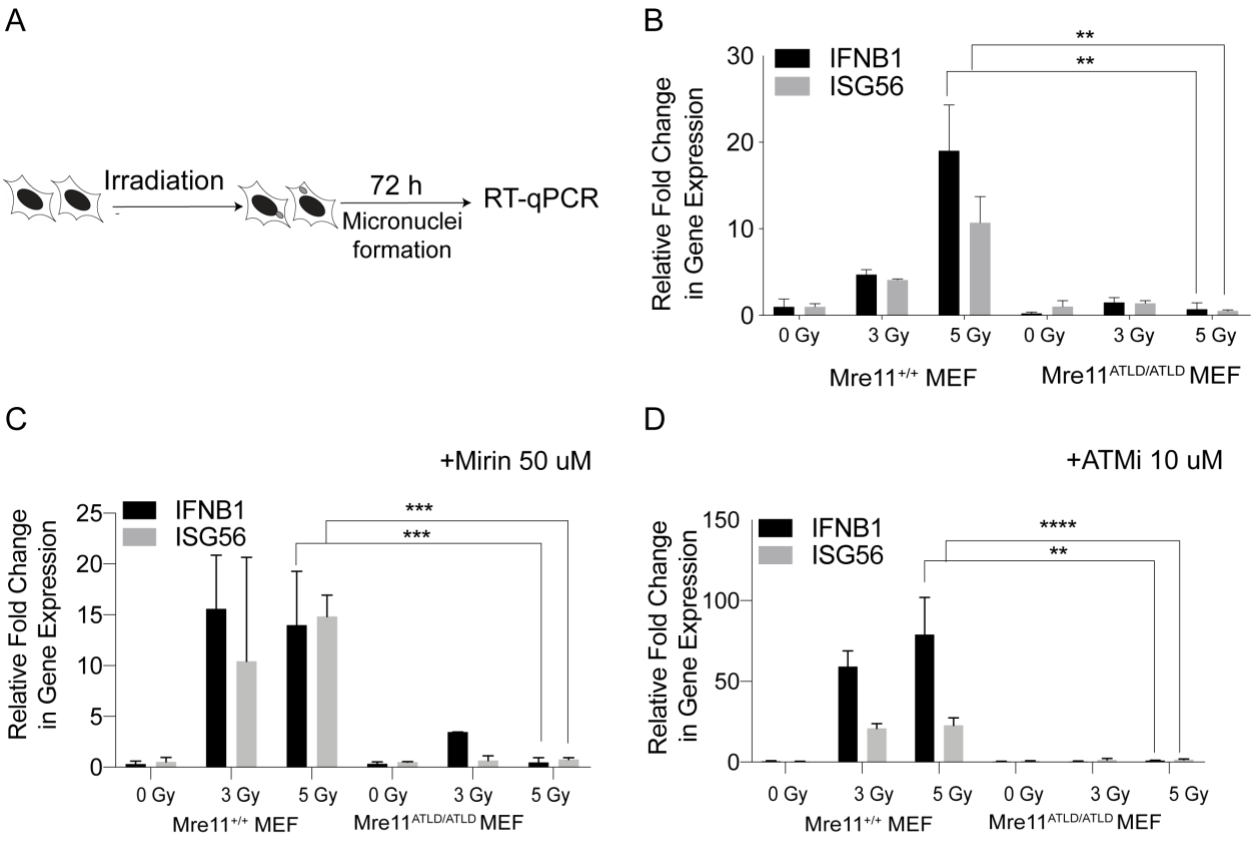

Figure 3.7 : Mre11 Deficient Cells have Impaired Interferon Signaling. A, Schematic describing the irradiation IR) induced micronucleus formation assay. 1x10^6 cells are plated in a 10cm dish 24 h prior to irradiation and media changed prior to IR. Cells are irradiated at 3 or 5 Gy and placed in 37C incubator for 72 hours for MN formation through mitosis. Cells are trypsnized and RNA extracted for cDNA synthesis and RT-qPCR. B, Irradiation induced Interferon B1 (IFNB1) and Interferon Stimulating Gene 56 (ISG56) transcriptional up-regulation in WT (Mre11+/+) MEFs compared to ATLD/ATLD MEFs. $p<0.01$ = **, results are average n=3 biological replicates. C, Cells were pre-treated with 50 uM Mirin (Mre11 inhibitor) 2 hours prior to irradiation. $p<0.001$ = ***., results are average n=3 biological replicates. C, Cells were pre-treated with 10 uM ATMi (KU55933) 2 hours prior to irradiation. $p<0.0001$ = ****, and $p<0.001$ = *** results are average n=3 biological replicates. Statistical analyses performed with Student's t-test

As we encountered these results, we additionally challenged the Mre11$^{ATLD/ATLD}$ deficient cells with a variety of classical interferon inducing agents to see if we could alter the IFN response in these cells compared to WT MEFs (Figure 3.8A). Due to several patient case reports of MRE11 mutations resulting in auto-inflammatory syndromes and new publications on cytosolic binding partners of Mre11, we hypothesized that Mre11

may have a cytosolic role in binding to dsDNA and initiating immune responses. We transfected dsDNA and ssDNA (as control) from Herpes Simplex Virus (HSV), Vaccinia Virus (VACV), and Interferon Stimulating DNA (ISD) into Mre11$^{ATLD/ATLD}$ vs. WT MEFs and measured interferon transcriptional responses (Figure 3.8B-D). These agents are often used by immunologists to trigger interferon responses in cells[191]. Intriguingly, the Mre11$^{ATLD/ATLD}$ MEFs significantly underperformed in their ability to induce transcription of IFNB1 by all three agents (VACV, ISD, and HSV) compared to the WT MEFs (Figure 3.8B-D, left panels). VACV also induced a significantly different ISG56 response in Mre11$^{ATLD/ATLD}$ vs. WT MEFs, while ISD and HSV induced differential responses with respect to ISG56 (Figure 3.8B-D, right panels). In summary, these results indicate that Mre11$^{ATLD/ATLD}$ cells have a functional deficiency in triggering interferon B1 signaling in response to cytosolic dsDNA from classical interferon stimulating agents.

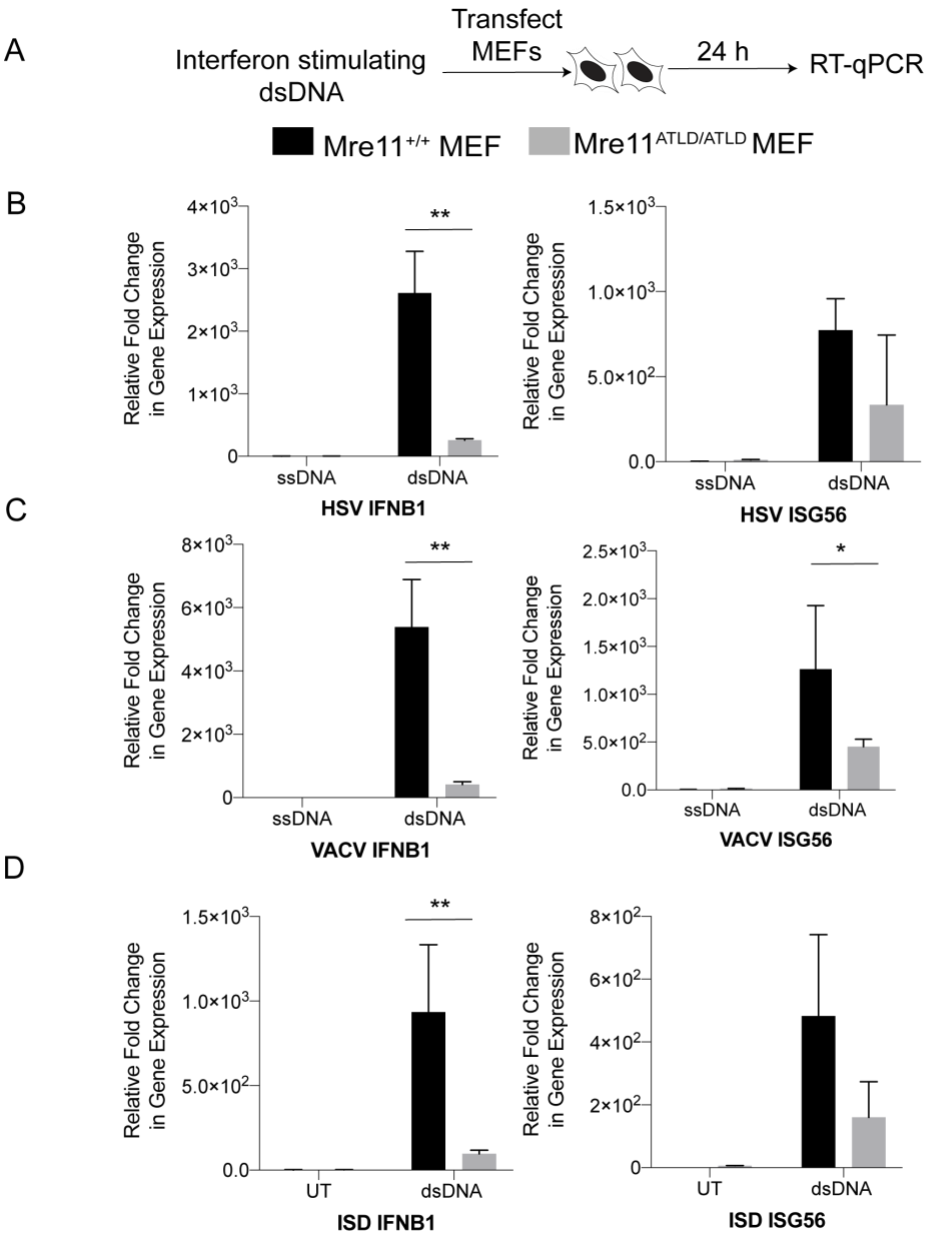

Figure 3.8 : Mre11 Deficient Cells have Functional Defects in Response to Classical Interferon Stimulating Agents. A, Schematic for RT-qPCR experimental set-up. Interferon stimulating dsDNA was transfected into 1x 10^6 mouse embryonic fibroblasts (MEFs) utilizing Lipofectamine 3000. 24 hours post transfection, cells were harvested and RNA extracted using Qiagen RNeasy Kit. RT-qPCR for two interferon stimulating genes were performed: interferon B1 (IFNB1) and interferon Stimulating Gene 56 (ISG56). B, RT-qPCR data for interferon response to transfected Herpes Simplex Virus (HSV) dsDNA, with ssDNA as negative control. dsDNA was created annealing ssDNA oligos.(p=0.002, IFNB1 and p=0.1, ISG56) C, RT-qPCR data for interferon response to transfected Vaccinia Virus (VACV) dsDNA, with ssDNA as negative control. (p=0.003, IFNB1 and p=0.0556 ISG56) D, RT-qPCR data for interferon response to transfected Interferon Stimulating DNA which is exists as duplex DNA. For this experiment, RNA from

untransfected (UT) cells was used as a negative control. (p=0.011, IFNB1 and p=0.066 ISG56). For all RT-qPCR experiments, the left panel (IFNB1) and the right panel (ISG56). Data from n=3 replicates are shown with +/- error.

In conclusion, our utilized a systematic *in vivo* DDR CRISPR library screen which revealed Mre11 to be a critical DDR gene in tumor suppression during early neoplasia. We then validated the results of the screen and investigated prior phenotypes associated with Mre11 deficiency to assess the role of Mre11 in regulating cell-cycle in pre-neoplasia. Our results highlight a key role for Mre11 in regulating G2-M checkpoint in response to oncogenic induction. This G2 checkpoint function is independent of p53-activation and is critical for restraining mitotic entry. Moreover, the same mechanism contributes to the loss of genome stability seen in Mre11 deficiency and as mitotic entry of UR-DNA is inherited by daughter cells in early G1 53BP1 nuclear bodies. Thus, Mre11 not only curtails initial tumor proliferation but also prevents ongoing genome instability in murine models of TNBC. Following close assessment of nuclear abnormalities seen in live-cell imaging, we reveal a novel interaction with Mre11 deficiency and micronucleus formation. Mre11 deficient cells have impaired formation of MN in response to radiation and importantly, lack functional interferon signaling that is critical for *in vivo* recruitment of innate immune cells and also for the abscopal response to radiotherapy. These results pave the way for future studies that investigate the clinical relevance of using DNA damage checkpoint inhibitors like ATRi and immune profiling in Mre11 deficiency with particular relevance of clinically, aggressive human TNBCs.

3.4. Materials and Methods

3.4.1. Cell Lines

WT and ATLD/ATLD Mouse Embryonic Fibroblasts (MEFs) were SV-40 large T antigen immortalized[12,20,22]. 293T cells were purchased from ATCC (CRL11268). These cell lines were maintained in Dulbecco's modified Eagle's medium (DMEM), with 10% Bovine Calf Serum (Hyclone BCS) and 2 mM L-glutamine (ThermoFisher). LA-7 cells were obtained from ATCC (CRL2283) and were maintained in DMEM/F12 medium supplemented with 10% fetabl bovine serum, 20mM HEPES, and 10ug/ml Insulin. LA-7 cells are irradiated at 70 Gy ionizing radiation using a Rad Source R2000 irradiator prior to use as feeder cells in experiments with primary mammary epithelial cells. All cells were maintained at 37 °C in an atmosphere of 5% CO_2. Cells in culture were routinely monitored for mycoplasma contamination using the Plasmo Test™ (Invivogen).

3.4.2. Primary Murine Mammary Epithelial Cells

pMMECs were grown as previously described in PMID: ***. were derived by harvesting the 4th and 5th mammary glands from 6-week-old female transgenic mice with the desired genotype. Glands were manually disrupted using surgical scissors and were incubated in Liberase digestion medium (EpiCult-B Mouse Medium Kit (Stem Cell Technologies, 285 Units Collagenase Type 3 (Worthington), 20mM HEPES (GIBCO), 20 ug/mL Liberase Blendzyme 2 (Roche) and shaken (vertically) at 37 ^{o}C overnight. The overnight digests were then spun down and resuspended in 3 mls trypsin with EDTA and 1000U DNase and incubated at 37 ^{o}C for 5 min. DMEM with 10% serum was used to quench the enzymatic digest. Cells were spun down and resuspended in 10U Dispase (Stem Cell Technologies) and 1000U DNase I (Worthington Biochemical) and incubated

at 37 ^{o}C for 5 min. Cells were washed twice with LA-7 medium and the resulting cells were resuspended in EpiCult-B Mouse Medium Kit (Stem Cell Technologies) and seeded onto Cultrex 3D-Culture Matrix (Trevigen) coated 6 well plates. To coat the 6-well plates, the 3D-culture collagen was mixed with 10mM Acetic Acid (at ratio specified by manufacture) and incubated for 40 minutes and washed 3x with PBS. For longer term cell growth experiments, pMMECs were seeded on lethally irradiated LA-7 cells and cultured in LA-7 medium. For cells that require viral transduction for experimentation purposes, pMMECs are infected for 48 hours in isolation after which cells are washed and grown for an additional 24 hours prior to trypsinization and addition to LA7 cells for long-term culture. All cells were cultured to 80% confluence then passaged by trypsinization. Cells were tested monthly for mycoplasma using PlasmoTest Kit.

3.4.3. DDR CRISPR Library

The sgGuide pooled library was previously published with sgGuide sequences on PMID: . The CRISPR library sgRNAs were PCR amplified using AmpliTaq Gold® 360 DNA Polymerase (ThermoFisher) with forward primer ArrayF and reverse primer ArrayR followed by PCR purification (Qiagen) to then use for Gibson Cloning. The CRISPR library cassette was cloned into lentiCRISPRV2-Lumifluor (derived from lenti-CrisprV2a gift from Feng Zhang, Addgene plasmid # 52961, see cloning). Post- the Gibson reaction, we transformed the plasmid into Endura Competent cells via electroporation and plated into twelve, 10 cm petri dishes (VWR) containing LB agar (ThermoFisher) with 100 µg/ml carbenicillin (ThermoFisher). Colonies were selected and combined for DNA extraction (Qiagen). The presence of the sgRNA was verified by Sanger sequencing using the ArrayF primers.

3.4.4. Viral Production And Infection

HEK 293T cells were transfected with viral packaging plasmids: psPax2 (Addgene #12260) and pMD2.G (Addgene #12259) using Linear Polyethlenimamine (PEI) and the desired plasmid containing sgRNA. 16 hours post transfection, cells were washed, and supernatant collected at 48h and 72h. Pooled supernatant was spun to eliminate cellular debris at 1000xg for 5 minutes and subsequently filtered at 0.45 um. To concentrate lentivirus, filtered supernatant was spun at 21,000 rpm for 2 hours at 16 ^{o}C. Post spin-down, the remaining media was removed and the viral pellet resuspended in 1:100th of initial volume in PBS overnight at 4 ^{o}C. Virus was then aliquoted into Eppendorf tubes in and stored in -80 ^{o}C until use. Viral aliquots were then thawed right before use to avoid freeze-thaw cycles.

3.4.5. Transgenic Mouse Models

Mice used in this study were previously described in PMID# were housed in the Division of Comparative Medicine at the University of North Carolina at Chapel Hill. R26LSL-Cas9 (JAX#024857) and R26LSL-MycOE (JAX#020458) transgenic mouse strains were obtained from the Jackson Laboratory. Trp53fl/fl mouse strains were gifts from the Perou laboratory, and originally obtained from the Frederick National Laboratory for Cancer Research (Strains #01XC1 and #01XC2). To create the desired genotype, R26LSL-Cas9 mice were crossed to R26LSL-MycOE to first create Cas9-MycOE mice which were then finally crossed to Trp53fl/fl to create R26Cas9/Cas9-MycOE-Trp53fl/fl female mice.

3.4.6. DDR In-vivo CRISPR Screen Tumor Generation

For the DDR In-vivo CRISPR screen, six to twelve-week-old female R26Cas9/Cas9-MycOE-Trp53fl/fl mice received bilateral intraductal injections, into the fourth mammary gland of LentiCRISPR-Cre-V2-DDR-Lumiflour lentivirus. Each gland received 10ul of virus into the ductal tree, fore ease of injection, virus was dyed with Evan's Blue powder. The intraductal injections were performed by Dr. Brian Cooley of the UNC Animal Surgery Core.

3.4.7. MYC-P53 Tumor Survival Studies

For tumor induction studies for the Mre11 deficiency vs. proficiency survival study, six to twelve-week-old female R26Cas9/Cas9-MycOE-Trp53fl/fl mice received bilateral intraductal injections, into the fourth mammary gland, containing 5x10^5 transduction units (TU) of either LentiCRISPR-Cre-V2-sgControl-Lumifluor (Cre-sgControl) or LentiCRISPR-Cre-V2-sgMre11-Lumifluor (Cre-sgMre11).

3.4.8. Tumor Harvest and Stable Cell Line Generation for all Tumor Studies

Tumor harvest guidelines used in this protocol were originally obtained from PMID# with. Mouse cohorts were bilaterally palpated for the development of mammary tumors twice weekly, and three times weekly after mammary tumors had formed to monitor tumor size. Mice were euthanized when tumors reached > 15 mm in size on either gland and in accordance with UNC Institutional Animal Care and Use Committee (IACUC) guidelines. At necropsy, each mammary tumor was sectioned into four pieces. Two pieces were banked as fresh frozen tissue for future studies and RNA/DNA extraction. One section (the part attached to gland 5) was fixed in 4% paraformaldehyde and processed for paraffin embedding and H&E staining (Histoserv Inc.). This ensured that a

non-injected control (Gland 5) would be present for histology analysis in the same sample. The final piece was taken for tumor line creation. The tumor pieces were mechanically disrupted using surgical blades on sterilized glass petri dishes to remove lipidaceous tissue. Tumor pieces were incubated in digestion medium (DMEM, 10% FBS, 1mg/ml Collagenase Type 3, 1mg/ml Hyaluronidase) and shaken (horizontally) at 37 ^{o}C for four hours. The resulting digestion was spun down and resuspended in trypsin with DNase and incubated at 37 ^{o}C for 5min. DMEM with 10% FBS was added to neutralize the trypsin. Cells were spun down and resuspended in Dispase and deoxyribonuclease and incubated at 37 for 5min. Cells were washed twice with 10% FBS in DMEM and passed through a 70 mm filter. The resulting cells were resuspended in LA-7 media and immediately seeded into co-culture with irradiated LA-7 feeder cells. The cells were cultured over 10 passages and analyzed via flow for GFP expression to monitor tumor cell outgrowth. Tumor lines were then utilized for downstream assays when GFP expression reached >90%.

3.4.9. Cloning

3.4.9.1. Lenticrispr-Cre-V2-Sgrna Plasmid

LentiCRISPR-Cre-V2 plasmid was previously described in (Cell Reports Paper PMID#). Using BSMB1 restriction sites, short-guide RNA sequences for a 53BP1 intron sequence (sgControl) and Mre11^{ATLD} (sgMre11) were inserted into the sgRNA scaffolding region.

3.4.9.2. Lenticrispr-Cre-V2-Sgrna-H2b-Gfp Plasmid

LentiCRISPR-Cre-V2-Lumifluor plasmid was previously described in (Cell Reports Paper PMID#). To insert H2B-GFP into the region we created a geneBlock (IDT) H2B fused to GFP using a sequence from a published H2B-GFP plasmid on Addgene (#11680). Using PCR based amplification of the LentiCRISPR-Cre-V2-Lumifluor plasmid, we used Gibson cloning (HiFi DNA Assembly Master Mix; NEB) to replace Lumifluor with H2B-GFP.

3.4.9.3. Immunofluorescence

Cells were fixed with 3% Paraformaldehyde for 15 min at RT, followed by permeabilization with 0.25% TritonX-100 in PBS. Cells were subsequently processed for immunostaining experiments using the antibodies listed below. For experiments in which S phase cells were imaged, cells were treated with 10uM EdU pulse for 30 minutes and washed 1x with PBS. Nuclei were visualized by staining with DAPI. The primary antibody used was 53BP1 (1:500 for immunofluorescence, Bethyl, A300-272A). The secondary antibodies were: FITC Goat Anti Rabbit IgG (H + L) (1:500, Jackson ImmunoResearch, 111-095-144).EdU was detected using the EdU-Click 647 Protocol (BaseClick). Images were acquired using the GE IN CELL 2200 high through-put imaging system at 20x magnification.

CHAPTER 4 – CONCLUSIONS

The research reported here identifies a novel role for the MRN complex in activating a p53-independent, G2/M checkpoint in response to oncogenic replication stress in pre-neoplastic lesions. We highlight the distinct mitotic phenotypes that cells with or without MRN deficiency incur. The presence of MRN is correlated with increased arrest frequency and catastrophic mitoses, suggesting that MRN is actively involved in eliminating cells with DNA damage via cell-cycle regulation. We demonstrate that MRN deficiency increases mitotic entry and results in propagation of replication stress into 53BP1 nuclear bodies in the early G1 phase of daughter cells. These results resolve the mechanism by which MRN deficiency gives rise to both a proliferative advantage and ongoing genomic instability.

In Chapter 3, we shed insights into how MRN complex may also have a role in tumor immunity. Our data indicate that MRN complex deficient cells have a functional defect in micronucleus formation which may have *in vivo* consequences for innate immune signaling and abscopal responses to radiotherapy. Interestingly, our data demonstrate that these cells may also have a defect in interferon responses. While this data is intriguing, the relationship between the DDR and the immune system is complex and more research is necessary to gain a better understanding of how the MRN complex functions to gives rise to micronuclei and helps to signal the presence of cytoplasmic DSBs. To do this, re-constitution experiments in MRN deficient lines with various

functional mutants (e.g. nuclease dead) of Mre11 are required to understand which functions of Mre11 are essential for micronucleus formation. Furthermore, immune profiling of MRN deficient tumors is also necessary to clarify whether the lack of interferon response is translates into reduced immune infiltration *in vivo.*

This dissertation also explored altered DNA damage responses in p53-deficiency. Currently, there is no consensus to explain why p53 deficiency in cells leads to resistance to DNA damaging therapy; even though the observation of therapeutic resistance has been documented for many decades. In Chapter 2, we demonstrate that p53 deficient cells have hyperactive end-joining repair capacities that render them less vulnerable to radio-mimetic drugs and by extension, other double strand break inducing agents. Using live-cell imaging we examine the accelerated repair of DNA damage foci in p53-deficient cells. Partial sensitivity to DSB-inducing agents can be restored with DNA-PKi treatment, which inhibits the key master regulatory kinase in the NHEJ pathway. Treatment with DNA-PKi promotes mitotic catastrophe in p53-deficient cells. However, some cells still escape cell-death. In these cells, we determined that up-regulated Polymerase Theta expression and alternative end-joining repair mediate resistance to DNA-PKi. Finally, combinatorial suppression of DNA-PK and Pol-Theta restores radiosensitivity of p53-deficient cells to the same level as p53 wildtype cells.

Clinically, our results indicate that the therapeutic benefit of radiotherapy in p53-deficient cancers can be potentiated with the use of DNA-PKi. Recent clinical reports have shown that p53 pathway alterations predict radioresistance in aggressive pediatric Diffuse Intrinsic Pontine Gliomas. Preliminary assessment of Rhabdomyosarcoma and Ewing Sarcoma (ES) patients in the MSK-IMPACT dataset identified an increased risk for

inferior irradiated tumor control in pediatric patients with p53-pathway mutations. To explore the therapeutic ramifications of our studies, future experiments should compare the efficacy of pre-treatment with DNA-PKi before radiotherapy to radiotherapy treatment alone in sarcoma cell lines and eventually, in *in vivo* mouse models of ES. Our results suggest that dual treatment may potentiate radiosensitivity only in p53-deficient cancer cell lines. DSB inducing chemotherapies present another therapeutic context in which end-joining repair is crucial, and should also be evaluated in combination with DNA-PKi treatment. Moreover, the current development of the first inhibitors to Polymerase-theta creates an exciting landscape to evaluate the use of DNA-PKi in combination with these newly synthesized compounds. Finally, as many DNA-PKi compounds are currently being evaluated in clinical trials as radiosensitizing agents, these results pave the way for potential selection criteria to determine which patients may benefit from these small molecular inhibitors.

BIBLIOGRAPHY

1. Davis, A., Gao, R. & Navin, N. Tumor evolution: Linear, branching, neutral or punctuated? *Biochim. Biophys. Acta - Rev. Cancer* **1867**, 151–161 (2017).

2. Nowell, P. C. The clonal evolution of tumor cell populations. *Science (80-.).* **194**, 23–28 (1976).

3. Kalimutho, M. *et al.* Patterns of Genomic Instability in Breast Cancer. *Trends in Pharmacological Sciences* **40**, 198–211 (2019).

4. Sansregret, L., Vanhaesebroeck, B. & Swanton, C. Determinants and clinical implications of chromosomal instability in cancer. *Nature Reviews Clinical Oncology* **15**, 139–150 (2018).

5. Dagogo-Jack, I. & Shaw, A. T. Tumour heterogeneity and resistance to cancer therapies. *Nature Reviews Clinical Oncology* **15**, 81–94 (2018).

6. Thompson, S. L., Bakhoum, S. F. & Compton, D. A. Mechanisms of Chromosomal Instability. *Current Biology* **20**, R285 (2010).

7. Zack, T. I. *et al.* Pan-cancer patterns of somatic copy number alteration. *Nat. Genet.* **45**, 1134–1140 (2013).

8. Li, Y. *et al.* Patterns of somatic structural variation in human cancer genomes. *Nature* **578**, 112–121 (2020).

9. Shlien, A. & Malkin, D. Copy number variations and cancer. *Genome Medicine* **1**, 62 (2009).

10. Jeggo, P. A. & Löbrich, M. DNA double-strand breaks: Their cellular and clinical impact? *Oncogene* **26**, 7717–7719 (2007).

11. Mehta, A. & Haber, J. E. Sources of DNA double-strand breaks and models of recombinational DNA repair. *Cold Spring Harb. Perspect. Biol.* **6**, (2014).

12. Giglia-Mari, G., Zotter, A. & Vermeulen, W. DNA damage response. *Cold Spring Harb. Perspect. Biol.* **3**, 1–19 (2011).

13. Jackson, S. P. & Bartek, J. The DNA-damage response in human biology and disease. *Nature* **461**, 1071–1078 (2009).

14. Tubbs, A. & Nussenzweig, A. Endogenous DNA Damage as a Source of Genomic Instability in Cancer. *Cell* **168**, 644–656 (2017).

15. Sulli, G., Di Micco, R. & Di Fagagna, F. D. A. Crosstalk between chromatin state and DNA damage response in cellular senescence and cancer. *Nature Reviews Cancer* **12**, 709–720 (2012).

16. Lamarche, B. J., Orazio, N. I. & Weitzman, M. D. The MRN complex in double-strand break repair and telomere maintenance. *FEBS Letters* **584**, 3682–3695 (2010).

17. Maréchal, A. & Zou, L. DNA damage sensing by the ATM and ATR kinases. *Cold Spring Harb. Perspect. Biol.* **5**, (2013).

18. Foster, S. S., De, S., Johnson, L. K., Petrini, J. H. J. & Stracker, T. H. Cell cycle- and DNA repair pathway-specific effects of apoptosis on tumor suppression. *Proc. Natl. Acad. Sci. U. S. A.* **109**, 9953–9958 (2012).

19. Featherstone, C. & Jackson, S. P. DNA double-strand break repair. *Curr. Biol.* **9**, R759–R761 (1999).

20. Shrivastav, M., De Haro, L. P. & Nickoloff, J. A. Regulation of DNA double-strand break repair pathway choice. *Cell Res.* **18**, 134–147 (2008).

21. Reid, D. A. *et al.* Organization and dynamics of the nonhomologous end-joining machinery during DNA double-strand break repair. *Proc. Natl. Acad. Sci. U. S. A.* **112**, E2575–E2584 (2015).

22. Davis, A. J., Chen, B. P. C. & Chen, D. J. DNA-PK: A dynamic enzyme in a versatile DSB repair pathway. *DNA Repair (Amst).* **17**, 21–29 (2014).

23. Chang, H. H. Y., Pannunzio, N. R., Adachi, N. & Lieber, M. R. Non-homologous DNA end joining and alternative pathways to double-strand break repair. *Nature Reviews Molecular Cell Biology* **18**, 495–506 (2017).

24. Williams, G. J. *et al.* Structural insights into NHEJ: Building up an integrated picture of the dynamic DSB repair super complex, one component and interaction at a time. *DNA Repair (Amst).* **17**, 110–120 (2014).

25. Rodgers, K. & Mcvey, M. Error-Prone Repair of DNA Double-Strand Breaks. *Journal of Cellular Physiology* **231**, 15–24 (2016).

26. Weterings, E. & Chen, D. J. The endless tale of non-homologous end-joining. *Cell Research* **18**, 114–124 (2008).

27. Bunting, S. F. & Nussenzweig, A. End-joining, translocations and cancer. *Nature Reviews Cancer* **13**, 443–454 (2013).

28. Sung, P. & Klein, H. Mechanism of homologous recombination: Mediators and helicases take on regulatory functions. *Nature Reviews Molecular Cell Biology* **7**, 739–750 (2006).

29. Li, X. & Heyer, W. D. Homologous recombination in DNA repair and DNA damage tolerance. *Cell Research* **18**, 99–113 (2008).

30. Michel, B. *et al.* Rescue of arrested replication forks by homologous recombination. *Proc. Natl. Acad. Sci. U. S. A.* **98**, 8181–8188 (2001).

31. Syed, A. & Tainer, J. A. The MRE11–RAD50–NBS1 Complex Conducts the Orchestration of Damage Signaling and Outcomes to Stress in DNA Replication and Repair. *Annu. Rev. Biochem.* **87**, 263–294 (2018).

32. Stracker, T. H. & Petrini, J. H. J. The MRE11 complex: Starting from the ends. *Nature Reviews Molecular Cell Biology* **12**, 90–103 (2011).

33. McVey, M., Khodaverdian, V. Y., Meyer, D., Cerqueira, P. G. & Heyer, W.-D. Eukaryotic DNA Polymerases in Homologous Recombination. *Annu. Rev. Genet.* **50**, 393–421 (2016).

34. Cooper, G. M. Recombination Between Homologous DNA Sequences. (2000).

35. Sung, P., Krejci, L., Van Komen, S. & Sehorn, M. G. Rad51 Recombinase and Recombination Mediators. *Journal of Biological Chemistry* **278**, 42729–42732

(2003).

36. Sung, P., Krejci, L., Van Komen, S. & Sehorn, M. G. Rad51 Recombinase and Recombination Mediators. *Journal of Biological Chemistry* **278**, 42729–42732 (2003).

37. Chen, Z., Yang, H. & Pavletich, N. P. Mechanism of homologous recombination from the RecA-ssDNA/dsDNA structures. *Nature* **453**, 489–494 (2008).

38. Repair of DNA double-strand breaks by DSBR and SDSA. | Learn Science at Scitable. Available at: https://www.nature.com/scitable/content/repair-of-dna-double-strand-breaks-by-41523/. (Accessed: 28th May 2020)

39. Wyatt, D. W. *et al.* Essential Roles for Polymerase θ-Mediated End Joining in the Repair of Chromosome Breaks. *Mol. Cell* **63**, 662–673 (2016).

40. Wood, R. D. & Doublié, S. DNA polymerase θ (POLQ), double-strand break repair, and cancer. *DNA Repair* **44**, 22–32 (2016).

41. Feng, W. *et al.* Genetic determinants of cellular addiction to DNA polymerase theta. *Nat. Commun.* **10**, 1–13 (2019).

42. Simsek, D. *et al.* DNA Ligase III Promotes Alternative Nonhomologous End-Joining during Chromosomal Translocation Formation. *PLoS Genet.* **7**, e1002080 (2011).

43. Malumbres, M. & Barbacid, M. Cell cycle, CDKs and cancer: A changing paradigm. *Nature Reviews Cancer* **9**, 153–166 (2009).

44. Zhou, B. B. S. & Elledge, S. J. The DNA damage response: Putting checkpoints in perspective. *Nature* **408**, 433–439 (2000).

45. Bertoli, C., Skotheim, J. M. & De Bruin, R. A. M. Control of cell cycle transcription during G1 and S phases. *Nature Reviews Molecular Cell Biology* **14**, 518–528 (2013).

46. Bartek, J. & Lukas, J. Pathways governing G1/S transition and their response to DNA damage. *FEBS Letters* **490**, 117–122 (2001).

47. Iyer, D. R. & Rhind, N. The intra-S checkpoint responses to DNA damage. *Genes* **8**, (2017).

48. Hu, J. *et al.* The intra-S phase checkpoint targets Dna2 to prevent stalled replication forks from reversing. *Cell* **149**, 1221–32 (2012).

49. Chao, H. X. *et al.* Orchestration of DNA Damage Checkpoint Dynamics across the Human Cell Cycle. *Cell Syst.* **5**, 445-459.e5 (2017).

50. Chaudhury, I. & Koepp, D. M. Recovery from the DNA Replication Checkpoint. *Genes (Basel).* **7**, (2016).

51. Bačević, K. *et al.* Cdk2 strengthens the intra-S checkpoint and counteracts cell cycle exit induced by DNA damage. *Sci. Rep.* **7**, 1–14 (2017).

52. Chung, J. H. & Bunz, F. Cdk2 is required for p53-independent G2/M checkpoint control. *PLoS Genet.* **6**, (2010).

53. Agarwal, M. L., Agarwal, A., Taylor, W. R. & Stark, G. R. p53 controls both the G2/M and the G1 cell cycle checkpoints and mediates reversible growth arrest in human fibroblasts. *Proc. Natl. Acad. Sci. U. S. A.* **92**, 8493–8497 (1995).

54. Vitale, I., Galluzzi, L., Castedo, M. & Kroemer, G. Mitotic catastrophe: a mechanism for avoiding genomic instability. *Nat. Rev. Mol. Cell Biol.* **12**, 385–392 (2011).

55. Paulovich, A. G., Toczyski, D. P. & Hartwell, L. H. When checkpoints fail. *Cell* **88**, 315–321 (1997).

56. Chao, W. C. H., Kulkarni, K., Zhang, Z., Kong, E. H. & Barford, D. Structure of the mitotic checkpoint complex. *Nature* **484**, 208–213 (2012).

57. Eytan, E., Sitry-Shevah, D., Teichner, A. & Hershko, A. Roles of different pools of the mitotic checkpoint complex and the mechanisms of their disassembly. *Proc. Natl. Acad. Sci. U. S. A.* **110**, 10568–73 (2013).

58. Pilié, P. G., Tang, C., Mills, G. B. & Yap, T. A. State-of-the-art strategies for targeting the DNA damage response in cancer. *Nature Reviews Clinical Oncology*

16, 81–104 (2019).

59. Dasika, G. K. *et al.* DNA damage-induced cell cycle checkpoints and DNA strand break repair in development and tumorigenesis. *Oncogene* **18**, 7883–7899 (1999).

60. Chao, H. X. *et al.* Evidence that the human cell cycle is a series of uncoupled, memoryless phases. *Mol. Syst. Biol.* **15**, (2019).

61. Purvis, J. E. *et al.* p53 dynamics control cell fate. *Science (80-.).* **336**, 1440–1444 (2012).

62. Reyes, J. *et al.* Fluctuations in p53 Signaling Allow Escape from Cell-Cycle Arrest. *Mol. Cell* **71**, 581-591.e5 (2018).

63. Jackson, S. P. & Bartek, J. The DNA-damage response in human biology and disease. *Nature* **461**, 1071–1078 (2009).

64. Taylor, A. M. R. *et al.* Chromosome instability syndromes. *Nature Reviews Disease Primers* **5**, 1–20 (2019).

65. Martin, S. A., Hewish, M., Lord, C. J. & Ashworth, A. Genomic instability and the selection of treatments for cancer. *Journal of Pathology* **220**, 281–289 (2010).

66. Knijnenburg, T. A. *et al.* Genomic and Molecular Landscape of DNA Damage Repair Deficiency across The Cancer Genome Atlas. (2018). doi:10.1016/j.celrep.2018.03.076

67. Alexandrov, L. B. *et al.* The repertoire of mutational signatures in human cancer. *Nature* **578**, 94–101 (2020).

68. Campbell, P. J. *et al.* Pan-cancer analysis of whole genomes. *Nature* **578**, 82–93 (2020).

69. O'Kane, G. M., Connor, A. A. & Gallinger, S. Characterization, Detection, and Treatment Approaches for Homologous Recombination Deficiency in Cancer. *Trends in Molecular Medicine* **23**, 1121–1137 (2017).

70. Sishc, B. J. & Davis, A. J. cancers The Role of the Core Non-Homologous End Joining Factors in Carcinogenesis and Cancer. (2017). doi:10.3390/cancers9070081

71. Kelley, M. R., Logsdon, D. & Fishel, M. L. Targeting DNA repair pathways for cancer treatment: What's new? *Future Oncology* **10**, 1215–1237 (2014).

72. Gavande, N. S. *et al.* DNA repair targeted therapy: The past or future of cancer treatment? *Pharmacology and Therapeutics* **160**, 65–83 (2016).

73. Huang, R. X. & Zhou, P. K. DNA damage response signaling pathways and targets for radiotherapy sensitization in cancer. *Signal Transduction and Targeted Therapy* **5**, 1–27 (2020).

74. Huen, M. S. Y. & Chen, J. The DNA damage response pathways: At the crossroad of protein modifications. *Cell Research* **18**, 8–16 (2008).

75. O'Neil, N. J., Bailey, M. L. & Hieter, P. Synthetic lethality and cancer. *Nature Reviews Genetics* **18**, 613–623 (2017).

76. Murai, J. & Pommier, Y. PARP Trapping Beyond Homologous Recombination and Platinum Sensitivity in Cancers. *Annu. Rev. Cancer Biol.* **3**, 131–150 (2019).

77. Brown, J. S., O'Carrigan, B., Jackson, S. P. & Yap, T. A. Targeting DNA repair in cancer: Beyond PARP inhibitors. *Cancer Discovery* **7**, 20–37 (2017).

78. Daniel, J. A. *et al.* Loss of ATM kinase activity leads to embryonic lethality in mice. *J. Cell Biol.* **198**, 295–304 (2012).

79. Yap, T. A., Plummer, R., Azad, N. S. & Helleday, T. The DNA Damaging Revolution: PARP Inhibitors and Beyond. *Am. Soc. Clin. Oncol. Educ. B.* 185–195 (2019). doi:10.1200/edbk_238473

80. Higgins, G. S. & Boulton, S. J. Beyond PARP—POLu as an anticancer target. *Science* **359**, 1217–1218 (2018).

81. Carvajal-Garcia, J. *et al.* Mechanistic basis for microhomology identification and genome scarring by polymerase theta. *Proc. Natl. Acad. Sci.* 201921791 (2020).

doi:10.1073/pnas.1921791117

82. Ma, J., Setton, J., Lee, N. Y., Riaz, N. & Powell, S. N. The therapeutic significance of mutational signatures from DNA repair deficiency in cancer. *Nature Communications* **9**, 1–12 (2018).

83. Meijer, T. G. *et al.* Functional ex vivo assay reveals homologous recombination deficiency in breast cancer beyond BRCA gene defects. *Clin. Cancer Res.* **24**, 6277–6287 (2018).

84. Konstantinopoulos, P. A., Ceccaldi, R., Shapiro, G. I. & D'Andrea, A. D. Homologous recombination deficiency: Exploiting the fundamental vulnerability of ovarian cancer. *Cancer Discovery* **5**, 1137–1154 (2015).

85. Donehower, L. A. *et al.* Integrated Analysis of TP53 Gene and Pathway Alterations in The Cancer Genome Atlas. *Cell Rep.* **28**, 1370-1384.e5 (2019).

86. Hafner, A., Bulyk, M. L., Jambhekar, A. & Lahav, G. The multiple mechanisms that regulate p53 activity and cell fate. *Nature Reviews Molecular Cell Biology* **20**, 199–210 (2019).

87. Skoulidis, F. *et al.* Co-occurring genomic alterations define major subsets of KRAS-mutant lung adenocarcinoma with distinct biology, immune profiles, and therapeutic vulnerabilities. *Cancer Discov.* **5**, 861–878 (2015).

88. Zhang, J., Wu, L. Y., Zhang, X. S. & Zhang, S. Discovery of co-occurring driver pathways in cancer. *BMC Bioinformatics* **15**, (2014).

89. TP53/ATM co-mutation associated with NSCLC checkpoint blockade response | oncology.medicinematters.com. Available at: https://oncology.medicinematters.com/non-small-cell-lung-cancer/checkpoint-blockade/tp53-atm-co-mutation-associated-with-nsclc-checkpoint-blockade/17333596. (Accessed: 28th May 2020)

90. Pawlik, T. M. & Keyomarsi, K. Role of cell cycle in mediating sensitivity to radiotherapy. *Int. J. Radiat. Oncol.* **59**, 928–942 (2004).

91. Lee, J. M. & Bernstein, A. p53 Mutations increase resistance to ionizing radiation. *Proc. Natl. Acad. Sci. U. S. A.* **90**, 5742–5746 (1993).

92. Huang, S. *et al.* P53 modulates acquired resistance to EGFR inhibitors and radiation. *Cancer Res.* **71**, 7071–7079 (2011).

93. Lowe, S. W. *et al.* p53 status and the efficacy of cancer therapy in vivo. *Science (80-.).* **266**, 807–810 (1994).

94. Kim, J. Y. *et al.* Tumor mutational burden and efficacy of immune checkpoint inhibitors: A systematic review and meta-analysis. *Cancers (Basel).* **11**, (2019).

95. Hollern, D. P. *et al.* B Cells and T Follicular Helper Cells Mediate Response to Checkpoint Inhibitors in High Mutation Burden Mouse Models of Breast Cancer. *Cell* **179**, 1191-1206.e21 (2019).

96. Mardis, E. R. Neoantigens and genome instability: Impact on immunogenomic phenotypes and immunotherapy response. *Genome Medicine* **11**, 71 (2019).

97. Ragu, S., Matos-Rodrigues, G. & Lopez, B. S. Replication stress, DNA damage, inflammatory cytokines and innate immune response. *Genes* **11**, (2020).

98. Li, T. & Chen, Z. J. The cGAS-cGAMP-STI NG pathway connects DNA damage to inflammation, senescence, and cancer. *Journal of Experimental Medicine* **215**, 1287–1299 (2018).

99. Takeuchi, O. & Akira, S. Pattern Recognition Receptors and Inflammation. *Cell* **140**, 805–820 (2010).

100. Coquel, F. *et al.* SAMHD1 acts at stalled replication forks to prevent interferon induction. *Nature* **557**, 57–61 (2018).

101. Harding, S. M. *et al.* Mitotic progression following DNA damage enables pattern recognition within micronuclei. *Nature* **548**, 466–470 (2017).

102. Investigating the Abscopal Effect as a Treatment for Cancer - National Cancer Institute. Available at: https://www.cancer.gov/news-events/cancer-currents-blog/2020/cancer-abscopal-effect-radiation-immunotherapy. (Accessed: 28th May 2020)

103. Crow, Y. J. *et al.* Characterization of human disease phenotypes associated with

mutations in TREX1, RNASEH2A, RNASEH2B, RNASEH2C, SAMHD1, ADAR, and IFIH1. *Am. J. Med. Genet. Part A* **167**, 296–312 (2015).

104. Cortés-Ciriano, I. *et al.* Comprehensive analysis of chromothripsis in 2,658 human cancers using whole-genome sequencing. *Nat. Genet.* **52**, 331–341 (2020).

105. Cortes-Ciriano, I., Lee, S., Park, W. Y., Kim, T. M. & Park, P. J. A molecular portrait of microsatellite instability across multiple cancers. *Nat. Commun.* **8**, 1–12 (2017).

106. Bartkova, J. *et al.* DNA damage response as a candidate anti-cancer barrier in early human tumorigenesis. *Nature* **434**, 864–70 (2005).

107. Bartkova, J. *et al.* Oncogene-induced senescence is part of the tumorigenesis barrier imposed by DNA damage checkpoints. *Nature* **444**, 633–7 (2006).

108. Dang, C. V. MYC on the path to cancer. *Cell* **149**, 22–35 (2012).

109. Lodish, H. *et al.* Proto-Oncogenes and Tumor-Suppressor Genes. (2000).

110. Fumagalli, M., Rossiello, F., Mondello, C. & D'Adda Di Fagagna, F. Stable cellular senescence is associated with persistent DDR activation. *PLoS One* **9**, (2014).

111. Broustas, C. G. & Lieberman, H. B. DNA Damage Response Genes and the Development of Cancer Metastasis. *Radiat. Res.* **181**, 111–130 (2014).

112. Daigh, L. H., Liu, C., Chung, M., Cimprich, K. A. & Meyer, T. Stochastic Endogenous Replication Stress Causes ATR-Triggered Fluctuations in CDK2 Activity that Dynamically Adjust Global DNA Synthesis Rates. *Cell Syst.* **7**, 17-27.e3 (2018).

113. Yang, H. W., Chung, M., Kudo, T. & Meyer, T. p53 of mother cells decide the cell division of daughter cells, 2017. *Nature* **549**, 404–408 (2017).

114. Arora, M., Moser, J., Phadke, H., Basha, A. A. & Spencer, S. L. Endogenous Replication Stress in Mother Cells Leads to Quiescence of Daughter Cells. *Cell Rep.* **19**, 1351–1364 (2017).

115. Lee, A. J. X. *et al.* Chromosomal instability confers intrinsic multidrug resistance. *Cancer Res.* **71**, 1858–1870 (2011).

116. Bakhoum, S. F. & Compton, D. A. Chromosomal instability and cancer: A complex relationship with therapeutic potential. *J. Clin. Invest.* **122**, 1138–1143 (2012).

117. Gronroos, E. & Lopez-García, C. Tolerance of chromosomal instability in cancer: Mechanisms and therapeutic opportunities. *Cancer Research* **78**, 6529–6535 (2018).

118. Salgueiro, L. *et al.* Acquisition of chromosome instability is a mechanism to evade oncogene addiction. *EMBO Mol. Med.* **12**, (2020).

119. Nigro, J., Baker, S., Preisinger, A., Nature, J. J.- & 1989, undefined. *Mutations in the p53 gene occur in diverse human tumour types*. *Springer* (1989).

120. Kastenhuber, E. R. & Lowe, S. W. Leading Edge Putting p53 in Context. (2017). doi:10.1016/j.cell.2017.08.028

121. Young, K. H. *et al.* Structural profiles of TP53 gene mutations predict clinical outcome in diffuse large B-cell lymphoma: An international collaborative study. *Blood* **112**, 3088–3098 (2008).

122. Miller, L. D. *et al.* An expression signature for p53 status in human breast cancer predicts mutation status, transcriptional effects, and patient survival. *Proc. Natl. Acad. Sci. U. S. A.* **102**, 13550–13555 (2005).

123. Robles, A. I. & Harris, C. C. Clinical outcomes and correlates of TP53 mutations and cancer. *Cold Spring Harbor perspectives in biology* **2**, (2010).

124. Freed-Pastor, W. A. & Prives, C. Mutant p53: one name, many proteins. *genesdev.cshlp.org* doi:10.1101/gad.190678.112

125. Lee, M. K. *et al.* Cell-type, Dose, and Mutation-type Specificity Dictate Mutant p53 Functions In Vivo. *Cancer Cell* **22**, 751–764 (2012).

126. Bykov, V. J. N. *et al.* Restoration of the tumor suppressor function to mutant p53 by a low-molecular-weight compound. *Nat. Med.* **8**, 282–288 (2002).

127. Aubrey, B. J., Kelly, G. L., Janic, A., Herold, M. J. & Strasser, A. How does p53 induce apoptosis and how does this relate to p53-mediated tumour suppression? *Cell Death and Differentiation* **25**, 104–113 (2018).

128. Xu, J. *et al.* Differential Radiation Sensitivity in p53 Wild-Type and p53-Deficient Tumor Cells Associated with Senescence but not Apoptosis or (Nonprotective) Autophagy. *Radiat. Res.* **190**, 538 (2018).

129. Mazzatti, D. J., Lee, Y.-J., Helt, C. E., O??Reilly, M. A. & Keng, P. C. p53 Modulates Radiation Sensitivity Independent of p21 Transcriptional Activation. *Am. J. Clin. Oncol.* **28**, 43–50 (2005).

130. Lee, C.-L., Blum, J. M. & Kirsch, D. G. Role of p53 in regulating tissue response to radiation by mechanisms independent of apoptosis. *Transl. Cancer Res.* **2**, 412–421 (2013).

131. Komarova, E. A., Christov, K., Faerman, A. I. & Gudkov, A. V. Different impact of p53 and p21 on the radiation response of mouse tissues. *Oncogene* **19**, 3791–3798 (2000).

132. Eriksson, D. & Stigbrand, T. Radiation-induced cell death mechanisms. *Tumor Biology* **31**, 363–372 (2010).

133. Nardella, C., Clohessy, J. G., Alimonti, A. & Pandolfi, P. P. Pro-senescence therapy for cancer treatment. *Nature Reviews Cancer* **11**, 503–511 (2011).

134. Hinohara, K. & Polyak, K. Intratumoral Heterogeneity: More Than Just Mutations. *Trends in Cell Biology* **29**, 569–579 (2019).

135. Hsu, C. H., Altschuler, S. J. & Wu, L. F. Patterns of Early p21 Dynamics Determine Proliferation-Senescence Cell Fate after Chemotherapy. *Cell* **178**, 361-373.e12 (2019).

136. Ryl, T. *et al.* Cell-Cycle Position of Single MYC-Driven Cancer Cells Dictates Their Susceptibility to a Chemotherapeutic Drug. *Cell Syst.* **5**, 237-250.e8 (2017).

137. Purvis, J. E. & Lahav, G. Encoding and decoding cellular information through signaling dynamics. *Cell* **152**, 945–956 (2013).

138. Zhang, X. P., Liu, F., Cheng, Z. & Wang, W. Cell fate decision mediated by p53 pulses. *Proc. Natl. Acad. Sci. U. S. A.* **106**, 12245–12250 (2009).

139. Chang, H. H. Y., Pannunzio, N. R., Adachi, N. & Lieber, M. R. Non-homologous DNA end joining and alternative pathways to double-strand break repair. *Nature Reviews Molecular Cell Biology* **18**, 495–506 (2017).

140. Williams, A. B. & Rn Schumacher, B. p53 in the DNA-Damage-Repair Process. *perspectivesinmedicine.cshlp.org* doi:10.1101/cshperspect.a026070

141. Krenning, L., Feringa, F. M., Shaltiel, I. A., vandenBerg, J. & Medema, R. H. Transient activation of p53 in G2 phase is sufficient to induce senescence. *Mol. Cell* **55**, 59–72 (2014).

142. Chao, H. X. *et al.* Orchestration of DNA Damage Checkpoint Dynamics across the Human Cell Cycle. *Cell Syst.* **0**, (2017).

143. Chao, H. X. *et al.* Evidence that the cell cycle is a series of uncoupled, memoryless phases. (2018). doi:10.1101/283614

144. Blackford, A. N. & Jackson, S. P. Molecular Cell Review ATM, ATR, and DNA-PK: The Trinity at the Heart of the DNA Damage Response. (2017). doi:10.1016/j.molcel.2017.05.015

145. Zhao, Y. *et al.* Preclinical evaluation of a potent novel DNA-dependent protein kinase inhibitor NU7441. *Cancer Res.* **66**, 5354–5362 (2006).

146. Chan, D. W. *et al.* Autophosphorylation of the DNA-dependent protein kinase catalytic subunit is required for rejoining of DNA double-strand breaks. *Genes Dev.* **16**, 2333–2338 (2002).

147. Attardi, L. D., De Vries, A. & Jacks, T. Activation of the p53-dependent G1 checkpoint response in mouse embryo fibroblasts depends on the specific DNA damage inducer. *Oncogene* **23**, 973–980 (2004).

148. Wyatt, D. W. *et al.* Essential Roles for Polymerase θ-Mediated End Joining in the Repair of Chromosome Breaks. *Mol. Cell* **63**, 662–673 (2016).

149. Brinkman, E. K. *et al.* Kinetics and Fidelity of the Repair of Cas9-Induced Double-Strand DNA Breaks Molecular Cell Article Kinetics and Fidelity of the Repair of Cas9-Induced Double-Strand DNA Breaks. *Mol. Cell* **70**, 801–813 (2018).

150. Brinkman, E. K., Chen, T., Amendola, M. & Van Steensel, B. Easy quantitative assessment of genome editing by sequence trace decomposition. *Nucleic Acids Res.* (2014). doi:10.1093/nar/gku936

151. Zhao, B. *et al.* The essential elements for the noncovalent association of two DNA ends during NHEJ synapsis. *Nat. Commun.* **10**, (2019).

152. Bétous, R. *et al.* DNA replication stress triggers Rapid DNA Replication Fork Breakage by Artemis and XPF. *PLoS Genet.* **14**, (2018).

153. Ma, Y., Pannicke, U., Schwarz, K. & Lieber, M. R. Hairpin opening and overhang processing by an Artemis/DNA-dependent protein kinase complex in nonhomologous end joining and V(D)J recombination. *Cell* **108**, 781–794 (2002).

154. Löbrich, M. & Jeggo, P. A Process of Resection-Dependent Nonhomologous End Joining Involving the Goddess Artemis. *Trends in Biochemical Sciences* **42**, 690–701 (2017).

155. Zhou, Y. & Paull, T. T. DNA-dependent protein kinase regulates DNA end resection in concert with Mre11-Rad50-Nbs1 (MRN) and Ataxia Telangiectasia-mutated (ATM). *J. Biol. Chem.* **288**, 37112–37125 (2013).

156. Arnoult, N. *et al.* Regulation of DNA repair pathway choice in S and G2 phases by the NHEJ inhibitor CYREN. *Nature* **549**, 548–552 (2017).

157. Ceccaldi, R. *et al.* Homologous recombination-deficient tumors are hyper-dependent on POLQ-mediated repair. *Nature* **518**, 258–262 (2015).

158. Huarte, M. *et al.* A large intergenic noncoding RNA induced by p53 mediates global gene repression in the p53 response. *Cell* **142**, 409–419 (2010).

159. Roy, S. *et al.* p53 orchestrates DNA replication restart homeostasis by suppressing mutagenic RAD52 and POLθ pathways. *Elife* **7**, (2018).

160. Sabapathy, K. & Lane, D. P. Therapeutic targeting of p53: All mutants are equal, but some mutants are more equal than others. *Nature Reviews Clinical Oncology* **15**, 13–30 (2018).

161. Baskar, R., Dai, J., Wenlong, N., Yeo, R. & Yeoh, K. W. Biological response of cancer cells to radiation treatment. *Frontiers in Molecular Biosciences* **1**, 24 (2014).

162. Higgins, G. S. & Boulton, S. J. Beyond PARP-POLθ as an anticancer target. *Science* **359**, 1217–1218 (2018).

163. Bartkova, J. *et al.* Oncogene-induced senescence is part of the tumorigenesis barrier imposed by DNA damage checkpoints. *Nature* **444**, 633–637 (2006).

164. Bartkova, J. *et al.* Aberrations of the MRE11-RAD50-NBS1 DNA damage sensor complex in human breast cancer: *MRE11* as a candidate familial cancer-predisposing gene. *Mol. Oncol.* **2**, 296–316 (2008).

165. Gupta, G. P. *et al.* The Mre11 complex suppresses oncogene-driven breast tumorigenesis and metastasis. *Mol. Cell* **52**, 353–65 (2013).

166. Bartek, J., Bartkova, J. & Lukas, J. DNA damage signalling guards against activated oncogenes and tumour progression. *Oncogene* **26**, 7773–9 (2007).

167. Di Micco, R. *et al.* Oncogene-induced senescence is a DNA damage response triggered by DNA hyper-replication. *Nature* **444**, 638–642 (2006).

168. Halazonetis, T. D., Gorgoulis, V. G. & Bartek, J. An oncogene-induced DNA damage model for cancer development. *Science* **319**, 1352–1355 (2008).

169. Hills, S. A. & Diffley, J. F. X. DNA replication and oncogene-induced replicative stress. *Current Biology* **24**, R435–R444 (2014).

170. Fagan-Solis, K. D. *et al.* A P53-Independent DNA Damage Response Suppresses Oncogenic Proliferation and Genome Instability. (2020). doi:10.1016/j.celrep.2020.01.020

171. Bian, L., Meng, Y., Zhang, M. & Li, D. MRE11-RAD50-NBS1 complex alterations

and DNA damage response: Implications for cancer treatment. *Molecular Cancer* **18**, (2019).

172. Castéra, L. *et al.* Next-generation sequencing for the diagnosis of hereditary breast and ovarian cancer using genomic capture targeting multiple candidate genes. *Eur. J. Hum. Genet.* **22**, 1305–1313 (2014).

173. Aloraifi, F. *et al.* Detection of novel germline mutations for breast cancer in non-BRCA1/2 families. *FEBS J.* **282**, 3424–3437 (2015).

174. Lilyquist, J. *et al.* Frequency of mutations in a large series of clinically ascertained ovarian cancer cases tested on multi-gene panels compared to reference controls. *Gynecol. Oncol.* **147**, 375–380 (2017).

175. Brandt, S. *et al.* Lack of MRE11-RAD50-NBS1 (MRN) complex detection occurs frequently in low-grade epithelial ovarian cancer. *BMC Cancer* **17**, (2017).

176. Fan, C.-W. *et al.* Prognostic Heterogeneity of MRE11 Based on the Location of Primary Colorectal Cancer Is Caused by Activation of Different Immune Signals. *Front. Oncol.* **9**, 1465 (2020).

177. Alemayehu, A. & Fridrichova, I. The MRE11/RAD50/NBS1 complex destabilization in Lynch-syndrome patients. *Eur. J. Hum. Genet.* **15**, 922–929 (2007).

178. Feng, W. *et al.* Genetic determinants of cellular addiction to DNA polymerase theta. *Nat. Commun.* **10**, 4286 (2019).

179. Hills, S. A. & Diffley, J. F. X. Review DNA Replication and Oncogene-Induced Replicative Stress. *CURBIO* **24**, R435–R444 (2014).

180. Hook, S. S., Lin, J. J. & Dutta, A. Mechanisms to control rereplication and implications for cancer. *Current Opinion in Cell Biology* **19**, 663–671 (2007).

181. Zeman, M. K. & Cimprich, K. A. Causes and consequences of replication stress. *Nature Cell Biology* **16**, 2–9 (2014).

182. Truong, L. N. & Wu, X. Prevention of DNA re-replication in eukaryotic cells. *J.*

Mol. Cell Biol. **3**, 13 (2011).

183. Liu, E. *et al.* The ATR-mediated S phase checkpoint prevents rereplication in mammalian cells when licensing control is disrupted. *J. Cell Biol.* **179**, 643–657 (2007).

184. Vaziri, C. *et al.* A p53-dependent checkpoint pathway prevents rereplication. *Mol. Cell* **11**, 997–1008 (2003).

185. Castedo, M. *et al.* Cell death by mitotic catastrophe: A molecular definition. *Oncogene* **23**, 2825–2837 (2004).

186. Lukas, C. *et al.* 53BP1 nuclear bodies form around DNA lesions generated by mitotic transmission of chromosomes under replication stress. *Nat. Cell Biol.* **13**, 243–253 (2011).

187. Saldivar, J. C. *et al.* An intrinsic S/G2 checkpoint enforced by ATR. *Science (80-.).* **361**, 806–810 (2018).

188. Fei, F. *et al.* The number of polyploid giant cancer cells and epithelial-mesenchymal transition-related proteins are associated with invasion and metastasis in human breast cancer. *J. Exp. Clin. Cancer Res.* **34**, 158 (2015).

189. MacKenzie, K. J. *et al.* CGAS surveillance of micronuclei links genome instability to innate immunity. *Nature* **548**, 461–465 (2017).

190. Zhang, C. Z. *et al.* Chromothripsis from DNA damage in micronuclei. *Nature* **522**, 179–184 (2015).

191. Ma, Z. *et al.* Modulation of the cGAS-STING DNA sensing pathway by gammaherpesviruses. *Proc. Natl. Acad. Sci. U. S. A.* **112**, E4306–E4315 (2015).